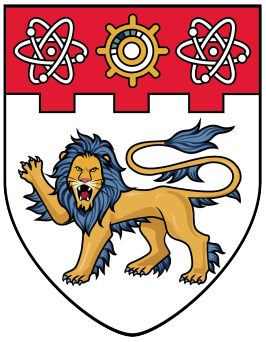

NANYANG TECHNOLOGICAL UNIVERSITY
SINGAPORE

HOLISTIC MANAGEMENT OF MOBILE ENERGY STORAGE FLEETS FOR MORE RESILIENT SERVICE RESTORATION

YAO SHUHAN

INTERDISCIPLINARY GRADUATE SCHOOL

INSTITUTE OF CATASTROPHE RISK MANAGEMENT

2019

HOLISTIC MANAGEMENT OF MOBILE ENERGY STORAGE FLEETS FOR MORE RESILIENT SERVICE RESTORATION

YAO SHUHAN

Interdisciplinary Graduate School

Institute of Catastrophe Risk Management

A thesis submitted to Nanyang Technological University

in partial fulfillment of the requirements for the degree of

Doctor of Philosophy

2019

Statement of Originality

I hereby certify that the work embodied in this thesis is the result of original research, is free of plagiarised materials, and has not been submitted for a higher degree to any other University or Institution.

16 October, 2019

. . . . . .

Date

. . . . . .

Yao Shuhan

Supervisor Declaration Statement

I have reviewed the content and presentation style of this thesis and declare it is free of plagiarism and of sufficient grammatical clarity to be examined. To the best of my knowledge, the research and writing are those of the candidate except as acknowledged in the Author Attribution Statement. I confirm that the investigations were conducted in accord with the ethics policies and integrity standards of Nanyang Technological University and that the research data are presented honestly and without prejudice.

16 October, 2019

. . . . . .

Date

. . . . . .

Wang Peng

Authorship Attribution Statement

This thesis contains material from three papers published in the following peer-reviewed journals and conferences where I was the first author.

Chapter 3 is published as S. Yao, P. Wang, T. Zhao, "Transportable Energy Storage for More Resilient Distribution Systems with Multiple Microgrids," *IEEE Trans. Smart Grid*, vol. 10, no. 3, pp. 3331-3341, 2019. DOI: 10.1109/TSG.2018.2824820.

The contributions of the co-authors are as follows:

- Prof. Wang Peng provided the research direction and revised the manuscript.
- I proposed the idea, developed the algorithm and prepared the manuscript drafts.
- Dr. Zhao Tianyang analyzed the algorithm and proofread the manuscript.

Chapter 4 is published as S. Yao, P. Wang, X. Liu, H. Zhang, T. Zhao, "Rolling Optimization of Mobile Energy Storage Fleets for Resilient Service Restoration," *IEEE Trans. Smart Grid*, vol. 11, no. 2, pp. 1030-1043, 2020. DOI: 10.1109/TSG.2019.2930012.

The contributions of the co-authors are as follows:

- Prof. Wang Peng provided the research direction and revised the manuscript.
- I proposed the idea, developed the algorithm and prepared the manuscript drafts.
- Dr. Zhao Tianyang, Mr. Liu Xiaochuan, Ms. Zhang Huajun analyzed the algorithm and proofread the manuscript.

Chapter 5 is published as S. Yao, J. Gu, P. Wang, T. Zhao, H. Zhang, X. Liu, "Resilient Load Restoration in Microgrids Considering Mobile Energy Storage Fleets: A Deep Reinforcement Learning Approach", *2020 IEEE Power & Energy Society General Meeting*, 2020.

The contributions of the co-authors are as follows:

- Prof. Wang Peng provided the research direction and revised the manuscript.
- I proposed the idea, developed the algorithm and prepared the manuscript drafts.
- Dr. Gu Jiuxiang, Dr. Zhao Tianyang, Ms. Zhang Huajun, Mr. Liu Xiaochuan analyzed the algorithm and proofread the manuscript.

Yao Shuhan

20 April, 2020

....

Date Yao Shuhan

Abstract

The world economy continues to electrify. The power grid constitutes a vital cornerstone of critical infrastructures and serves as an essential foundation for the economy and society. Recent major blackouts caused by extreme weather events lead to catastrophic consequences. The impacts of extreme weather events pose unprecedented challenges to power grids and emphasize the importance of improving system resilience. It is indispensable to restore the electric service effectively in response to severe power outages, thus achieving more resilient distribution systems. When severe blackouts occur, a variety of local resources, e.g., microgrids and distributed energy resources, can be utilized to restore critical loads in distribution systems. Moreover, the emerging mobile energy storage systems (MESSs) can provide temporal-spatial mobility and coordinate with stationary local resources for an integrated distribution system restoration.

To fully leverage the mobility and flexibility of MESS fleets in distribution system restoration, this thesis proposes a joint post-disaster restoration scheme for MESS fleets and generation scheduling in microgrids and network reconfiguration to minimize the total system cost, including customer interruption cost, generation cost, and MESS related costs. A temporal-spatial MESSs model that is related to both transportation networks and distribution systems is proposed to represent the difference between MESSs and energy storage systems (ESS)s in terms of flexibility and cost reduction of ESSs sharing among microgrids. The proposed restoration problem is formulated as a mixed-integer linear program (MILP) with considering various network and MESS constraints. Compared to conventional restoration strategy, the MESS can efficiently transfer energy among multiple micros within the distribution systems in appropriate times and locations,

facilitating critical loads service restoration.

Moreover, this thesis develops restoration strategies under uncertainties. A novel stochastic service restoration strategy is studied to coordinate the dynamic scheduling of MESS, resource dispatching of microgrids, and distribution network reconfiguration. It takes into account damage and repair to both the roads in transportation networks and the branches in distribution systems. The uncertainties in load consumption and the status of roads and branches are modeled as scenario trees using Monte Carlo simulation method. The operation strategy of MESSs is modeled by a stochastic multi-layer time-space network technique. In order to take advantages of multiple source data that improve situational awareness during the restoration process, a rolling optimization framework is adopted to dynamically update system damage, and the coordinated scheduling at each time interval over the prediction horizon is formulated as a two-stage stochastic mixed-integer linear program with temporal-spatial and operation constraints. The integrated restoration strategy is demonstrated to perform effectively under uncertainties in coupled transportation and distribution systems.

Finally, this thesis investigates an on-line optimization framework inspired by deep reinforcement learning (DRL) for solving challenging large scale decision-making problems. The decision-making problem under uncertainties is formulated using Markov decision process (MDP) and solved iteratively by data-driven DRL algorithms. An MDP formulation for an integrated service restoration strategy is investigated to coordinate the scheduling of MESSs and resource dispatching of microgrids. The uncertainties in load consumption are taken into account. The deep reinforcement learning (DRL) algorithm is utilized to solve the MDP for optimal scheduling. The deep deterministic policy gradient (DDPG) and twin delayed DDPG (TD3) are applied to train the deep Q-network and policy network, then the well-trained policy can be deployed in on-line manner

for solving restoration strategy efficiently.

All the proposed methodologies and algorithms are verified by simulations and implemented in Python. Numerical results demonstrate the effectiveness and superiority of the proposed methods.

Acknowledgements

After four years of a fantastic PhD journey with a wonderful research team, I am heading on to new adventures. Thanks to everyone who made my PhD journey special.

First and foremost, I would like to express my sincere gratitude and appreciation to my supervisor, Prof. Wang Peng for his continuous guidance, invaluable advice and encouragement. His enthusiasm for academic research and attitude towards life have great impacts on my future career.

I would also like to give great appreciation to my co-supervisor Asst. Prof. Cheung Sai Hung and mentor Assoc. Prof. Lo Yat Man, Edmond, who provide valuable suggestions on research work. I am particularly grateful to Asst. Prof. Xu Yan and Asst. Prof. Tang Yi for sharing their valuable knowledge.

I would like to thank Future Resilient Systems, Singapore-ETH Centre for financial support for research scholarship and overseas conference support. Special thanks go to my friends and colleagues. They are Dr. Zhao Tianyang, Dr. Gu Jiuxiang, Dr. Cao Zhiguang, Dr. Xiao Jianfang, Dr. Li Song, Dr. Yang Shunfeng, Dr. Zhu Dexuan, Dr. Ju Chengquan, Dr. Xu Qianwen, Dr. Tu Pengfei, Dr. Hu Xiaolei, Dr. Jin Chi, Dr. Huang Jingjing, Mr. Gu Yang, Mr. Lin Pengfeng, Ms. Zhang Huajun, Mr. Chen Shuxin, Mr. Liu Xiaochuan, Mr. Qiu Huan. My sincere gratitude extends to Mr. Tan Peng Chye, Mr. Lee Chew Siong from WERL, Ms. Lim Hwei Li and Ms. Goh Li Hoon from ICRM, as well as Mr. Aaron Ang from FRS for their continuous help.

Last but not least, I also wish to express my appreciation and gratitude to my parents for their invaluable understanding and support. I sincerely express my love to my wife Ms. He Mengxi for her persistent encouragement and warmest

love. Such an accomplishment would not have been possible without them.

Table of Contents

List of Tables

List of Figures

List of Abbreviations

DDPG	Deep Deterministic Policy Gradient
DER	Distributed Energy Resource
DG	Distributed Generator
DRL	Deep Reinforcement Learning
ESS	Energy Storage System
MDP	Markov Decision Process
MESS	Mobile Energy Storage System
MILP	Mixed-integer Linear Programming
SOC	State of Charge
TD3	Twin Delayed Deep Deterministic Policy Gradient

Chapter 1

Introduction

This chapter starts with the backgrounds of the related research work, detailing the smart grid resilience and new challenges to tackle increasing extreme events. Then, the motivations and main contributions of this thesis are summarized, this thesis aims to bridge the gap in the joint coordination of multiple stationary and mobile energy resources to improve smart grid resilience. Finally, detailed thesis organizations are presented.

1.1 Background

Over the next few decades, the world will encounter increasing energy challenges [1]. Current energy system architecture are unsustainable in terms of both resource and environmental issues. The world economy continues to electrify, with nearly two-thirds of the increase in global energy going into the power sector [2]. The power grid constitutes a vital cornerstone of the critical infrastructures and serves as an essential foundation for economy and society. A resilient electric power system is indispensable to meeting the demands in terms of economy and security.

There has been a significant increase in extreme weather events over the last few decades [3], the consequence of both large power outages and extreme weather is increasing. Extreme weather is the primary cause of blackouts in the United States [4], leading to a significant economic loss of billions of dollars a year and interrupting the lives of millions of customers.

Due to the changing scenarios, a reliable mechanism that takes effect today may not be able to tackle perils effectively in future, since the incentives and patterns of threats and hazards continually mutate, no matter by setups of an intentional cyber-attack or through unanticipated natural disasters. Therefore, the concept of resilience has gained much attraction, and policy makers, practitioners and academics have been using it widely and enthusiastically [5].

With regard to power systems, the concept of power systems resilience has only arisen in the last decade. The Presidential Policy Directive (PPD-21) defines resilience as the ability to prepare for and adapt to changing conditions and withstand and recover rapidly from disruptions. Resilience includes the ability to withstand and recover from deliberate attacks, accidents, or naturally occurring threats or incidents [6]. U.S. Department of Energy features five

requisites for resilient distribution systems [7]: a). Develop resilience metrics; b). Enhance system design for resiliency; c). Improve preparedness and mitigation measures; d). Improve system response and recovery; e). Analyze and manage interdependencies.

Several key trends that will shape the future electricity sector [8]. The most critical transformation and evolution of the smart grid are from a one-way flow system to a two-way flow supply chain by distributed energy resources (DERs) and demand side management.

Recent major blackouts caused by extreme weather events lead to catastrophic consequences for the economy and society [9], [10]. The impacts of extreme weather events pose unprecedented challenges to power grids and emphasize the importance of improving system resilience [11]–[13]. As distribution systems remain vulnerable to natural disasters, it is indispensable to restore the electric service effectively in response to severe power outages, thus achieving more resilient distribution systems [14]. When severe blackouts occur, a variety of local resources [15], [16], e.g., microgrids and DERs (energy storage systems, etc.), can be utilized to restore critical loads in distribution systems. Microgrids could serve as a aggregators to actively regulate distributed generators (DGs) and other DERs to implement restoration against natural disasters [11]. A significant property of microgrids compared with conventional grids is that microgrids provide active network ingredients at the distribution level. This feature enables much more flexible operation and mitigates typical power grid susceptibilities associated with centralized generation and control framework and long transmission distances between electricity generation and consumption. Microgrids would be able to facilitate power system restoration under the circumstance of natural disasters. The benefit of microgrids to accomplish network resilience has been identified, several U.S. state governments and utilities have been embracing microgrids as

key components in fast changing architecture of power industry, and investigating the technical, regulatory and financial obstacles for large-scale applications [17], [18].

With the increasing installation of charging/discharging facilities [19], microgrids can provide plug-and-play integration of MESSs for effective service restoration at distribution level. The emerging mobile energy storage systems (MESSs) [20] can provide temporal-spatial mobility and coordinate with stationary local resources for an integrated distribution system restoration. MESSs are generally vehicle-mounted container battery energy storage systems with standard interfaces that allow for plug-and-play [20]. In comparison to stationary energy storage systems (ESSs), MESSs have a sort of advantages in terms of transportability, operational flexibility, which enable MESS to provide power supply to critical loads under emergency conditions.

1.2 Motivation

The importance of the integration of MESS fleets with smart grid operation has been increasingly recognized. The scheduling of MESSs and network reconfiguration of distribution systems should be jointly optimized in the post-disaster restoration. However, to the best of our knowledge, a joint scheduling of MESSs and network reconfiguration in the post-disaster restoration has not been considered yet, especially from the resilience perspective. In this context, this thesis aims to fill the gap in the application of MESS fleets into distribution system restoration. A joint post-disaster restoration scheme is proposed, in which MESS fleets are dynamically scheduled in coordination with distribution system reconfiguration through microgrids, to minimize the total cost in the wake of catastrophes.

Moreover, existing researches are either deterministic or do not thoroughly investigate the potential subsequent damage and repair during the system restoration process, and more detailed stochastic modeling of MESS in transportation network are still needed. Furthermore, extreme weather events can destroy not only the distribution systems but also some other interdependent infrastructures, e.g., transportation networks, which in turn will impact the scheduling of MESSs and impose more challenges to service restoration. Few existing studies have considered the electric service restoration in an integrated distribution and transportation system. In addition, during the disasters, multiple sources of information can be utilized to improve situational awareness of damage status, i.e. weather forecast combined with the geographic information systems, distribution system data from smart meters and micro-phasor measurement can provide information on damage and repair to both the roads in transportation networks and the branches in distribution systems. Therefore, an integrated restoration strategy is needed to coordinate the mobile and stationary resources for service restoration with dynamically updated system damage information in coupled transportation and distribution systems. To overcome the aforementioned technical challenges, this paper aims to bridge the gap in the coordination of MESS fleets with microgrids into distribution system restoration and leveraging dynamically updated information during the restoration process. A rolling integrated restoration strategy is proposed to coordinate the dynamic scheduling of MESS, resource dispatching of microgrids and distribution network reconfiguration.

The optimal scheduling is generally formulated as a mixed-integer convex program, which is NP-hard and computationally expensive, in terms of a large number of integer or binary variables in large-scale systems. In addition, accurate forecast information is necessary for the optimization model. Recent advances in deep reinforcement learning (DRL) give rise to tremendous success in solving

challenging decision-making problems. In general, the decision-making problem under uncertainties is formulated using Markov decision process (MDP) and solved iteratively by data-driven DRL algorithms. The application of DRL in energy management systems has been increasingly recognized. However, research in this area is still in the early stage, the benefit of applying DRL in coordinated scheduling of stationary and mobile energy resources has not yet been fully investigated and further studies are needed. To address the aforementioned issue, a novel MDP formulation for critical load restoration in microgrids is proposed considering the stationary and mobile energy resources. Uncertainties in load consumption are taken into account. The agent aims to maximize the service restoration in microgrids by jointly coordinating the resource dispatching of microgrids and scheduling of MESS. The MESS fleets are dynamically dispatched among microgrids for load restoration in coordination with microgrid operation.

1.3 Main Contributions

The main objective of this thesis is to improve smart grid resilience by coordination of multiple stationary and mobile energy resources. The main contributions of this research are summarized as follows.

1) To fill the gap in the application of MESSs into distribution system restoration and fully leverage the mobility and flexibility of MESS fleets, this thesis proposes an integrated restoration scheme for coordinating stationary and mobile energy resources. A temporal-spatial MESS model, connecting the transportation networks and distribution systems, is presented. Compared to conventional restoration strategy, the MESS can efficiently transfer energy among multiple micros within the distribution systems in appropriate times

and locations, facilitating critical loads service restoration without violating network topology and operation constraints.

2) To deal with uncertain information and thoroughly investigate the potential subsequent damage and repair during the restoration process, A novel stochastic model is developed. The scheduling of MESS fleet is modeled by a stochastic multi-layer time-space network, which reduces the computational complexity with a fewer number of binary variables and constraints and can be utilized for practical transportation networks. Moreover, to make the most of updated information, a rolling optimization framework is adopted to dynamically update system information and the coordinated scheduling over the prediction horizon. The integrated restoration strategy is demonstrated to perform effectively under uncertainties in coupled transportation and distribution systems.

3) Motivated by great progress in DRL for solving large scale decision optimization problems, this thesis further investigates an on-line optimization framework by applying DRL for more resilient service restoration in an on-line manner, tackling scalability issues and the need for accurate uncertainty modeling. A novel MDP formulation for critical load restoration in microgrids is proposed considering the stationary and mobile energy resources. The proposed model is solved by twin delayed deep deterministic policy gradient (TD3), which is an actor-critic algorithm that can deal with discrete or continuous variables in state and action space. The well-trained model can be deployed for on-line implementation for solving the coordinated service restoration problem.

1.4 Organization of the Thesis

This thesis consists of six chapters organized as follows.

Chapter 1 presents the background, motivation and contribution of the thesis.

Chapter 2 provides a literature review on smart grid resilience. The emerging MESSs have great potential to provide temporal-spatial mobility and coordinate with stationary local resources to improve smart grid resilience.

Chapter 3 proposes a joint post-disaster restoration scheme for MESS and generation scheduling in microgrids and network reconfiguration, to minimize the total system cost including customer interruption cost, generation cost, and MESS related costs. A temporal-spatial MESS model that is related to both transportation networks and distribution systems is proposed to represent the difference between MESS and ESS in terms of flexibility and cost reduction of ESS sharing among microgrids. The proposed restoration problem is formulated as an MILP with considering various network and MESS constraints.

Chapter 4 further develops the deterministic model in Chapter 3 to a stochastic one. This chapter proposes a rolling integrated service restoration strategy to minimize the total system cost by coordinating the scheduling of MESS fleets, resource dispatching of microgrids and network reconfiguration of distribution systems. The integrated strategy takes into account damage and repair to both the roads in transportation networks and the branches in distribution systems. The uncertainties in load consumption and the status of roads and branches are modeled as scenario trees using Monte Carlo simulation method. The operation strategy of MESSs is modeled by a stochastic multi-layer time-space network technique. A rolling optimization framework is adopted to dynamically update system damage, and the coordinated scheduling at each time interval over the prediction horizon

is formulated as a two-stage stochastic MILP with temporal-spatial and operation constraints.

In Chapter 5, to address the scalability issues to implement an on-line optimization framework, an MDP formulation for an integrated service restoration strategy is presented that coordinates the scheduling of MESSs and resource dispatching of microgrids. The uncertainties in load consumption are taken into account. The DRL algorithm is utilized to solve the MDP for optimal scheduling. Specifically, the twin delayed deep deterministic policy gradient (TD3) is applied to train the deep Q-network and policy network, then the well-trained policy can be deployed in an on-line manner for solving the optimization problems efficiently.

Chapter 6 concludes the research work and recommends prospective areas for further investigation.

Chapter 2

Literature Review

In this chapter, a comprehensive review of the resilient smart grid is presented in detail. First, the changing scenario in energy systems and new challenges to tackle increasing extreme events are introduced, followed by a brief introduction of smart grid resilience. The most critical transformation and evolution of the smart grid are from a one-way flow system to a two-way flow supply chain by DERs and demand side management. Microgrids are utilized to coordinate multiple energy resources. Finally, the emerging MESSs are presented, which have great potential to provide temporal-spatial mobility and coordinate with stationary local resources to improve smart grid resilience.

2.1 Changing Threats to Critical Infrastructures

2.1.1 Electrification of Energy Systems

Over the next few decades, the world will encounter increasing challenges [1]. Current energy system architecture are unsustainable in terms of both resource and environmental issues. The outlook for energy use worldwide presented in [2] continues to rise over the next three decades, Electricity consumption is an important part of this change. It is expected that electricity consumption is projected to grow by about 18 percent between 2014 and 2040 [21].

The extensive exploitation and utilization of fossil fuel have caused various consequences, including energy shortages, environmental pollution and climate changes [1]. The renewables-led transformation of energy systems has given focus to electrical power systems [22]. Renewable electricity generation will make a significant contribution to achieving climate change goals and sustainable energy use [23].

The world economy continues to electrify, with nearly two-thirds of the increase in global energy going into the power sector [2]. The share of energy exploited worldwide for electricity generation is projected to rise from 42% in 2015 to 47% by 2035 [23]. Fig. 2.1 and Fig. 2.2 track the U.S consumption of energy resources in 2012 and 2018, respectively [24]. Overall energy consumption rises to a record high level of 101.2 quadrillion BTU. The rapidly increasing renewable energy would be transformed into electricity and delivered to end-use customers.

The IEC justifies the electrification of energy systems to be the most critical ingredients in dealing with the energy concerns [1]. It argues that electricity is the most sensible way to consume energy. The electricity is conveniently

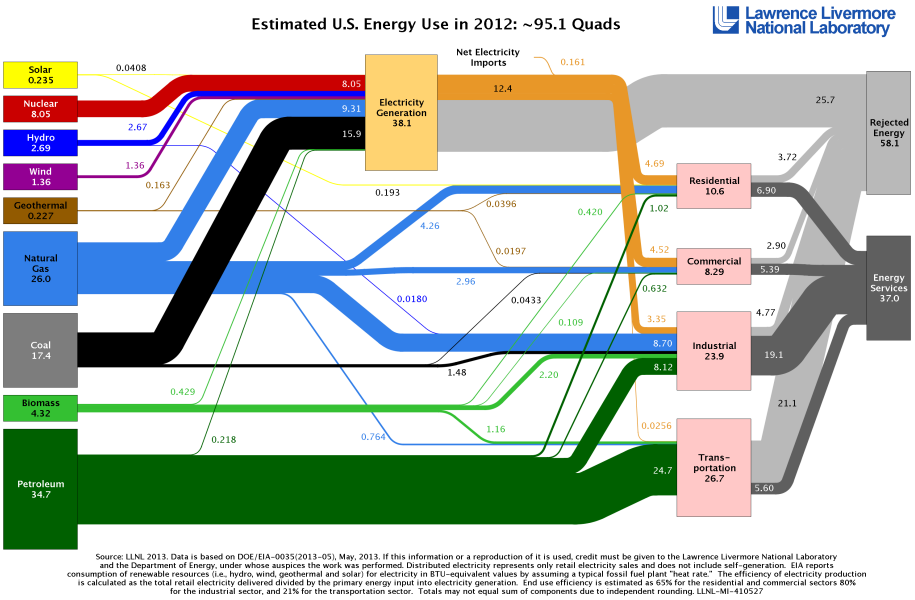

Figure 2.1: The 2012 energy flow chart.

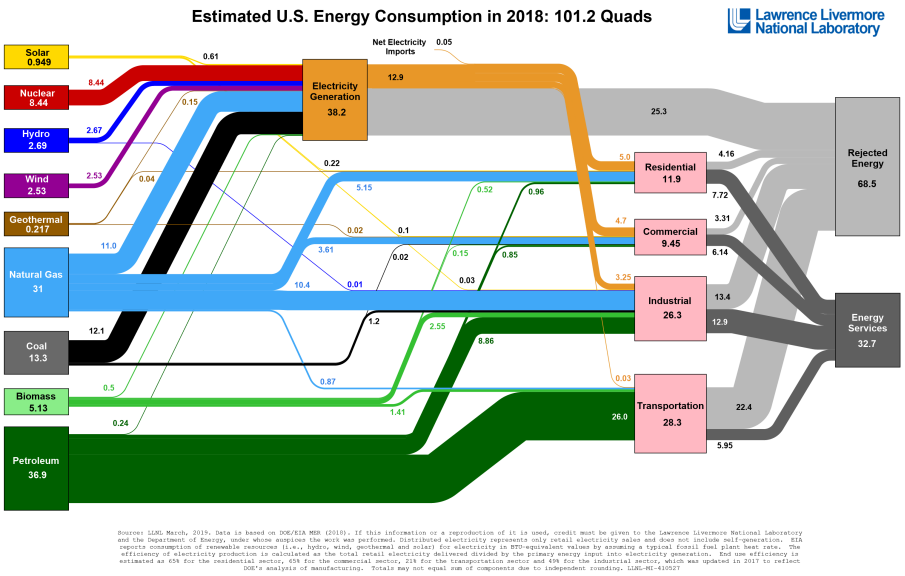

Figure 2.2: The 2018 energy flow chart.

managed, much more effortless to transmit and deliver than most other energy sources, essentially would not cause environmental contamination at the end-use customers and could be eco-friendly at the generation part in consideration of progressive penetration of renewable energy. It is demonstrated to be the most efficient and effective path for future global efforts to economize energy [8], [22].

In Fig. 2.3, key critical infrastructure interdependencies represent the core underlying framework that supports the economy and society [21]. Electricity is at the center of key infrastructure systems that support these sectors, including transportation, oil and gas production, water, communications and information, and finance [21]. The power grid constitutes a vital cornerstone of the critical infrastructures and serves as an essential foundation for economy and society. A resilient electric power system is indispensable to meeting the demands in terms of health, safety and national security. Physical incidents, cyber incidents, or natural disasters would affect the power grid and evoke catastrophes for life. A reliable mechanism that takes effect today may not be able to tackle perils effectively in future, since the incentives and patterns of threats and hazards continually mutate, no matter by setups of an intentional cyber-attack or through unanticipated natural disasters. Associated stakeholders must make provision for interruptive contingencies and respond to the potential risks, jeopardizes, susceptibilities, and consequences.

2.1.2 Catastrophic Impacts of Blackouts

Electric power systems are complex, critical to modern society, and interdependent with other critical infrastructure. The electricity system faces a range of growing threats to its reliability and security.

Various blackouts took place all over the world in the past few decades.

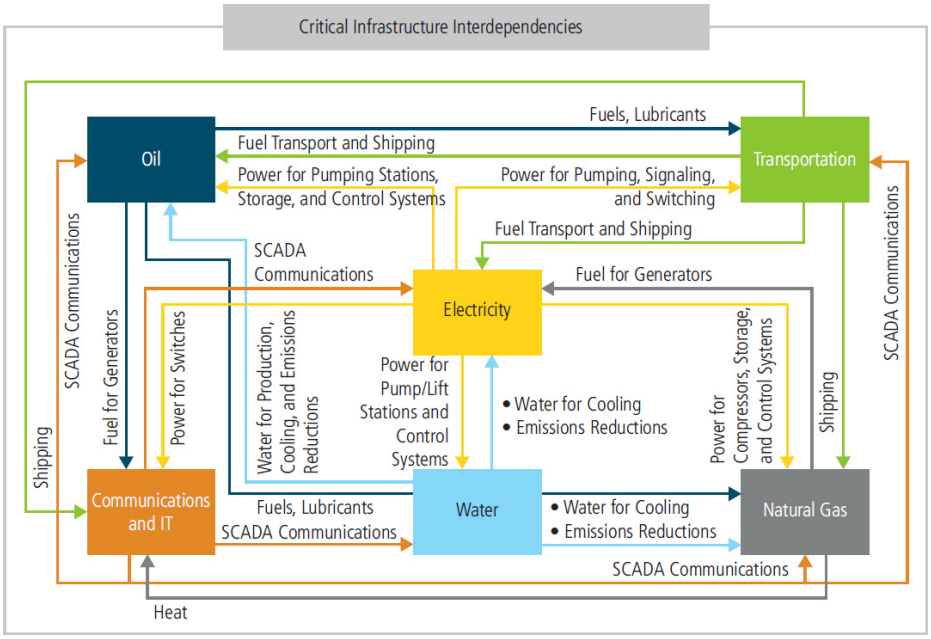

Figure 2.3: Critical infrastructure interdependencies.

power system outages lead to economic loss between $104 and $164 billion a year in the U.S. [25]. Severe power outages arise from time to time. For instance, in August 1996, a major system disturbance split the Western Electricity Coordinating Council (WECC) system into four islands, impacting 7.5 million customers for about nine hours. The 1998 Auckland blackout disrupted electricity service for a long period of two months, rendering a serious lawsuit against the utility company. In August, 2003, a large area blackout triggered by cascading failures in the east of North America caused eight states in U.S. and two provinces in Canada to lose power, affecting about 50 million people for a period up to several days. On August 18, 2005, numerous power stations were forced out following the power grid imbalance in Indonesia, knocking out power supply to 100 million people for five hours. In November 2006, Western Europe suffered a large blackout resulting from a high voltage line switching. On November 10, 2009, Brazil and Paraguay experienced a massive power outage caused by

cascading failure under storms, impacting an estimated 67 million consumers. In July, 2012, a wide area outage strikes the power systems in India, causing approximately half of India without electricity supply. This is the biggest ever blackout in the world, disrupting a variety of sectors for two days. These large blackouts let us recognize that the N-1 principle that works for several years for power system planning and operation may not be able to assure an acceptable reliability level under the rapidly changing scenario.

2.1.3 Increasing Exposure to Extreme Weather Events

There has been a significant increase in extreme weather events over the last few decades [3], as shown in Fig. 2.4. Between 1980 and 2012, more than 21000 natural catastrophes occurred, of which 87% were weather-related. These catastrophes brought 2.3 million fatalities, $3,800 billion of overall losses and $970 billion of insured losses [26]. Most of the increase in economic losses from weather-related disasters over the past two decades can be attributed to socio-economic factors. As populations and economics continue to grow, the total value and human life at risk will increase. In 2012 alone, natural catastrophes caused $160 billion in overall losses and $65 billion in insured losses worldwide, of which 67% were attributable to the U.S [8]. Fig. 2.5 summarizes the major natural disasters worldwide registered by Munich Re NatCatSERVICE in 2018 [27].

Weather outages triggered by thunderstorms, hurricanes and blizzards and other extreme weather events account for 58% of blackouts witnessed since 2002 and 87% of outages impacting more than 50000 customers [28]. Generally, 679 wide area blackouts taking place between 2003 and 2012 are related to extreme weather. Additionally, the consequence of both large power outages and extreme weather is increasing, the highest insured loss was caused by Hurricane

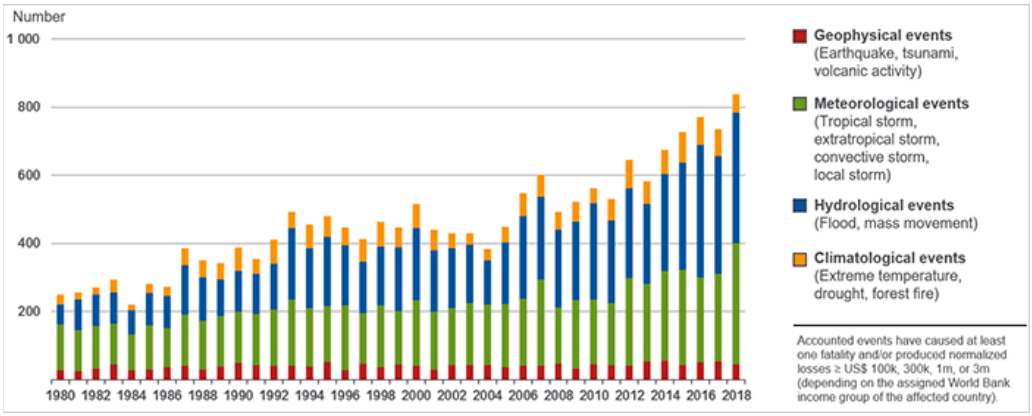

Figure 2.4: Number of natural catastrophes, 1980-2018.

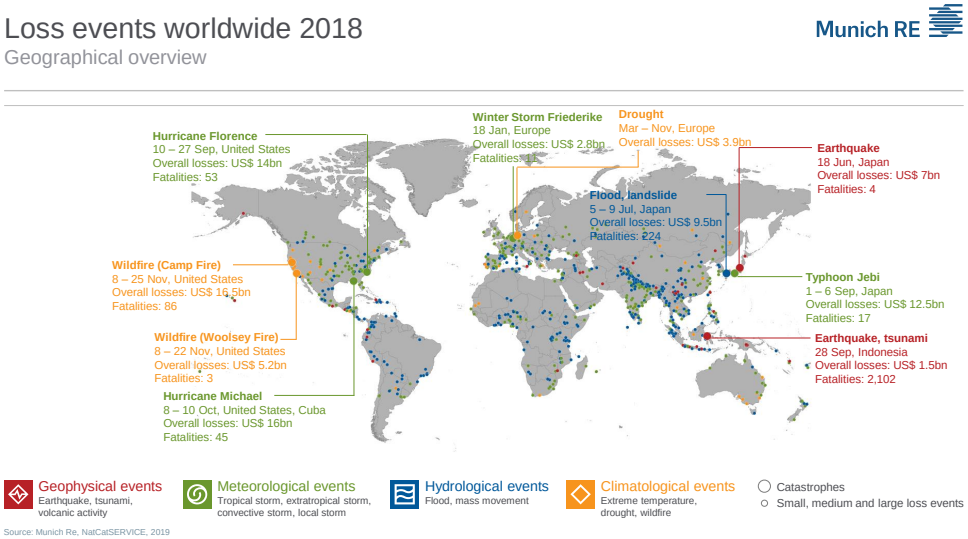

Figure 2.5: World natural catastrophes in 2018.

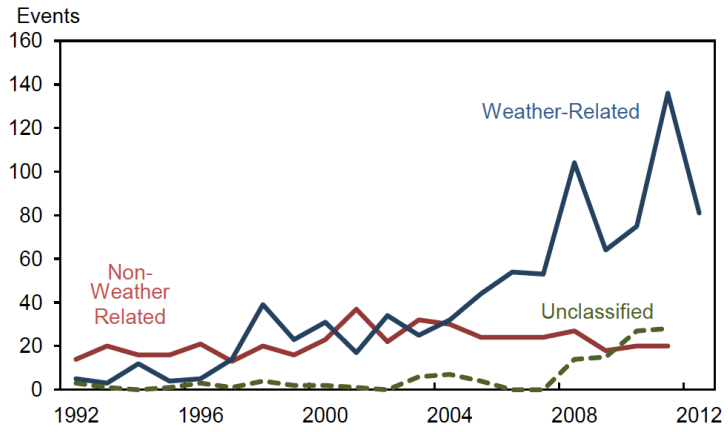

Figure 2.6: Outages to the bulk power systems, 1992-2012.

Sandy, with an estimated insurance cost of $25 billion [26]. Statistics and data demonstrate that weather-related blackouts have increased notably since 1992, as shown in Fig. 2.6 [4].

Extreme weather is the primary cause of blackouts in the United States [4], leading to a significant economic loss of billions of dollars a year and interrupting the lives of millions of customers. In the past decade, there have been over 500 severe weather events in North America that have affected 50,000 customers each [29]. For example, more than 8 million end-use customers suffered blackouts as a result of Hurricane Sandy's devastating impact in 2012, with the overall losses in New York and New Jersey exceeding $70 billion [30]. In 2008, when a disastrous ice storm hit southern China, 2000 substations and 8500 towers were collapsed and 13 provinces, 170 cities were suffering power outages lasting from several days to a month [31]. Meanwhile, the number of weather related outages is projected to enhance because of the aging nature of grid combined with climate change which increases the frequency and intensity of hurricanes, storms, blizzards and floods. Therefore, in addition to being reliable to the most typical outages, the power system resilience is critically important as a key part of the

infrastructure's defense against high impact low probability extreme events.

Comparison between typical and weather-related outages are are highly dependent on the attributes of natural disasters. For instance, multiple failures can take place concurrently and locations are associated with the pathway of disastrous events. Some extreme disasters could even break down the transmission network, impair substations and generators to evoke severe blackouts. Additionally, extreme weather events may also devastate other interdependent infrastructures (e.g., transportation, communications, water and gas supply networks) [11].

It is imperative to learn from the lessons and develop resilient responses and strategies [29]. In addition to being reliable to the most typical outages, the power grid resilience is progressively critical as climate change promotes the probability and consequence of extreme weather events [4].

2.2 Smart Grid Resilience

2.2.1 Concepts of Resilience

The Presidential Policy Directive (PPD-21) defines resilience as the ability to prepare for and adapt to changing conditions and withstand and recover rapidly from disruptions. Resilience includes the ability to withstand and recover from deliberate attacks, accidents, or naturally occurring threats or incidents [6]. A conceptual resilience curve associated with an event in [31] is adopted for better illustration, as shown in Fig. 2.7. R refers to an index of system resilience level. The system states involve: pre-disturbance resilient state (t_0, t_e), event progress (t_e, t_{pe}), post-event degraded state (t_{pe}, t_r), restorative state (t_r, t_pr), post-restoration state (t_pr, t_ir) and infrastructure recovery (t_ir, t_pir).

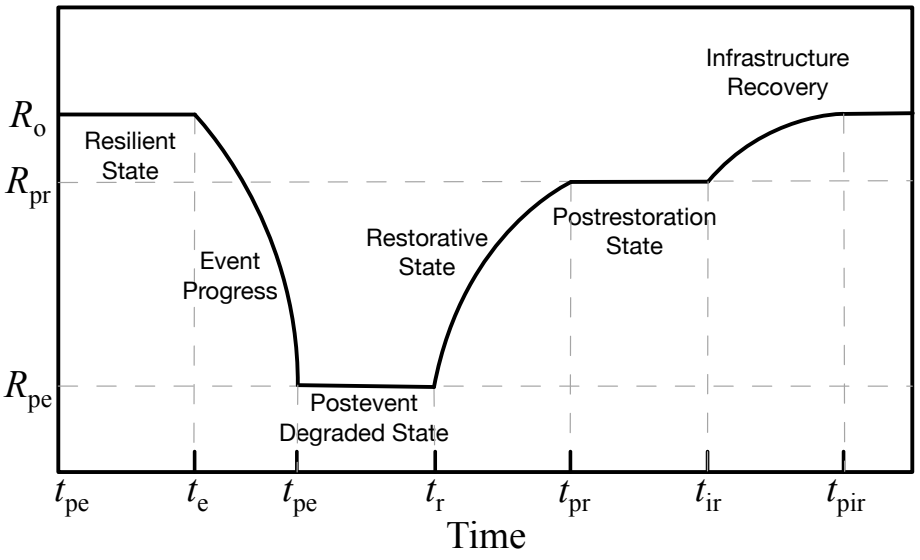

Figure 2.7: A conceptual resilience curve associated with an event.

The Resilience Engineering Research Centre of the University of Tokyo was established in 2013 to promote research on principles and methodologies to realize resilient systems, thus contributing to a safe and secure society [32]. Following the 2011 Tohoku earthquake and Fukushima nuclear power plant disaster, Tohoku University established the International Research Institute of Disaster Resilience [33]. The research is action-oriented, complementing widely applied prevention with preparation and response policies, strategies and practices. The Japanese initiative seems to become an international benchmark of how resilience can become part of social development.

The American Recovery and Reinvestment Act of 2009 ("Recovery Act") apportioned $4.5 billion to the U.S. department of energy for improvements in modernizing power grids [34]. The initiatives aim to enhance the power systems resilience and reliability in response to severe weather. Smart grid technology utilizes remote control and automation to enhance situational awareness and better monitor and control the grid.

The U.S. department of energy highlights resilience against climate change and extreme weather. The Smart Grid R&D Program has commenced a national effort on distribution system resilience [35]. In addition to acting as a backbone to enhance resilience against extreme events, this effort also bolsters Executive Order 13653 "Preparing the United States for the Impacts of Climate Change" [36] and the goal of "building stronger and safer communities and infrastructure" [7]. Sandia National Laboratory has developed an iterative process for resilience analysis and resilience metrics. Argonne National Laboratory has investigated the infrastructure survey tool. This infrastructure survey tool is able to capture and evaluate protection and resilience data acquired from facilities in other critical infrastructures. Los Alamos National Laboratory makes efforts to build up a decision-making support system, which supports resilient distribution system design and modernization of legacy distribution networks. Washington State University and Pacific Northwest National Laboratory cooperate to justify using microgrids as resilience resources. U.S. Department of Energy features five requisites for resilient distribution systems [7]: a). Develop resilience metrics; b). Enhance system design for resiliency; c). Improve preparedness and mitigation measures; d). Improve system response and recovery; e). Analyze and manage interdependencies.

2.2.2 Evolution of Smart Grids

Electric power systems are evolving to smarter grids, which can use digital communications technology, information systems, and automation to detect and react to local changes in usage, improve system operating efficiency, and in turn reduce operating costs while maintaining high system reliability [37].

For over 100 years, the electricity system has been operated through one-way

Figure 2.8: Traditional one-way flow electricity supply chain.

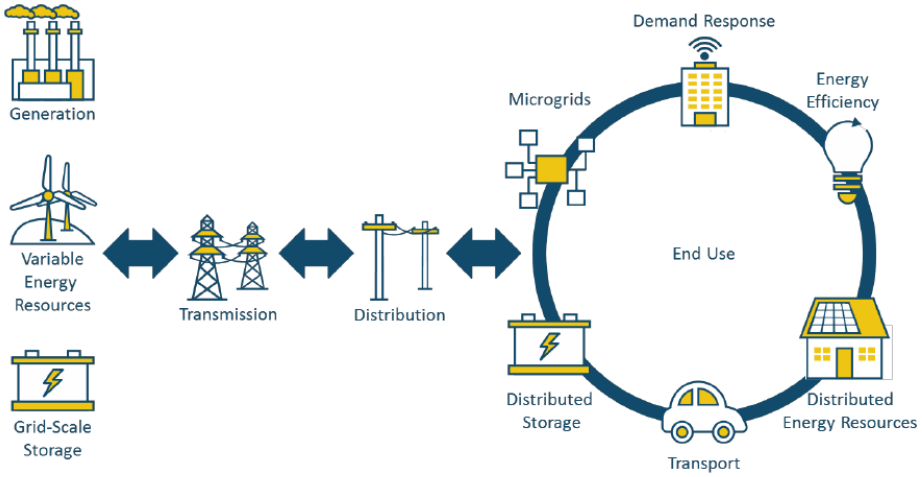

Figure 2.9: Evolution of smart grid to two-way flow supply chain.

flows of electricity and information, as shown in Fig. 2.8 [8]. The generation and smart grid technology innovations can reduce grid costs and improve efficiency. Fig. 2.9 indicates that these technologies have enabled an electricity system where two-way flows are possible and more common, and where digitization is a key enabler of a new range of services, including increased flexibility, higher system efficiency, reduced energy consumption, and increased consumer options and value [21].

2.2.3 Microgrids as Resilience Resources

Recent major blackouts caused by extreme weather events lead to catastrophic consequences for the economy and society [9], [10]. The impacts of extreme

weather events pose unprecedented challenges to power grids and emphasize the importance of improving system resilience [11]–[13]. As distribution systems remain vulnerable to natural disasters, it is indispensable to restore the electric service effectively in response to severe power outages, thus achieving more resilient distribution systems [14]. When severe blackouts occur, a variety of local resources [15], [16], e.g., microgrids and DERs (ESSs, etc.), can be utilized to restore critical loads in distribution systems.

Great progress has been made in the utilization of stationary resources for service restoration in distribution systems after major blackouts [11], [38]. To cope with generation unavailability during and after natural disasters, distributed generation units, such as fuel cells, micro turbines, wind turbines, photovoltaic panels, could be employed as flexible resources to increase system resilience. DGs are widely adopted in the restoration when the distribution system is isolated from the main grid [39]. Furthermore, microgrids can be used to aggregate a wide range of DERs for service restoration [11], [38], [40]

In the light of the CIGRE Working Group C6.22, microgrids comprise low voltage distribution systems with DERs, storage devices, and controllable loads, operated connected to the main power network or islanded, in a controlled, coordinated way [41]. Microgrids could serve as aggregators to actively regulate DGs and other DERs to implement restoration against natural disasters [11]. A significant property of microgrids compared with conventional grids is that microgrids provide active network ingredients at the distribution level. This feature enables much more flexible operation and mitigates typical power grid susceptibilities associated with centralized generation and control framework and long transmission distances between electricity generation and consumption. Microgrids would be able to facilitate power system restoration under the circumstance of natural disasters. The benefit of microgrids to accomplish network

resilience has been identified, several U.S. state governments and utilities have been embracing microgrids as key components in fast changing architecture of power industry, and investigating the technical, regulatory and financial obstacles for large-scale applications [17], [18].

Reference [39] develops an integrated operating and self-healing strategy for distribution system. micro turbines are dispatchable with frequency and voltage regulation functions whereas wind turbines and photovoltaic generators are deemed nondispatchable. An optimization problem is formulated and solved over the time window. Only the solution for the first period in the window is carried out while the solution for other time intervals would be neglected. This process iterates untill the time window has been traversed [39]. The formed self-adequate networked microgrids are more resilient to potential cascading failures since the power balance is achieved locally within each section. Besides, those networked microgrids can support each other [42]. Dynamic formation of multiple microgrids with DGs offers a resilient solution to restore critical loads against natural disasters. In [40], a distribution system operational approach by using DGs to restore critical load after major disruptions. The optimization is formulated as a MILP subject to self-adequacy and electrical constraints. However, more dummy binary and continuous variables are needed with the increase of the number of DGs, reference [43] presents a new mathematical formulation for the model in [40] to scale down the number of decision variables and improve the computational performance.

Reference [44] develops a graph-theoretic approach for distribution system restoration. The microgrids ameliorate the self-healing ability and enable the distribution system to recover faster after disturbances. The presented approach employs the spanning tree search algorithm in order to maximize load pickup and minimize the number of switching operations without violating operational

constraints. The microgrids connected to distribution system through point of common coupling are represented as virtual feeders. In [38], the stability of microgirds, constraints on frequency deviation, and limits to transient voltage and current of DGs are integrated to describe transient property. The authors demonstrate the concepts of restoration tree and load group to come up with restoration measures. The restoration problem is modeled as a maximum coverage problem and formulated as a linear integer program. Reference [45] considers the scarcity of power generation resources, and introduce the concept of continuous operating time to determine the availability of microgrids for critical load restoration and assess the service time. A two-stage heuristic is developed. First, a strategy table containing all feasible restoration path is established, Then the critical load restoration strategy is obtained by solving a linear integer program.

Reference [46] proposes a resilience response framework by generator redispatch, topology switching, and load shedding. A Markov model is proposed to construct sequential proactive strategies against extreme weather events in [47]. In [48], a microgrid proactive management framework is proposed to coordinate generation reschedule, conservation voltage regulation and demand-side resources. Proactive scheduling in multiple energy carrier microgrids is proposed in response to approaching hurricane [49] and floods [50]. Reference [51] proposes an optimal restoration strategy that coordinates multiple sources at multiple locations to serve critical loads after blackouts. These studies illustrate the value of coordination of multiple resources to enhance grid resilience.

2.3 Mobile Energy Storage Systems

2.3.1 Development of Mobile Energy Storage Systems

With the increasing installation of charging/discharging facilities [19], microgrids can provide plug-and-play integration of MESSs for effective service restoration at distribution level. The emerging MESSs [20] can provide temporal-spatial mobility and coordinate with stationary local resources for an integrated distribution system restoration.

MESSs are generally vehicle-mounted container battery energy storage systems with standard interfaces that allow for plug-and-play [20]. They are characterized by utility-scale capacity [52]. In an MESS, an array of batteries is installed on a transport truck, where power converters and controllers are integrated. Under the demonstration stage, MESSs are attractive players in the resilient power systems, along with the cost reduction and profitable benefits.

Various demonstration projects of MESS applications have been deployed in recent years. In the U.S., electric utility company Premium Power's 0.5-MW/2.8-MWh transportable Zinc-Bromine ESS was deployed by Electric Power Research Institute (EPRI) [53]. EPRI and Department of Defense of the U.S. initiated a project to demonstrate a containerized grid support storage system featuring utility capacity up to 2 MWh committed to enhancing energy security at military facilities [54]. Li-ion developer Altair Nanotechlogoies has 1-MW/250-kWh trailer-mounted Li-ion battery systems in service with both AES corporation and PJM interconnection [53].

In comparison to stationary ESSs, MESSs have a sort of advantages in terms of transportability, operational flexibility, which enable MESS to provide power

supply to critical loads under emergency conditions. Furthermore, the installed capital cost of MESS is expected to reduce to a competitive level in about 5 to 10 years [54]. MESSs have the potential to rival distributed generation units like fuel cells and micro turbines in the coming years [54]. In terms of techno-economic benefits, it is promising to utilize MESSs to provide of various ancillary services [55], [56].

2.3.2 Integration of Mobile Energy Storage Systems into Smart Grid

For the integration of MESSs, some researches have been conducted to apply MESSs into power systems operation under both normal [57], [58] and extreme conditions [52]. Under normal conditions, MESSs are utilized to provide ancillary services to both transmission networks [55], [59] and DSs [56]. For transmission networks, MESSs are applied to realize load shifting in [57], [58]. To alleviate the transmission line congestion and reduce the operating cost, a battery-based energy transportation system integrated unit commitment problem is presented in [55]. Aside from boosting system economics, the battery-based energy transportation system is used to reduce the wind power curtailment in [59]. To regulate the voltage profiles in DSs, a transition model is developed to schedule MESSs' position and operation plans in [56].

In response to extreme events, MESS fleets can be utilized in both pre and post stage. The economic feasibility of MESSs is demonstrated in [60] by optimizing the investments and relocation of MESSs in case of natural disasters. Reference [61] proposes a sequential framework for the pre-positioning of mobile generators to staging locations and real-time dispatching to distribution systems. In [62], the resource allocation of electric buses and transportable batteries is

formulated for proactive preparedness for extreme weather events. Dynamic microgrids formation is applied to accommodate mobile and stationary distributed generation and energy resources after disruptions in [63]. Reference [64] presents a microgrid-based critical load restoration by adaptively forming microgrids and positioning mobile emergency resources. Nevertheless, the resource allocation is for one-time dispatching of MESSs in the pre or initial stage of disasters instead of optimizing the temporal-spatial behaviors throughout the restoration process, so the mobility and flexibility of MESS fleets are underutilized. Reference [65] implements resilient routing and scheduling of mobile power sources via a two-stage framework, in which the pre-position and dynamic dispatch are used to coordinate with conventional restoration efforts. For post-disaster restoration, [66] proposes a resilient scheme for disaster recovery logistics that involves scheduling of repair crews and mobile power source and network reconfiguration. A joint scheme is proposed in [67] to integrate the dynamic scheduling of MESSs, generation re-dispatching and network reconfiguration.

2.4 Summary

This chapter reviews the background literature. The electrification of energy systems and changing threats are introduced. Extreme events with high-impact, low-probability have catastrophic impacts on electricity infrastructure in terms of extensive interruptions in service to end-use customers. In addition to reliability, it is increasingly evident that smart grid resilience is necessary for dealing with extreme events. Then The transformation and evolution of smart grid are reviewed, microgrids are adopted to serve as resilience resource after major blackouts. Moreover, the emerging MESSs can provide temporal-spatial mobility and coordinate with stationary local resources for disaster relief efforts.

Chapter 3

Mobile Energy Storage for More Resilient Distribution Systems with Multiple Microgrids

MESSs have great potential to enhance the resilience of distribution systems against large area blackouts. A joint post-disaster restoration scheme for MESS and generation scheduling in microgrids and network reconfiguration is proposed to minimize the total system cost including customer interruption cost, generation cost, and MESS related costs. A temporal-spatial MESS model that is related to both transportation networks and distribution systems is proposed to represent the difference between MESS and ESS in terms of flexibility and cost reduction of ESS sharing among microgrids. The proposed restoration problem is formulated as an MILP with considering various network and MESS constraints. The proposed model and scheme are tested in a modified 33-bus test system with three microgrids and four MESSs. The results verify that a distribution system with MESS is more resilient compared with conventional ESS because of the benefit from total cost reduction.

3.1 Introduction

Large area blackouts lead to widespread catastrophic consequences for economy and society [4], [21]. It highlights the importance of power systems resilience against major disruptions [9], [46], especially for distribution systems [7], [14], [68]. In a more resilient distribution system, electric service restoration can be implemented efficiently using stationary [15], [16] and mobile sources [61], [62]. After a disaster, stationary sources, e.g., DERs and microgrids, can be adopted for one island of the distribution system [15], [16]. Equipped with vehicles, mobile sources, e.g., MESSs, have great potential to enhance the resilience through optimal scheduling among multiple islands within the distribution system.

Considerable progress has been made with respect to the utilization of stationary sources in distribution system restoration [10], [69]. DGs are widely adopted in the restoration when the distribution system is isolated from the main grid [39]. When DGs are insufficient to meet the energy requirements, microgrids can be used to aggregate a wide range of DERs for service restoration [11], [38], [40]. In addition, the distribution system can be sectionalized into multiple islands, where each island has one microgrid [45]. These researches illustrate that distribution system can benefit enormously from the stationary DERs, especially microgrids, in enhancing resilience against large area blackouts. Furthermore, with the increasing penetration of public charging/discharging facilities [19], [70], microgrids provide opportunities to integrate MESSs for distribution system service restoration.

For the integration of MESSs, some researches have been conducted to apply MESSs into power systems operation under both normal [57], [58] and extreme conditions [52]. Under normal conditions, MESSs are utilized to provide ancillary

services to both transmission networks [24], [25] and distribution systems [26]. For transmission networks, MESSs are applied to realize load shifting in [57], [58]. To alleviate the transmission line congestion and reduce the operating cost, a battery-based energy transportation system integrated unit commitment problem is presented in [55]. Aside from boosting system economics, the battery-based energy transportation system is used to reduce the wind power curtailment in [59]. To regulate the voltage profiles in distribution systems, a transition model is developed to schedule MESSs' position and operation plans in [56].

Under extreme conditions, MESSs can be scheduled in pre and post stage of the extreme events. Before the advent of extreme events, MESSs have been deployed as uninterruptible power supplies in [71]. In [62], electric buses and transportable batteries are allocated as proactive preparedness for hurricanes. A joint pre and post-dispatch framework is proposed for the mobile emergency generators, where the position is optimized before natural disasters and real-time output is optimized after the disasters in [61]. As there is no trip chain scheduling, one mobile emergency generator is dispatched to form microgrids and then stand still at the same place to serve as the root bus [61]. In conclusion, the status of MESSs scheduling for resilient response to blackouts is either pre-positioned or only implemented one time after outages, which is not coordinated with the network reconfiguration and operation of distribution systems.

The scheduling of MESSs and network reconfiguration of distribution systems should be jointly optimized in the post-disaster restoration. After a disaster, there exist multiple faults in the distribution system, and the network reconfiguration is necessary to improve the resilience via forming multiple islands [38], [40]. MESSs can affect the power balance in each island through a sequence of trips e.g., optimal scheduling of MESSs [55]. To the best of our knowledge, a joint scheduling of MESSs and network reconfiguration in the post-disaster restoration

has not been considered yet, especially from the resilience perspective.

In this context, this chapter aims to fulfill the gap in the application of MESSs into distribution system restoration. A joint post-disaster restoration scheme is proposed, in which MESSs are dynamically scheduled in coordination with distribution system reconfiguration through microgrids, to minimize the total cost in the wake of catastrophes. Specifically, microgrids make the most of available generating resources and act as root buses to dynamically form islands for loads pickup, while the time-space network is adopted and customized in vehicle scheduling problem [72], [73] to mathematically model the scheduling problem of MESSs. The optimization problem is formulated as a MILP model. Main contributions are concluded as follows.

1) A joint post-disaster restoration scheme for coordination of MESSs and distribution systems with multiple microgrids is proposed to bridge the gap in the application of MESSs to achieve a more resilient distribution system. A temporal-spatial MESS model, connecting the transportation networks and distribution systems, is proposed to represent the difference between MESS and ESS in terms of flexibility and cost reduction of ESS sharing among microgrids.

2) The total cost, considering both the benefits (mitigating the customer interruption cost) and operation costs (microgrid generation cost, and MESS transportation cost and battery maintenance cost), is proposed to evaluate the feasibility of using MESS in distribution system restoration.

The remainder of the chapter consists of five sections. Section 3.2 defines the resilience and illustrates the system architecture in detail. Section 3.3 presents the modeling of MESSs. Section 3.4 proposes the mathematical formulation of a joint post-disaster restoration scheme. Section 3.5 provides the numerical results and analysis, and this chapter is summarized in Section 3.6.

3.2 Resilient Distribution Systems with Mobile Energy Storage Systems

3.2.1 Power System Resilience Evaluation

Resilience is defined as the ability to prepare for and adapt to changing conditions and withstand and recover rapidly from disruptions [7]. A conceptual resilience curve associated with an event in [31] is adopted in this work for illustration, as shown in Fig. 2.7. R refers to an index of system resilience level. The system states involve: pre-disturbance resilient state (t_0, t_e), event progress (t_e, t_{pe}), post-event degraded state (t_{pe}, t_r), restorative state (t_r, t_{pr}), post-restoration state (t_{pr}, t_{ir}) and infrastructure recovery (t_{ir}, t_{pir}). Specifically, a catastrophic event strikes the distribution system at t_e, resulting in a prolonged outage as electric service to end users is disrupted. The faults and consequences are identified in (t_{pe}, t_r) to improve distribution system operator's situational awareness. The proposed joint restoration scheme is implemented from tr to enhance system resilience level to R_{pr}. The distribution systems remain in the post-restoration state until the upstream transmission systems come back into operation.

In this chapter, the concerned period is (t_r, t_{ir}), i.e., the restorative state and post-restoration state. In the aftermath of extreme events, by analyzing the outage information, the distribution system operator is able to estimate the time period for full recovery [45], [62]. It is assumed that the upstream transmission system is restored at t_{ir} and the joint, as shown in Fig. 2.7. The restoration scheme for distribution system is carried out over the optimization horizon T.

In the wake of major disturbances, a restoration scheme is implemented over the optimization horizon T to reach a higher level of R_{pr}. The resilience level, R_{pr},

is the index to quantify the performance of a distribution system.

3.2.2 Mobile Energy Storage Systems

MESSs are truck-mounted ESSs characterized by utility-scale capacity [52]. In an MESS, an array of batteries is installed on a transport truck, where power converters and controllers are integrated. Under the demonstration stage, MESSs are attractive players in the resilient power systems, along with the cost reduction and profitable benefits.

Various demonstration projects of MESS applications have been deployed in recent years. In the U.S., electric utility company Premium Power's 0.5-MW/2.8-MWh transportable Zinc-Bromine ESS was deployed by Electric Power Research Institute (EPRI) [53]. EPRI and Department of Defense of the U.S. initiated a project to demonstrate a containerized grid support storage system featuring utility capacity up to 2 MWh committed to enhancing energy security at military facilities [54]. Li-ion developer Altair Nanotechlogoies has 1-MW/250-kWh trailer-mounted Li-ion battery systems in service with both AES corporation and PJM interconnection [53].

In comparison to stationary ESSs, MESSs have a sort of advantages in terms of transportability, operational flexibility, which enable MESS to provide power supply to critical loads under emergency conditions. Furthermore, the installed capital cost of MESS is expected to reduce to a competitive level in about 5 to 10 years [54]. MESSs have the potential to rival distributed generation units like fuel cells and micro turbines in the coming years [54].

In terms of techno-economic benefits, it is promising to utilize MESSs to provide of various ancillary services [55], [56]. For the more resilient distribution

systems, MESSs can follow the trip chains among multiple islands to engage in the restoration. The trip chains can specify the MESSs' assigned locations in the corresponding intervals to describe the spatiotemporal driving pattern of MESSs.

3.2.3 Distribution System Restoration with Mobile Energy Storage Systems

A novel application of MESS in distribution system is studied to propose a joint post-disaster restoration scheme, which leverages MESSs and generating resources in microgrids for post-disaster restoration, as shown in Fig. 3.1. In the aftermath of extreme events, the distribution system can no longer be supplied by transmission grids as a result of multiple faults across the power systems, including substation faults, broken feeders. Under this circumstance, microgrids will be utilized to pick up critical loads by sectionalizing the distribution system into multiple islands. MESSs are assumed to be owned and controlled by utility companies, and they can be dispatched in time horizon T. In addition, it is assumed that there exists a transportation network connecting all microgrids within the distribution system.

The idea is to optimally coordinate scheduling of MESSs and distribution network reconfiguration with microgrids, enabling a resilient service restoration in distribution system after natural hazards. On the one hand, the distribution system is reconfigured and sectionalized into a few islands through controlling the ON/OFF status of remote-controlled switches. In each island, a microgrid is the root bus to supply electricity to critical loads and works as an interface to couple distribution systems and transportation systems. On the other hand, by solving vehicle scheduling problem, MESSs can be scheduled to travel among microgrids through the transportation network to transfer energy, alleviating dis-

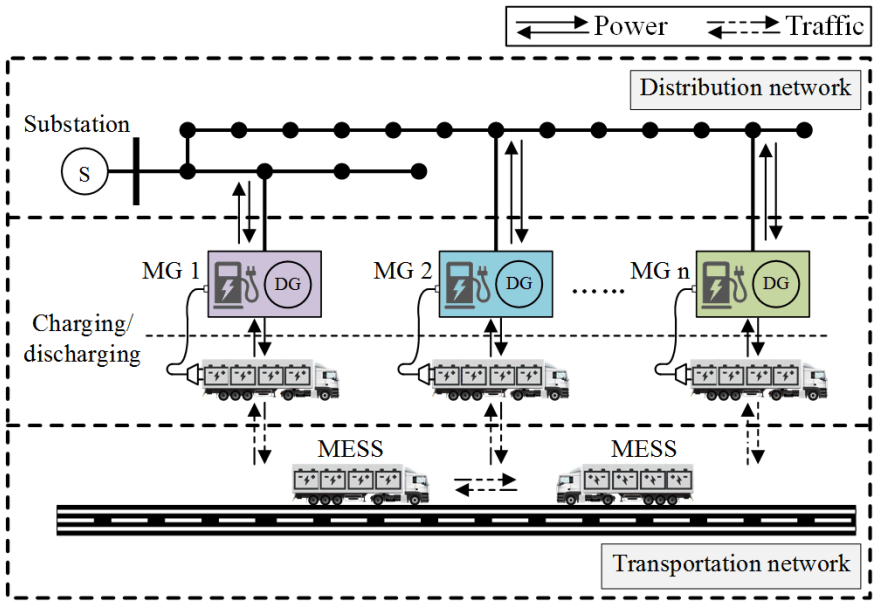

Figure 3.1: Overview of system architecture.

tribution network energy imbalance posed by operation and topology constraints in scenarios of multiple faults, in order to improve the resilience level.

To indicate the resilience level for a distribution system with MESSs as shown in Fig. 3.1, the total cost, considering both the benefits (mitigating the customer interruption cost) and operation costs (microgrid generation cost, and MESS transportation cost and battery maintenance cost), is utilized. The effort is characterized by mitigating the customer interruption cost and microgrid generation cost. Moreover, the operation costs of MESS are considered with the transportation cost and battery maintenance cost. In this sense, the defined total cost can be adopted to evaluate the feasibility of the joint restoration scheme, and the minimization of total cost leads to an optimal restoration scheme.

3.3 Modeling of Mobile Energy Storage Systems

In contrast to stationary ESSs, MESSs can transport energy to designated locations over the transportation network. In order to deal with scheduling problems more efficiently in both time and spatial domains, a time-space network model is adopted to model the trip chain of MESSs. This section proposes a temporal-spatial MESS model to investigate the driving dynamics and charging/discharging behaviors of MESSs, and studies their impacts on distribution system restoration.

3.3.1 Temporal-spatial Constraints of Mobile Energy Storage Systems

In order to deal with scheduling problems more efficiently in both time and spatial domains, new modeling methods have been applied, such as continuous time modeling and time-space network modeling [74]. In contrast to the continuous time modeling method [74], the time-space network model is more suitable for scheduling problems involving both space decisions and discrete time intervals [72], which is in line with the discrete intervals in planning horizon for distribution system. In addition, the time-space network-based scheduling model can be formulated as an MILP problem, which could be effectively solved by off-the-shelf solvers.

A transportation network connecting multiple microgrids is considered, as shown in Fig. 3.2. Each arc is marked with associated travel time. For example, it takes two intervals for MESSs to travel between microgrid #2 and microgrid #3, whereas only one interval for any other transit. In order to enable arcs to represent the corresponding status in each interval, a virtual node, i.e., microgrid #4 is introduced in between microgrid #2 and microgrid #3, so that travel time of

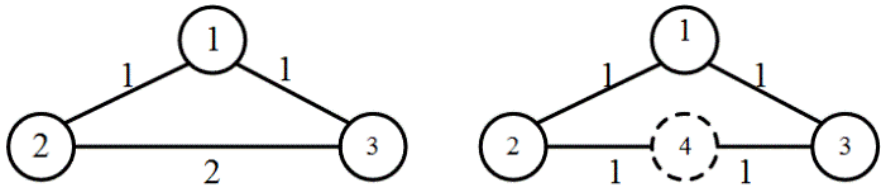

Figure 3.2: Transportation network with virtual nodes.

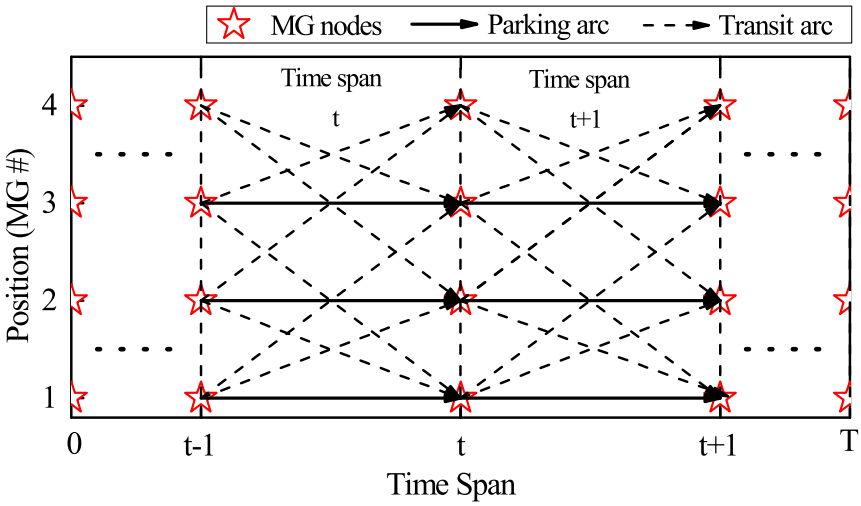

Figure 3.3: Time-space network model.

each arc in the network is exactly one interval [55].

The transportation network with travel time is modeled by a time-space network, as shown in Fig. 3.3, which has been broadly used to model airline and public transportation scheduling problems [72], [75]. In this work, a mathematical model for MESS scheduling problem is presented based on the time-space network involving microgrid nodes and trip arcs. The trip chain can be represented by a sequence of arcs, which indicate the departure microgrid nodes and destination microgrid nodes in a given timetable.

As illustrated in Fig. 3.3, the MESSs traveling and parking behavior is described by different types of arcs to indicate the spatiotemporal dynamics of

MESSs. The time-space network comprises microgrid nodes and the arcs linking various microgrids, indicating the feasible transit routes. There are two types of arcs in the time-space network. One type is referred to as the transit arc, which allows MESSs to transport energy among microgrids. Another type is the parking arc, which represents the MESS stays at a certain microgrid for exchanging power with distribution systems through charging or discharging. Therefore, a trip chain for each MESS can be determined to schedule MESSs to different microgrids over the time horizon $\mathcal{T}$.

The time-space network-based MESS model is formulated as follows.

$$\sum_{(m,u)\in Z} \zeta^t_{\omega,mu} = 1, \forall \omega \in \Omega, t \in \mathcal{T} \tag{3.1}$$

$$\sum_{(m,u)\in Z^-_m} \zeta^t_{\omega,mu} = \sum_{(m,u)\in Z^+_m} \zeta^{t+1}_{\omega,mu}, \forall \omega \in \Omega, m \in \mathcal{M} \cup \mathcal{M}_v, t \in \mathcal{T} \setminus \{T\} \tag{3.2}$$

$$\sum_{(m,u)\in Z^+_m} \zeta^1_{\omega,mu} = \zeta^0_{\omega,m}, \forall \omega \in \Omega, m \in \mathcal{M} \cup \mathcal{M}_v \tag{3.3}$$

$$\zeta^t_{\omega,mu} + \zeta^{t+1}_{\omega,um} \leq 1, \forall \omega \in \Omega, (m,u) \in Z, m \neq u, t \in \mathcal{T} \setminus \{T\} \tag{3.4}$$

where $\mathcal{T}$ is the set of time intervals. $\mathcal{M}$ is the set of microgrids. $\mathcal{M}_v$ is the set of virtual nodes in time-space networks. Ω is the set of MESS fleet. Z is the set of arcs in time-space network, indexed by (m,u). Z^+_m is the set of arcs in time-space network starting from microgrid m. Z^-_m is the set of arcs in time-space network ending at microgrid m. $\zeta^t_{\omega,mu}$ is a binary variable, 1 if MESS ω is on arc (m,u) in interval t, 0 otherwise.

Equation (3.1) ensures that MESS ω can be either on transit arcs or parking arcs. Constraints (3.2) and (3.3) refer to the flow conservation for both microgrid nodes and virtual stations. In (3.2), MESS ω, which ends the trip in interval t at microgrid node m, is certain to keep staying on one of the arcs which start

from a node (t, m) in the next interval $t + 1$. Particularly, constraint (3.3) declares the initial position. The constraint (3.4) guarantees that under no circumstances MESSs are able to make an immediate round trip, i.e., MESSs moving from one microgrid to another one are not permitted to go directly back to the previous microgrid.

3.3.2 Operation Constraints of Mobile Energy Storage Systems

When arrives at one microgrid, i.e., on parking arcs shown in Fig. 3.3, MESS can charge from or discharge to this microgrid, while satisfying the following operation constraints.

$$0 \leq P^t_{\text{ch},\omega m} \leq \zeta^t_{\omega,mm} P^{\max}_{\text{ch},\omega}, \forall \omega \in \Omega, m \in \mathcal{M}, t \in \mathcal{T} \tag{3.5}$$

$$0 \leq P^t_{\text{dch},\omega m} \leq \zeta^t_{\omega,mm} P^{\max}_{\text{dch},\omega}, \forall \omega \in \Omega, m \in \mathcal{M}, t \in \mathcal{T} \tag{3.6}$$

$$0 \leq \sum_{m \in \mathcal{M}} P^t_{\text{ch},\omega} \leq I^{\max}_{\text{ch},\omega}, \forall \omega \in \Omega, t \in \mathcal{T} \tag{3.7}$$

$$0 \leq \sum_{m \in \mathcal{M}} P^t_{\text{dch},\omega} \leq I^{\max}_{\text{dch},\omega}, \forall \omega \in \Omega, t \in \mathcal{T} \tag{3.8}$$

$$I^t_{\text{dch},\omega} + I^t_{\text{ch},\omega} \leq \sum_{m \in \text{M}} \zeta^t_{\omega,mm}, \forall \omega \in \Omega, t \in \mathcal{T} \tag{3.9}$$

$$SOC^{t+1}_\omega = SOC^t_\omega - \frac{\Delta T}{E^{\text{cap}}_{\text{MESS}}} \left(\frac{\sum_{m \in \mathcal{M}} P^t_{\text{dch},\omega}}{\eta_{\text{dch},\omega}} - \eta_{\text{ch},\omega} \sum_{m \in \mathcal{M}} P^{t+1}_{\text{ch},\omega m} \right), \forall \omega \in \Omega, t \in \mathcal{T} \setminus \{T\} \tag{3.10}$$

$$SOC_{\min} \leq SOC^t_\omega \leq SOC_{\max}, \forall \omega \in \Omega, t \in \mathcal{T} \tag{3.11}$$

where $P^t_{\text{ch},\omega m}$, $P^t_{\text{dch},\omega m}$ represent charging/discharging power of MESS ω from/to microgrid m in interval t. $P^{\max}_{\text{ch}}$, $P^{\max}_{\text{dch}}$ are maximum charging/discharging power

of MESSs. $I^t_{\text{ch},\omega}$, $I^t_{\text{dch},\omega}$ is binary variable, representing charging/discharging state of MESS ω in interval t. SOC^t_ω represents the state of charge of MESS ω by the end of interval t. $SOC_{\max/\min}$ are maximum/Minimum SOC level of MESSs. Δt is the length of time intervals. $E^{\text{cap}}_{\text{MESS}}$ is the energy capacity of MESSs. η^ω_{ch}, η^ω_{dch} represent charging/discharging efficiency.

Constraints (3.5) and (3.6) establish the feasible sets of charging/discharging power of MESS ω to microgrid m. Equations (3.7) and (3.8) define the MESS charging/discharging constraints associated with its operation mode. The operation mode constraint is described in (3.9), indicating that MESS can operate in charging/discharging mode for exchanging power with microgrids only if it is on parking arcs to stay in a certain microgrid. For instance, if MESS ω stays at any microgrid and we can obtain that $\sum_{m\in\mathcal{M}} \zeta^t_{\omega,mm} = 1$, thus MESS ω can be operated either in charging/discharging or idle mode, otherwise, the sign of charging/discharging status would be sandwiched to zero. Constraint (10) determines the state of charge (SOC) of MESS ω by the end of interval t. Finally, the SOC upper and lower bounds limitations are denoted in (3.11).

3.4 Joint Post-disaster Restoration Scheme

Incorporating MESSs into distribution systems, a more resilient restoration solution can be obtained through the coordination of MESSs and distribution systems. To achieve the optimal restoration, the mathematical formulation of joint post-disaster restoration scheme is presented in this section. The objective is to minimize the total cost, subject to operation and topology constraints. Partial load restoration is adopted by introducing continuous variables for each load as in [43], [76]. Customer interruption cost is used to distinguish critical loads [25], [77], [78]. The objective function and constraint sets are described as follows.

3.4.1 Objective Function

The objective function aims to minimize the total cost, considering the customer interruption cost, microgrid generation cost, and MESS transportation cost and battery maintenance cost, as follows.

$$\begin{aligned}\min \sum_{t\in\mathcal{T}}[\sum_{i\in\mathcal{N}_{\mathrm{D}}} W_i(P^t_{\mathrm{D},i} - P^t_{\mathrm{r},i})\Delta T + \sum_{m\in\mathcal{M}} C_{\mathrm{gen},m} P^t_{\mathrm{DG},m}\Delta T \\ + \sum_{\omega\in\Omega} C_{\mathrm{tran},\omega} \sum_{(m,u)\in Z, m\neq u} \zeta^t_{\omega,mu} \\ + \sum_{\omega\in\Omega} C_{\mathrm{bat},\omega} \sum_{m\in\mathcal{M}} |P^t_{\mathrm{ch},\omega m} + P^t_{\mathrm{dch},\omega m}|\Delta T] \end{aligned} \tag{3.12}$$

where W_i is unit interruption cost for load at bus i. $C_{\mathrm{gen},m}$ is unit generation cost of microgrid m. $C_{\mathrm{bat},\omega}$ is unit battery maintenance cost for MESS ω. $C_{\mathrm{tran},\omega}$ is unit transportation cost for MESS ω. $P^t_{\mathrm{D},i}$, $Q^t_{\mathrm{D},i}$ are active/reactive load at bus i in interval t. $P^t_{\mathrm{DG},m}$, $Q^t_{\mathrm{DG},i}$ are active/reactive power generation of equivalent dispatchable DG in microgrid m in interval t.

The first term $\sum_{i\in\mathcal{N}_{\mathrm{D}}} W_i(P^t_{\mathrm{D},i} - P^t_{\mathrm{r},i})\Delta T$ calculates the customer interruption cost in interval t. The second term $\sum_{m\in\mathcal{M}} C_{\mathrm{gen},m} P^t_{\mathrm{DG},m}\Delta T$ indicates the microgrids generation cost in interval t. The third term $\sum_{(m,u)\in Z, m\neq u} C_{\mathrm{tran},\omega}\zeta^t_{\omega,,mu}$ is regarding the transportation cost in interval t, where $\sum_{(m,u)\in Z, m\neq u} \zeta^t_{\omega,,mu}$ describes whether the transporting cost takes effect. When it equals to 1, the MESS ω is in transit in interval t, resulting in transportation cost. Otherwise, the transportation cost would not be incurred. The last term $\sum_{\omega\in\Omega} C_{\mathrm{bat},\omega} \sum_{m\in\mathcal{M}} |P^t_{\mathrm{ch},\omega m} + P^t_{\mathrm{dch},\omega m}|\Delta T$ provides the MESS battery maintenance cost for charging/discharging.

3.4.2 Distribution Network Topology Constraints

The distribution system is modeled as an undirected graph $\mathcal{G} = (\mathcal{N}_{\mathrm{D}}, \mathcal{E})_{\mathrm{D}}$ [38]. In the case of multiple faults, there might be some isolated areas without connection to any generating resources. These completely isolated areas will be removed. For the sake of notational simplicity, each microgrid m is denoted by the node i at which the microgrid is connected to the distribution network, i.e., $m = i$. It can be concluded that $\mathcal{M} \subseteq \mathcal{N}_{\mathrm{D}}$.

The network reconfiguration should retain the radial structure [38], [45], [61]. There is only one microgrid in each island, and no loop or overlap region exists. The radiality and connectivity features in [79] are extended to the circumstance with multiple microgrids over the distribution network. The formulation can be described as following.

$$\sum_{(i,j)\in\mathcal{E}_{\mathrm{D}}} \alpha_{ij} = |\mathcal{N}_{\mathrm{D}}| - |\mathcal{M}| \tag{3.13}$$

$$\beta_{ij} + \beta_{ji} = \alpha_{ij}, \forall (i,j) \in \mathcal{E}_{\mathrm{D}} \tag{3.14}$$

$$\sum_{j\in\Psi(i)} \beta_{ij} = 1, \forall i \in \mathcal{N}_{\mathrm{D}} \setminus \mathcal{M} \tag{3.15}$$

$$\beta_{ij} = 0, \forall i \in \mathcal{M}, j \in \Psi(i) \tag{3.16}$$

where $|\mathcal{N}_{\mathrm{D}}|$ and $|\mathcal{M}|$ denote the cardinality of the set. α_{ij} is binary variable, 1 if the line (i, j) is connected, 0 otherwise. β_{ij} is binary variable, 1 if bus j is the parent of bus i, 0 otherwise. $\Psi(i)$ is set of buses connected to bus i by a branch.

The network reconfiguration is achieved by one-time switching operation decisions. The necessary condition for the spanning tree is denoted by (3.13). Equation (3.14) determines if a line is connected by checking that either $\beta_{ij} = 1$

or $\beta_{ji} = 1$. Equation (3.15) represents that every bus other than the microgrid buses has exactly one parent, while constraint (3.16) enforces that the microgrid buses, serving as the root buses, has no parent.

3.4.3 Operation Constraints of Distribution Systems

In this chapter, a linearized DistFlow model [40], [43], [61] is adopted in the power flow analysis of distribution systems as follows.

$$P^t_{\mathrm{G},i} - P^t_{\mathrm{r},i} = \sum_{(i,j)\in\mathcal{E}_\mathrm{D}} P^t_{ij} - \sum_{(k,i)\in\mathcal{E}_\mathrm{D}} P^t_{ki}, \forall i \in \mathcal{N}_\mathrm{D}, t \in \mathcal{T} \tag{3.17}$$

$$Q^t_{\mathrm{G},i} - Q^t_{\mathrm{r},i} = \sum_{(i,j)\in\mathcal{E}_\mathrm{D}} Q^t_{ij} - \sum_{(k,i)\in\mathcal{E}_\mathrm{D}} Q^t_{ki}, \forall i \in \mathcal{N}_\mathrm{D}, t \in \mathcal{T} \tag{3.18}$$

$$V^t_j - V^t_i \le M(1-\alpha_{ij}) + \frac{r_{ij}P^t_{ij} + x_{ij}Q^t_{ij}}{V_0}, \forall (i,j) \in \mathcal{E}_\mathrm{D}, t \in \mathcal{T} \tag{3.19}$$

$$V^t_j - V^t_i \ge -M(1-\alpha_{ij}) + \frac{r_{ij}P^t_{ij} + x_{ij}Q^t_{ij}}{V_0}, \forall (i,j) \in \mathcal{E}_\mathrm{D}, t \in \mathcal{T} \tag{3.20}$$

$$-\alpha_{ij}S^{\max}_{ij} \le P^t_{ij} \le \alpha_{ij}S^{\max}_{ij}, \forall (i,j) \in \mathcal{E}_\mathrm{D}, t \in \mathcal{T} \tag{3.21}$$

$$-\alpha_{ij}S^{\max}_{ij} \le Q^t_{ij} \le \alpha_{ij}S^{\max}_{ij}, \forall (i,j) \in \mathcal{E}_\mathrm{D}, t \in \mathcal{T} \tag{3.22}$$

$$-\sqrt{2}\alpha_{ij}S^{\max}_{ij} \le P^t_{ij} + Q^t_{ij} \le \sqrt{2}\alpha_{ij}S^{\max}_{ij}, \forall (i,j) \in \mathcal{E}_\mathrm{D}, t \in \mathcal{T} \tag{3.23}$$

$$-\sqrt{2}\alpha_{ij}S^{\max}_{ij} \le P^t_{ij} - Q^t_{ij} \le \sqrt{2}\alpha_{ij}S^{\max}_{ij}, \forall (i,j) \in \mathcal{E}_\mathrm{D}, t \in \mathcal{T} \tag{3.24}$$

$$V^{\min}_i \le V^t_i \le V^{\max}_i, \forall i \in \mathcal{N}_\mathrm{D} \setminus \mathcal{M}, t \in \mathcal{T} \tag{3.25}$$

$$V^t_i = V_0, \forall i \in \mathcal{M}, t \in \mathcal{T} \tag{3.26}$$

$$0 \le P^t_{\mathrm{r},i} \le P^t_{\mathrm{D},i}, \forall i \in \mathcal{N}_\mathrm{D}, t \in \mathcal{T} \tag{3.27}$$

$$Q^t_{\mathrm{r},i} = P^t_{\mathrm{r},i} \tan\left(\cos^{-1}\varphi_i\right), \forall i \in \mathcal{N}_\mathrm{D}, t \in \mathcal{T} \tag{3.28}$$

where $P^t_{\mathrm{G},i}, Q^t_{\mathrm{G},i}$ are real/reactive power generation at bus i in interval t. $P^t_{\mathrm{r},i}$, $Q^t_{\mathrm{r},i}$ are load restoration at bus i in interval t. P^t_{ij}, Q^t_{ij}] represent active/reactive power

from bus i to bus j in interval t. V_i^t is voltage magnitude at bus i in interval t. $V_i^{\max}$, $V_i^{\min}$ are maximum/minimum voltage magnitude at bus i. V_0 is voltage reference at root bus. M is a large number. $S_{ij}^{\max}$ is apparent power capacity of line (i, j). $P_{\mathrm{D},i}^t Q_{\mathrm{D},i}^t$ are active/reactive load at bus i in interval t. φ_i is power factor of load at bus i.

Equations (3.17) and (3.18) are constraints regarding real and reactive power balance at each bus in interval t. Equations (3.19) and (3.20) enforce constraints on line voltage drop by using the big-M method [76], [80]. Constraints (3.21)-(3.24) provide the branch capacity limitations, which is a linearized approximation as given in [81]. Constraint (3.25) enforces the upper and lower bounds on voltage magnitude. Constraint (3.26) sets the voltage of microgrid buses to V_0. Constraints (3.27) and (3.28) require that power factor of each load should be maintained.

3.4.4 Operation Constraints of Microgrids

Microgrids are entities that coordinate DERs and behave as a single producer or load from the grids' perspective [82]. In this chapter, a microgrid is modeled as a single bus with an equivalent dispatchable DG aggregating the whole generating resources, an equivalent local load, and charging/discharging facilities. When integrated with MESS, microgrids operation constraints can be expressed as follows.

$$P_{\mathrm{G},m}^t = P_{\mathrm{DG},m}^t - \sum_{\omega\in\Omega} P_{\mathrm{ch},\omega m}^t + \sum_{\omega\in\Omega} P_{\mathrm{dch},\omega m}^t - P_{\mathrm{D},m}^t, \forall m \in \mathcal{M}, t \in \mathcal{T} \tag{3.29}$$

$$Q_{\mathrm{G},m}^t = Q_{\mathrm{DG},m}^t - Q_{\mathrm{D},m}^t, \forall m \in \mathcal{M}, t \in \mathcal{T} \tag{3.30}$$

$$0 \le P_{\mathrm{DG},m}^t \le P_{\mathrm{DG},m}^{\max}, \forall m \in \mathcal{M}, t \in \mathcal{T} \tag{3.31}$$

$$-Q_{\mathrm{DG},m}^{\max} \le Q_{\mathrm{DG},m}^t \le Q_{\mathrm{DG},m}^{\max}, \forall m \in \mathcal{M}, t \in \mathcal{T} \tag{3.32}$$

$$E_{\mathrm{DG},m}^{t+1} = E_{\mathrm{DG},m}^{t} - P_{\mathrm{DG},m}^{t+1}\Delta t, \forall m \in \mathcal{M}, t \in \mathcal{T}\backslash\{T\} \tag{3.33}$$

$$E_{\mathrm{DG},m}^{\min} \leq E_{\mathrm{DG},m}^{t} \leq E_{\mathrm{DG},m}^{\max}, \forall m \in \mathcal{M}, t \in \mathcal{T} \tag{3.34}$$

where $P_{\mathrm{DG},m}^{t}$, $Q_{\mathrm{DG},m}^{t}$ are active/reactive power generation of equivalent dispatchable DG in microgrid m. $P_{\mathrm{DG},m}^{\max}$, $Q_{\mathrm{DG},m}^{\max}$] are maximum active/reactive power of equivalent dispatchable DG in microgrid m. $E_{\mathrm{DG},m}^{t}$] is energy of equivalent dispatchable DG in microgrid m by the end of interval t. $E_{\mathrm{DG},m}^{\max}$, $E_{\mathrm{DG},m}^{\min}$ are energy capacity/minimum reserve in microgrid m.

Equations (3.29) and (3.30) stand for the active and reactive power support from microgrids to distribution systems via point of common coupling bus m, considering MESS charging from and discharging to microgrids. Constraints (3.31) and (3.32) enforce the real and reactive power capacity constraints upon dispatchable DG in each microgrid. Equation (3.33) calculates the energy in each microgrid. The energy limitations of microgrids are given in (3.34).

Together with the MESS models in Section 3.3, the joint post-disaster restoration scheme is formulated as an MILP problem, which can be solved by off-the-shelf solvers effectively, and the constraints are classified into the following 5 categories.

(1) Temporal-spatial constraints of MESSs: (3.1)-(3.4);

(2) Operation constraints of MESSs: (3.5)-(3.11);

(3) Distribution network topology constraints: (3.13)-(3.16);

(4) Operation constraints of distribution systems: (3.17)-(3.28);

(5) Operation constraints of microgrids: (3.29)-(3.34).

Table 3.1: Number of Variables

Type	Binary Variables	Continuous Variables
Variables	α_{ij}, β_{ij}, $I^t_{\mathrm{ch},\omega}$, $I^t_{\mathrm{dch},\omega}$, $\eta^t_{\omega,m}$	$P^t_{\mathrm{G},i}$, $Q^t_{\mathrm{G},i}$, $P^t_{\mathrm{r},i}$, $Q^t_{\mathrm{r},i}$, P^t_{ij}, Q^t_{ij}, V^t_i, $P^t_{\mathrm{DG},m}$, $Q^t_{\mathrm{DG},m}$, $E^t_{\mathrm{DG},m}$, $P^t_{\mathrm{ch},\omega m}$, $P^t_{\mathrm{dch},\omega m}$, SOC^t_ω
Number of Variables	$3\lvert\mathcal{E}_{\mathrm{D}}\rvert+(2+\lvert Z\rvert)\times \lvert\Omega\rvert\times\lvert\mathrm{T}\rvert$	$(2\lvert\mathcal{E}_{\mathrm{D}}\rvert+3\lvert\mathcal{N}_{\mathrm{D}}\rvert+2\lvert\mathcal{M}\rvert)\times\lvert\mathcal{T}\rvert+3\lvert\mathcal{M}\rvert\times \lvert\mathcal{T}\rvert+(2\lvert\mathcal{M}\rvert+1)\times\lvert\mathcal{M}\rvert\times\lvert\mathcal{T}\rvert$

The number of variables in the formulated problem is shown in Table 3.1. Since distribution systems cover merely several to tens of kilometers of power supply radius due to relatively low voltage levels, so the $|\mathcal{M}|$ and $|Z|$ are within an acceptable range. Consequently, the problem scale is tractable and can be solved optimally and efficiently by commercial solvers like Gurobi. Furthermore, for further extension of this model to a large-scale MILP, it can be increasingly challenging to solve directly, some decomposition algorithms, e.g., Benders decomposition [83] and progressive hedging [84] can be adopted.

3.5 Numerical Results

In this section, the case studies are performed on a modified 33-bus test system [85] to corroborate the effectiveness of the proposed reconfiguration method. The optimization model is implemented using Python 3.6 and solved by Gurobi [86] (or other off-the-shelf solvers), on a computer with an Intel Core i7 3.4GHz CPU and 8GB RAM.

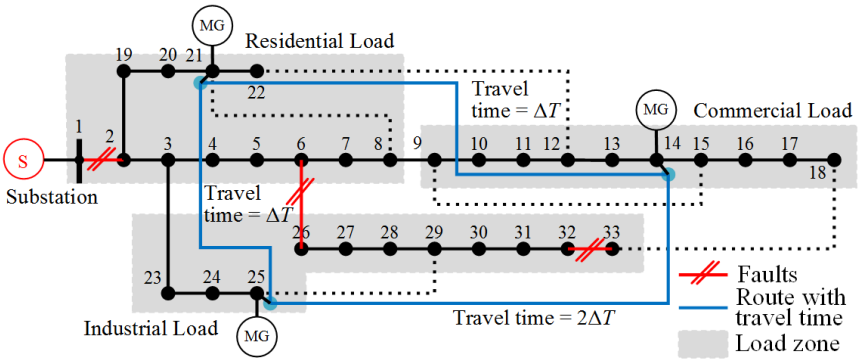

Figure 3.4: A modified 33-bus test system with 3 microgrids and multiple faults.

3.5.1 Test Systems

The modified 33-bus test feeder is shown in Fig. 3.4. The entire distribution system is disconnected from the utility grid, the substation and three lines (1, 2), (6, 26) and (32, 33) are at fault as a result of disastrous events. In this study, loads are classified into 3 types of end-use customers: industrial, commercial and residential. Fig. 3.5 gives the load profile [80] and Fig. 3.6 describes two load priority levels with unit interruption cost [25], [77].

Three microgrids are connected to distribution network at buses 14, 21, 25, respectively, as depicted in Fig. 3.4. The transportation routes connecting three microgrids are marked with the travel time between any two microgrids. Table 3.2 provides the generation and load information for microgrids. The local load in each microgrid follows the load profile as given in Fig. 3.5. Four MESSs are considered and the MESS fleet ω is supposed to be homogeneous, meaning that all MESSs have identical properties. Parameters of MESSs are shown in Table 3.3. The time horizon is set to 24 hours and time step is 1 hour. The unit generation cost for microgrids is \$0.5/kWh. The unit transportation cost for MESS is 80\$ per transit. The unit battery maintenance cost for MESS is 0.2\$/kWh. The V_0 is

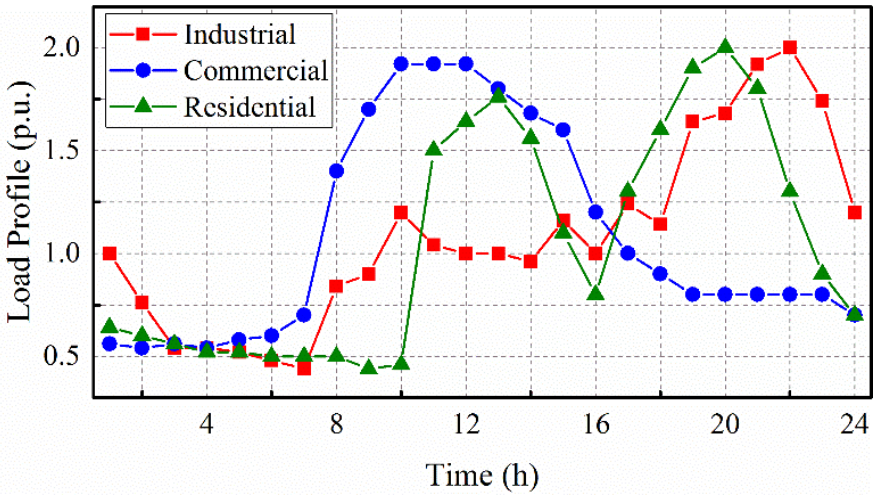

Figure 3.5: Load profile.

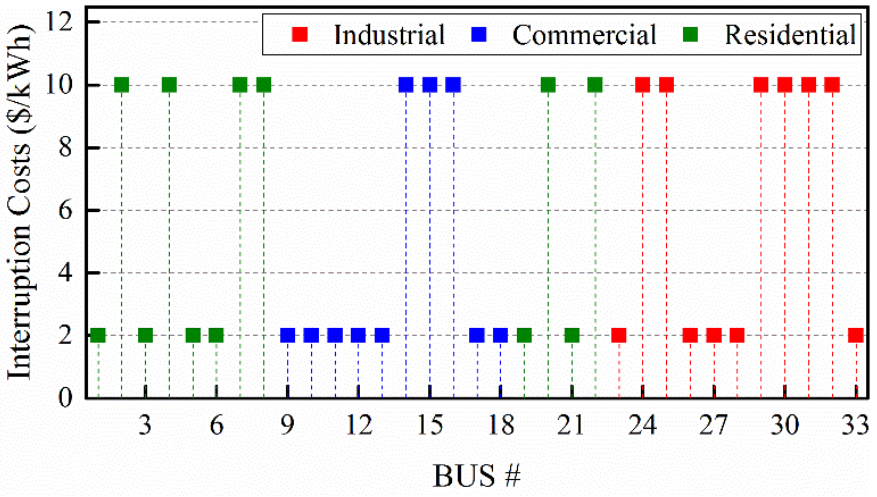

Figure 3.6: Unit interruption cost.

set to 1.0 p.u. The $V_{\max}$ and $V_{\min}$ are 1.05 p.u. and 0.95 p.u., respectively.

In the remaining section, three cases are investigated to show the feasibility of joint scheduling of MESSs and distribution systems, as follows.

(1) Distribution system has microgrids without ESSs;

(2) Distribution system has microgrids with stationary ESSs;

Table 3.2: Generation Resources and Local Loads for Microgrids

Microgrid bus #		14	21	25
Generation	Real Power (MW)	1.60	1.60	1.80
	Reactive power (MVar)	1.28	1.28	1.44
Energy Capacity (MWh)		23.04	23.04	25.92
Minimum fuel reserve (MWH)		2.30	2.30	2.59
Local load	Peak load (MW)	0.5	0.5	0.7
	Power factor		0.9	
	Load type	C	R	I

Note: C - commercial, R - residential, I - industrial

Table 3.3: MESS Parameters

MESS #	1	2	3	4
Initial position (Microgrid bus #)	14	21	21	25
Charging/discharging power (MW)	0.2			
Energy Capacity (MWh)	1.0			
Initial SOC (%)	50			
$SOC_{\max}/SOC_{\min}$ (%)	90/10			
Charging/discharging efficiency (%)	95/95			

Table 3.4: Simulation Statistics for Distribution System Restoration

Results		Case 1	Case 2	Case 3
Objective values ($)	Interruption cost	115395	96639	71365
	Microgrids generation cost	32400	32400	32400
	Transportation cost	0	0	800
	Battery maintenance cost	0	497	1875
	Total cost	147795	129536	106440
Load Restoration (%)	Priority I	89.65	92.66	97.60
	Priority II	19.94	18.22	6.05
	Total	68.01	69.55	69.60

(3) Distribution system has microgrids with MESSs

3.5.2 Simulation Results

The techno-economic results under three cases are compared in TABLE 3.4.

Case 1) Distribution system has microgrids without ESSs. In this base case, microgrids can utilize their available generating resources to support distribution system restoration. By solving the optimization problem, the network topology and optimal hourly generation dispatch for microgrids are acquired. The network reconfiguration result is to open switches (3, 4), (8, 21), (12, 22), (13, 14) and (24, 25). As shown in Table 3.4, the total cost is $147795, load pickup for priority I and II are 89.65% and 19.94%, respectively.

Case 2) Distribution system has microgrids with Stationary ESSs. In this case, ESSs are assumed to be fixed at microgrids. In the obtained results, the open switches are (3, 4), (8, 21), (11, 12), (12, 13) and (24, 25). The total cost

decreases by 12.35% to $129536, as compared to that without MESSs in case 1. The load restored for priority I and II are 92.66% and 18.22%, respectively. It is worth noting that incorporating MESSs into microgrids not only reduces total cost through introducing more energy of 2 MWh, but also that stationary ESSs can work in coordination with microgrids to better supply critical loads. It is noticed that total load percentage only increases by 1.54% while the load restoration for priority I rises by 3.01%. The results reveal that microgrids can manage stationary ESSs to effectively restore critical loads.

Case 3) Distribution system has microgrids with MESSs: In this case, the network topology, microgrids generation dispatch and scheduling of MESSs are optimized simultaneously to obtain a more resilient restoration solution. Compared with cases 1 and 2, the total cost decreases by 27.98% and 17.83%, respectively, to $106440. The load restored for priority I enhances to 97.60% and reduces to 6.05% for priority II, respectively. These results illustrate that MESSs can improve the resilience significantly.

Fig. 3.7 denotes the distribution network reconfiguration results in case 3. The distribution system is sectionalized into 3 islands, i.e., islands 14, 21 and 25, which is denoted by the corresponding microgrid bus number in each island. The opening line switches are (3, 4), (8, 21), (12, 13), (21, 22), and (24, 25). In addition, each one is energized by a corresponding microgrid to satisfy radial topology, i.e., constraints (3.13)-(3.16).

Fig. 3.8 provides the charging/discharging schedule and spatio-temporal dynamics of MESSs. Note that a positive power indicates discharging of MESSs, while a negative power means the charging of MESSs. The projection on XY plane indicates the trajectory of MESSs' trip chains, while the Zaxis indicates the active power generation for each MESS. Take MESS #3 for instance to illustrate the

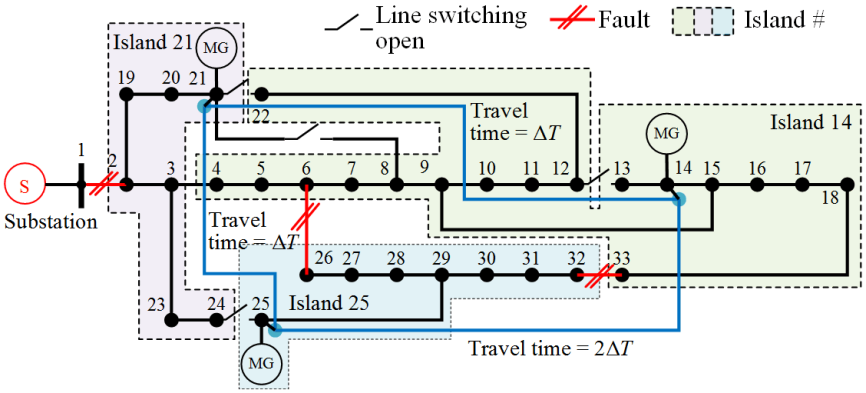

Figure 3.7: Network reconfiguration result for the 33-bus test system in case 3.

schedule. MESS #3 stays at initial position microgrid #21 for 9 hours (00:0009:00) and charges in (00:0002:00) and (08:0009:00). Next, it moves from microgrid #21 to microgrid #14 in (09:0010:00) and discharges for 4 hours (10:0014:00). Then, it returns to microgrid #21 to get charged in (15:0018:00). The final transition is made to microgrid #25 in (18:0019:00) and it starts to discharge from 19:00 for 4 hours to 23:00.

Fig. 3.9 shows the stacked generation dispatch for microgrids and MESSs. It can be seen that the active power within each island is balanced along the optimization horizon. Fig. 3.10 11 denotes the SOC of MESS and Fig. 3.11 depicts energy transfer from MESS to microgrids through charging and discharging behaviors. Positive energy transfer represents that microgrid receives energy from MESSs whereas negative value represents that microgrid transfers energy to MESSs. It can be observed that energy transfer is mainly from microgrid #21 to microgrid #25 in the obtained solution.

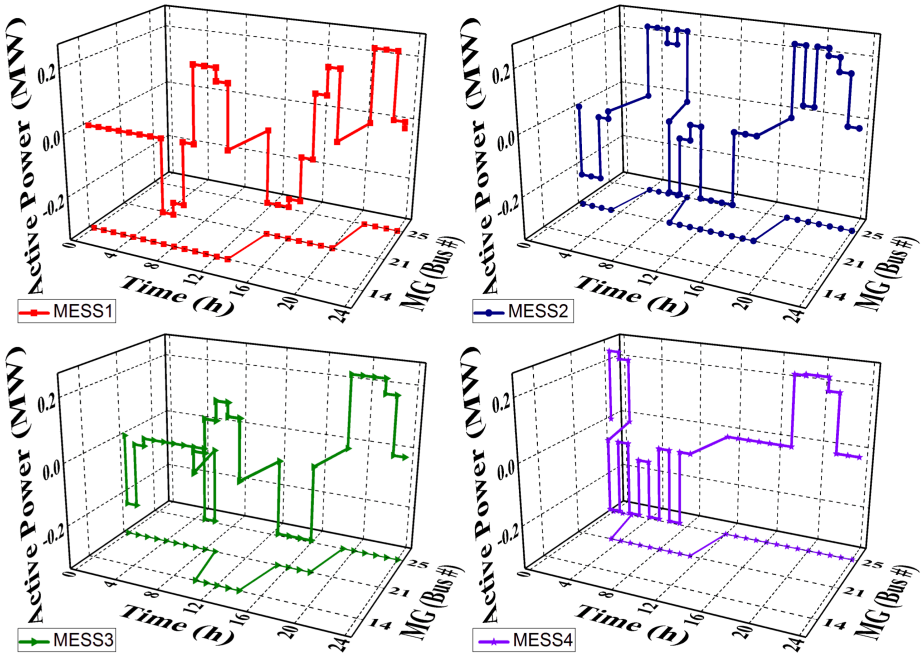

Figure 3.8: MESS scheduling results in case 3.

3.5.3 Analysis and Discussions

A. Transfer of Energy Among Microgrids

In the simulations, it is observed that MESSs are charged where and when the power generation resource is relatively surplus for critical loads and discharged to the grid where and when the power or energy is insufficient. Energy imbalance posed by topology and operation constraints deters the effective utilization of microgrids' generating resource. Thus, MESSs can decrease the total cost through transferring power and energy among microgrids to serve critical loads in distribution system. It can be observed in TABLE IV that the total load restoration only rises by 0.15%, while the load restored for priority I increase by 4.97% compared to that in case 2. In this case, the MESS #2 is fully charged from 00:00 to 03:00 in microgrid #21 (see Fig. 3.8 and Fig. 3.9) to the SOC of

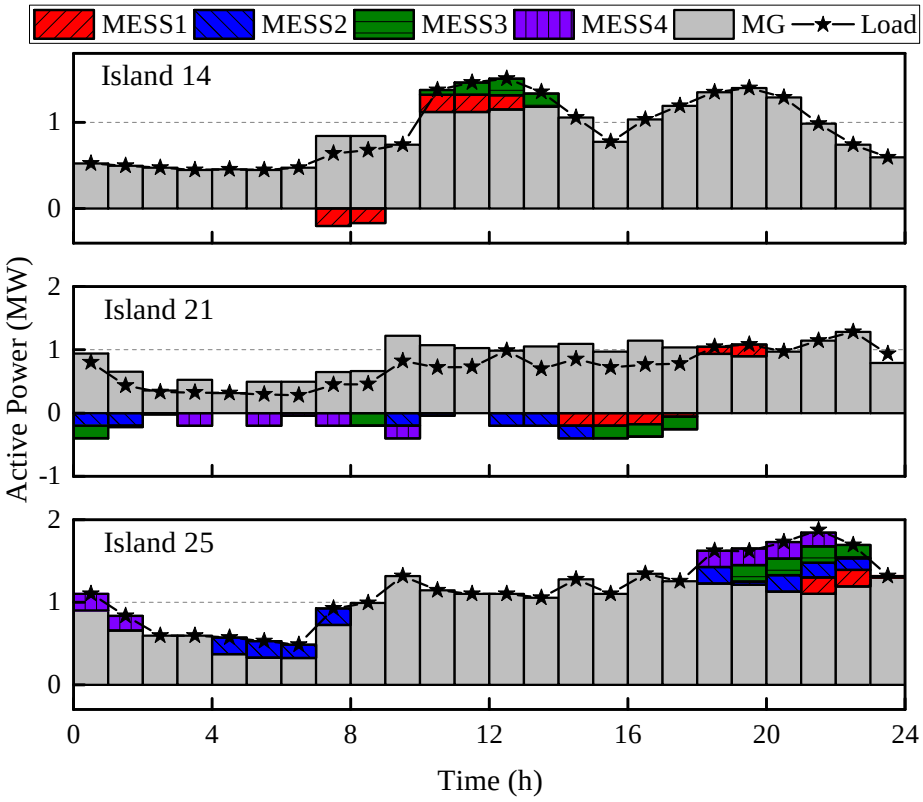

Figure 3.9: Generation dispatch and load restored in case 3.

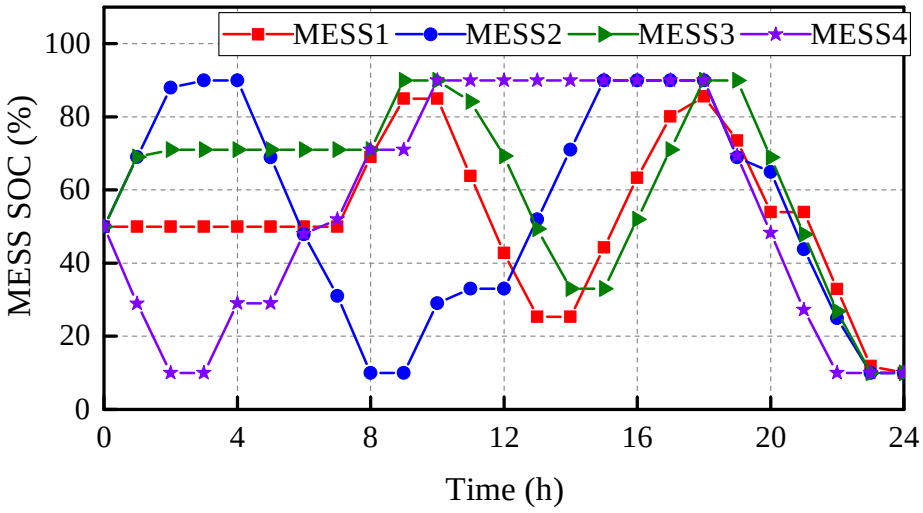

Figure 3.10: SOC of MESS in case 3.

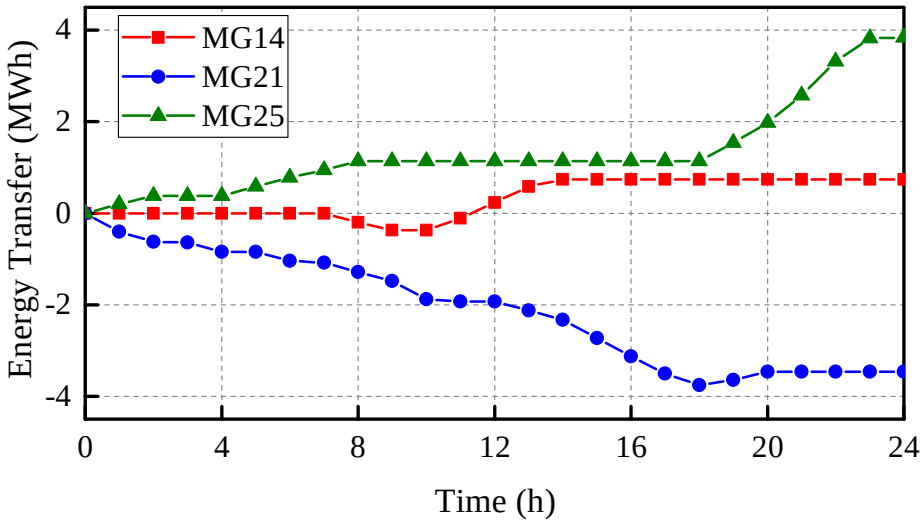

Figure 3.11: Energy transfer among microgrids in case 3.

90% (see Fig. 3.10. Then MESS #2 travels to microgrid #25 in (03:00-04:00) and discharges to microgrid #25 from 04:00 to 08:00, while the SOC reduces to the minimum level of 10%. Here, energy is transferred from microgrid #21 to microgrid #25 through MESS #2. Similar phenomena can be observed from other MESSs.

B. Implementation of Load Shifting within Microgrids

Meanwhile, MESSs can also serve as stationary ESSs to achieve load shifting within the same microgrids. For instance, MESS #1 stays at microgrid #14 in (00:00-13:00), it charges in (07:00-09:00) and discharges to microgrid #14 from 10:00 to 13:00. As noticed in Fig. 3.10, the SOC of MESS #1 changes from 50% to 84.9% and then to 25.3%. This is because, during the early intervals, the load is low as the load profile only ranges from 0.22 to 0.32, as shown in Fig.6. MESS #1 would charge in energy sufficient hours and when it comes to the peak hour, the MESS #1 can discharge to microgrid #14 to achieve efficient utilization of

energy resources within microgrid #14.

The comparison of three cases illustrates the importance of MESS mobility. The integration of MESSs would reduce the total cost through transferring energy among microgrids. The application of MESSs is more effective to serve critical loads to attain an effective restoration scheme, in terms of that their flexibility and transportability can tackle energy imbalance posed by topology and operation constraints. Also, the MESSs act as stationary ESSs in some intervals to perform load shifting within microgrids.

C. Effect of Unit Interruption Cost and Unit Transportation Cost on Total Cost

Fig. 3.12 illustrates the variation of total cost reduction as a function of the unit interruption cost and unit transportation cost. The X-axis of unit interruption cost is measured in p.u. on the basis of \$10/kWh for priority I load and \$2/kWh for priority II load, which ranges from 0.01 p.u. to 100 p.u. The Y-axis of unit transportation cost is changing from \$0 to \$2000 /interval. The Z-axis of the percentage of total cost reduction is calculated by a comparison between the total cost in Case 2 and Case 3.

It can be seen that the total cost reduction improves with the increasing unit interruption cost and the decreasing unit transportation cost. It is because the lower the unit interruption cost and the higher the unit transportation cost, the fewer benefits will the distribution system gets from the MESS and vice versa. MESS will stay at initial microgrids to act as stationary ESSs if unit transportation cost is high enough (See the purple area in Fig. 3.12). Moreover, the contours on the XY-plane further indicate the correlation between unit interruption cost and unit transportation cost given a certain level of total cost reduction. It is also noted

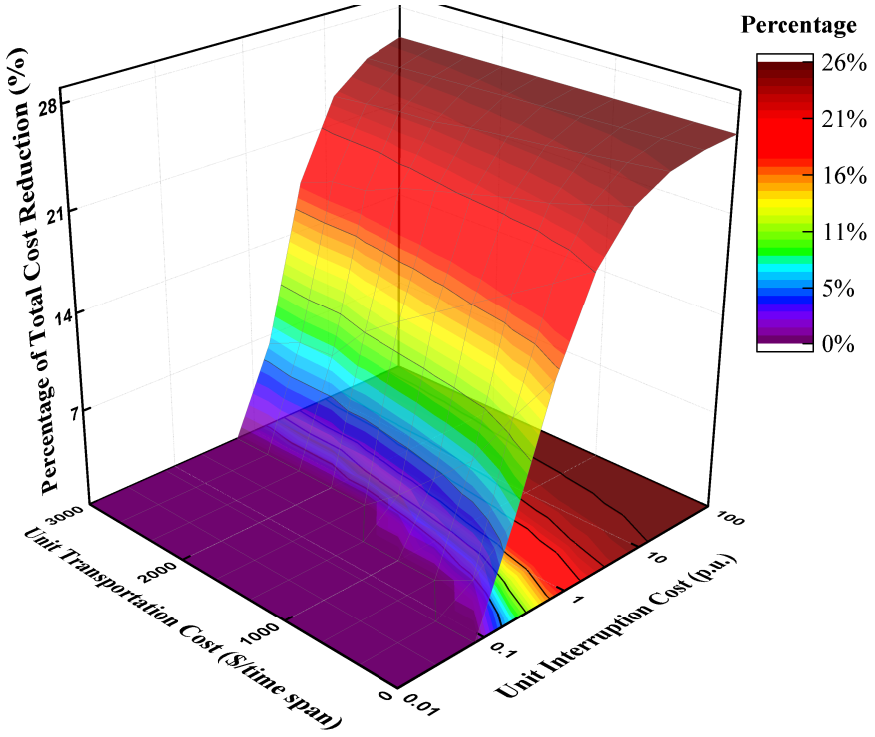

Figure 3.12: Sensitivity analysis of unit interruption cost and unit transportation cost.

that the total cost reduction will remain stable as the continuous increase of unit interruption cost. The reason is that when unit interruption cost is too high and thus the transportation cost can be neglected in the scheduling of MESS, resulting in the same scheduling trip chain. In that case, the total cost is only dependent on the unit interruption cost and the total cost reduction will hit the upper bound.

Therefore, this sensitivity study can serve as a decision support tool to determine the correlation of the unit interruption cost and unit transportation cost with respect to the desired resilience level.

D. Fairness for Scheduling

In terms of fairness of each MESS, MESSs are fully owned and controlled by utility companies in this chapter, so they can be dispatched after major blackouts to minimize the total cost. Thus, there is only one entity involved in this optimization problem. However, the fairness analysis is important if this work is extended to a cooperative game, in which MESS are owned by different entities. There have been research efforts on fair and efficient revenue sharing among providers through the Shapely value [87]. TABLE 3.5 shows the Shapely value as follows.

The Shapely value indicates a single payoff for each MESS, which is the average of all marginal contribution of that MESS to the total cost reduction. It can be used to identify each MESS's contribution to ensure fairness in a cooperative game.

3.6 Conclusions

The chapter investigated a novel application of MESSs into distribution system to propose a post-disaster joint restoration scheme, which aims to minimize

Table 3.5: Shapely Values

Order	Marginal Contribution ($)			
	MESS #1	MESS #2	MESS #3	MESS #4
(1, 2, 3, 4)	13590	12969	8697	6100
(1, 2, 4, 3)	13590	12969	6148	8648
(1, 3, 2, 4)	13590	8697	12969	6100
(1, 3, 4, 2)	13590	6148	12969	8648
(1, 4, 2, 3)	13590	9069	6148	12549
(1, 4, 3, 2)	13590	6148	9069	12549
(2, 1, 3, 4)	12557	14002	8697	6100
(2, 1, 4, 3)	12557	14002	6148	8648
(2, 3, 1, 4)	7988	14002	13266	6100
(2, 3, 4, 1)	6167	14002	13266	7921
(2, 4, 1, 3)	8209	14002	6148	12997
(2, 4, 3, 1)	6167	14002	8190	12997
(3, 1, 2, 4)	12557	8697	14002	6100
(3, 1, 4, 2)	12557	6148	14002	8648
(3, 2, 1, 4)	7988	13266	14002	6100
(3, 2, 4, 1)	6167	13266	14002	7921
(3, 4, 1, 2)	8209	6148	14002	12997
(3, 4, 2, 1)	6167	8190	14002	12997
(4, 1, 2, 3)	11823	9069	6148	14315
(4, 1, 3, 2)	11823	6148	9069	14315
(4, 2, 1, 3)	8209	12684	6148	14315
(4, 2, 3, 1)	6167	12684	8190	14315
(4, 3, 1, 2)	8209	6148	12684	14315
(4, 3, 2, 1)	6167	8190	12684	14315
Shapely Value ($)	10051	10043	10043	10417

the total cost by scheduling MESSs in coordination with distribution network reconfiguration and microgrid operations. With charging/discharging facilities, microgrids serve as root buses to dynamically form islands by controlling ON/OFF status of remote-controlled switches. A modified TSN-based MESS scheduling model is presented and integrated into distribution network reconfiguration to allocate MESSs among microgrids. The optimization problem is formulated as an MILP model, which can derive a MESS scheduling sequence and generation dispatches for both MESSs and resources in microgrids. The effectiveness of the proposed restoration scheme is demonstrated by case studies on a modified 33-bus test system.

The comparative simulations have been implemented to demonstrate the impacts of MESS on distribution system restoration. The MESSs transportability can efficiently transfer energy among multiple microgrids within the distribution system in appropriate times and locations to facilitate critical loads service restoration without violating network topology and operation constraints. Meanwhile, MESSs can also serve as stationary ESSs to implement load shifting within microgrids. Finally, sensitivity analysis shows the impacts of unit interruption cost and unit transportation cost on the total cost, indicating the cost-effectiveness of scheduling MESS in distribution system restoration.

Chapter 4

Rolling Optimization of Mobile Energy Storage Fleets for Resilient Service Restoration

MESSs provide promising solutions to enhance distribution system resilience in terms of mobility and flexibility. This Chapter proposes a rolling integrated service restoration strategy to minimize the total system cost by coordinating the scheduling of MESS fleets, resource dispatching of microgrids and network reconfiguration of distribution systems. The integrated strategy takes into account damage and repair to both the roads in transportation networks and the branches in distribution systems. The uncertainties in load consumption and the status of roads and branches are modeled as scenario trees using Monte Carlo simulation method. The operation strategy of MESSs is modeled by a stochastic multi-layer time-space network technique. A rolling optimization framework is adopted to dynamically update system damage, and the coordinated scheduling at each time interval over the prediction horizon is formulated as a two-stage stochastic MILP with temporal-spatial and operation constraints. The proposed model is verified on two integrated test systems, one is with Sioux Falls transportation network and four 33-bus distribution systems, and the other is the Singapore transportation network-based test system connecting six 33-bus distribution systems. The results demonstrate

the effectiveness of MESS mobility to enhance distribution system resilience due to the coordination of mobile and stationary resources.

4.1 Introduction

Recent major blackouts caused by extreme weather events lead to catastrophic consequences for the economy and society [9], [10]. The impacts of extreme weather events pose unprecedented challenges to power grids and emphasize the importance of improving system resilience [11]–[13]. As distribution systems remain vulnerable to natural disasters, it is indispensable to restore the electric service effectively in response to severe power outages, thus achieving more resilient distribution systems [14]. When severe blackouts occur, a variety of local resources, e.g., microgrids and DERs (ESSs, etc.), can be utilized to restore critical loads in distribution systems. Moreover, the emerging MESSs [20] can provide temporal-spatial mobility and coordinate with stationary local resources for an integrated distribution system restoration.

Great progress has been made in the utilization of stationary resources for service restoration in distribution systems after major blackouts [11], [38]. Microgrids can consolidate and manage a wide range of DERs to alleviate the hazardous impacts of extended outages [14]. Reference [46] proposes a resilience response framework by generator re-dispatch, topology switching, and load shedding. A Markov model is proposed to construct sequential proactive strategies against extreme weather events in [47]. In [48], a microgrid proactive management framework is proposed to coordinate generation reschedule, conservation voltage regulation and demand-side resources. Proactive scheduling in multiple energy carrier microgrids is proposed in response to approaching hurricane [49] and floods [50]. Reference [51] proposes an optimal restoration strategy that coordinates multiple sources at multiple locations to serve critical loads after blackouts. These studies illustrate the value of coordination of multiple resources to enhance grid resilience. In addition, with the increasing installation

of charging/discharging facilities [19], microgrids can provide plug-and-play integration of MESSs for effective service restoration.

MESSs are generally vehicle-mounted container battery ESSs with standard interfaces that allow for plug-and-play [20]. The importance of the integration of MESS fleets with power system operation has been increasingly recognized in recent researches. For normal operations, MESSs are employed to achieve load shifting [56] and relieve transmission congestion [88]. In response to extreme events, MESS fleets can be utilized in both pre and post stage. The economic feasibility of MESSs is demonstrated in [60] by optimizing the investments and relocation of MESSs in case of natural disasters. Reference [61] proposes a sequential framework for pre-positioning of mobile generators to staging locations and real-time dispatching to distribution systems. In [62], the resource allocation of electric buses and transportable batteries is formulated for proactive preparedness for extreme weather events. Dynamic microgrids formation is applied to accommodate mobile and stationary distributed generation and energy resources after disruptions in [63]. Reference [64] presents a microgrid-based critical load restoration by adaptively forming microgrids and positioning mobile emergency resources. Nevertheless, the resource allocation is for one-time dispatching of MESSs in the pre or initial stage of disasters instead of optimizing the temporal-spatial behaviors throughout the restoration process, so the mobility and flexibility of MESS fleets are underutilized. Reference [65] implements resilient routing and scheduling of mobile power sources via a two-stage framework, in which the pre-position and dynamic dispatch are used to coordinate with conventional restoration efforts. For post-disaster restoration, [66] proposes a resilient scheme for disaster recovery logistics that involves scheduling of repair crews and mobile power source and network reconfiguration. A joint scheme is proposed in [67] to integrate the dynamic scheduling of MESSs, generation re-dispatching and

network reconfiguration. However, these researches are either deterministic or do not thoroughly investigate the potential subsequent damage and repair during the restoration process, and more detailed stochastic modeling of MESS in transportation network are still needed.

Furthermore, extreme weather events can destroy not only the distribution systems but also some other interdependent infrastructures [9], [11], e.g., transportation networks, which in turn will impact the scheduling of MESSs and impose more challenges to service restoration. Few existing studies have considered electric service restoration in an integrated distribution and transportation system. In addition, during the disasters, multiple sources of information can be utilized to improve situational awareness of damage status [14], [89], i.e. weather forecast combined with the geographic information systems, distribution system data from smart meters and micro-phasor measurement can provide information on damage and repair to both the roads in transportation networks and the branches in distribution systems. Therefore, an integrated restoration strategy is needed to coordinate the mobile and stationary resources for service restoration with dynamically updated system damage information in coupled transportation and distribution systems.

In this context, this chapter aims to bridge the gap in the coordination of MESS fleets with microgrids into distribution system restoration and leveraging dynamically updated information during the restoration process. A rolling integrated restoration strategy is proposed to coordinate the dynamic scheduling of MESS, resource dispatching of microgrids and distribution network reconfiguration. In order to take advantages of multiple source data that improves situational awareness during the restoration process, a rolling optimization is adopted to dynamically update system damage status. The optimization problem at each interval over the prediction horizon is formulated as a two-stage stochastic MILP,

aiming to minimize the total cost by co-optimizing the scheduling problem of an MESS fleet, generation dispatching of microgrids and network topology reconfiguration. The contributions of the chapter are concluded as follows.

1) A novel integrated restoration strategy is proposed that coordinates the MESS fleet and microgrids to minimize the total system cost. The scheduling of MESS fleet is modeled by a stochastic multi-layer time-space network, which reduces the computational complexity with a fewer number of binary variables and constraints and can be utilized for practical transportation networks.

2) The proposed model takes into account both damage and repair to the roads in transportation networks and the branches in distribution systems. The uncertainties in load consumption and the status of the roads and branches are considered to generate scenarios by Monte Carlo simulation method. A rolling optimization framework is adopted to dynamically update system information and the coordinated scheduling over the prediction horizon is formulated as a two-stage stochastic MILP.

The remainder of this chapter is organized as follows. Section 4.2 describes the construction of time-space networks and the stochastic scheduling of MESSs. Section 4.3 presents the rolling optimization framework for integrated service restoration. Section 4.4 conducts case studies on two integrated test systems to verify the effectiveness of the proposed method. Section 4.5 summarizes this chapter.

4.2 Stochastic Modeling of Mobile Energy Storage System

The increasing penetration of MESSs highlights the superiorities over stationary resources in terms of mobility and flexibility. When major blackout happens,

MESS can be dispatched among microgrids to transport energy for service restoration. This section formulates the stochastic modeling of MESSs via a time-space network, which has been employed to investigate the vehicle routing and scheduling problem [90]–[92]. In order to take into account the uncertainties in damage and repair to the roads in the transportation networks, a scenario-based stochastic time-space network is proposed to model the temporal-spatial behavior of MESSs over the transportation network, while the charging/discharging schedule is described by battery operation and temporal-spatial constraints.

4.2.1 Construction of Multi-layer Time-space Networks

A transportation network is modeled as a weighted graph $\mathcal{G}_{\mathrm{T}} = (\mathcal{N}_{\mathrm{T}}, \mathcal{E}_{\mathrm{T}}, \mathcal{W}_{\mathrm{T}})$, where $\mathcal{N}_{\mathrm{T}}$ is the nodes set and $\mathcal{E}_{\mathrm{T}}$ denotes the edges set of roads with the edge distance $\mathfrak{w} \in \mathcal{W}_{\mathrm{T}}$.

A set of microgrids $\mathcal{M}$ indexed by m and a set of depots $\mathcal{D}$ are located in the transportation network $\mathcal{G}_{\mathrm{T}}$. The mappings $\mathfrak{F}_{\mathrm{T}} : \mathcal{M} \rightarrow \mathcal{N}_{\mathrm{T}}$ and $\mathfrak{F}_{\mathrm{D}} : \mathcal{D} \rightarrow \mathcal{N}_{\mathrm{T}}$ denotes microgrids and depots' locations in the transportation network, respectively. Ω represents an MESS fleet. An MESS $\omega \in \Omega$ is initially located at a depot $d \in \mathcal{D}$, where it starts and travels among microgrids to provide power supply to power grids, finally it goes back to a depot.

In order to account for the uncertainties in damage and repair to the roads in transportation networks, a scenario-based stochastic model is adopted. The uncertainty modeling and scenario generation are detailed in Section 4.3-B. In a scenario s, the shortest path matrix $\mathfrak{P}^s$ is utilized to define the shortest paths for all pairs of microgrids or depots, where the superscript s represents scenario s and the element $\mathfrak{p}_{ij}^s$ denotes the set of nodes $\mathcal{N}_{ij}^s$ and edges $\mathcal{E}_{ij}^s$ with edge distances $\mathcal{W}_{ij}^s$ in the route, which is calculated by the Dijkstra's algorithm [93]. It is noted that

data-driven approach can be integrated in the future research to find the optimal path considering uncertainties in travel time [94], [95]. In this section, a distance matrix $\mathfrak{D}^s$ describes the distances between every two microgrids or depots through the shortest path, the element $\mathfrak{d}_{ij}^s$ is calculated by the sum of the edge distances along the shortest path. A travel time matrix $\mathfrak{T}^{\omega,s}$ with elements $\mathfrak{t}_{ij}^s$ indicates the travel time in the number of intervals considering MESSs' average speed V_{avg}^{ω}.

$$\mathfrak{p}_{ij}^s = (\mathcal{N}_{ij}^s, \mathcal{E}_{ij}^s, \mathcal{W}_{ij}^s), \forall i, j \in \mathcal{M} \cup \mathcal{D}, s \tag{4.1}$$

$$\mathfrak{d}_{ij}^s = \sum_{\mathfrak{w} \in \mathcal{W}_{ij}^s} \mathfrak{w}, \forall s \tag{4.2}$$

$$\mathfrak{t}_{ij}^{\omega,s} = \lceil \mathfrak{d}_{ij}^s / V_{\text{avg}}^{\omega} / \Delta t \rceil, \forall \omega \in \Omega, i, j \in \mathcal{M} \cup \mathcal{D}, s \tag{4.3}$$

where $\lceil\ \rceil$ is the ceiling function and Δt is the length of time intervals.

A modified multi-layer time-space network is proposed to formulate the vehicle scheduling problem of MESSs over a transportation network. For instance, a transportation network connecting four microgrids and one depot is used for illustration, as shown in 4.1. Time horizon $\mathcal{T}$ is the set of time intervals indexed by t. The MESS ω starts at the depot, and obtains the matrix $\mathfrak{P}^s$, $\mathfrak{D}^s$, $\mathfrak{T}^{\omega,s}$. Then its temporal-spatial behavior will be modeled through a time-space network.

In the time-space network, as shown in Fig. 4.2, the horizontal axis shows the time horizon which is discretized into multiple time intervals, the vertical axis represents the spatial dimension and consists of microgrids and depots. In a scenario s, the time-space network is separated into several layers, each one is associated with an MESS ω. That is, $|\Omega|$ layers of the time-space network are assigned to schedule MESSs, where $|\Omega|$ is the total number of MESSs. In a time-space network layer $\mathcal{G}_{\text{S}}^{\omega,s} = (\mathcal{N}_{\text{S}}^{\omega,s}, \mathcal{E}_{\text{S}}^{\omega,s})$ for MESS ω, the set of time-space node $\mathcal{N}_{\text{S}}^{\omega,s}$ represents microgrids or depots' locations at specific time points. There are

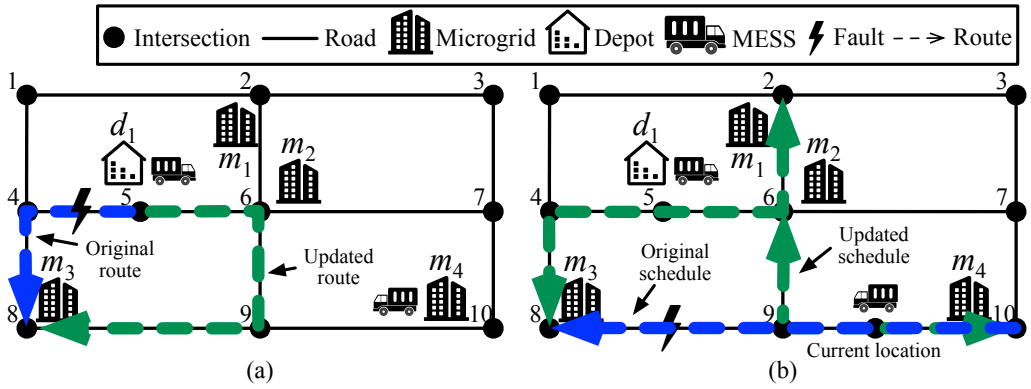

Figure 4.1: A transportation network connecting microgrids and depots: (a) impacts of damage to roads, (b) rescheduling or rerouting at each interval.

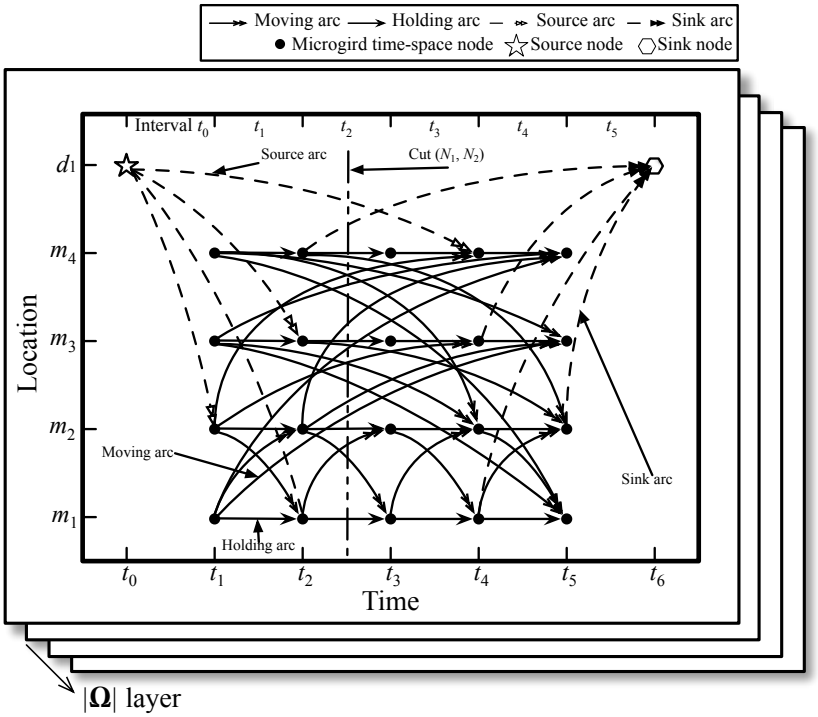

Figure 4.2: A multi-layer time-space network for modeling temporal-spatial behavior of MESSs over the transportation network.

three types of time-space nodes as follows. *1) Microgrid time-space nodes* $\tilde{\mathcal{N}}_S^{\omega,s}$: represent the microgrids at specific time points in the scenario s. *2) Source nodes* $\hat{\mathcal{N}}_S^{\omega,s}$: represent the MESS ω's initial depot position in scenario s. *3) Sink nodes* $\check{\mathcal{N}}_S^{\omega,s}$: indicate the MESS's final depot positions in scenario s.

In addition, the time-space arcs $\mathcal{E}_{\mathrm{S}}^{\omega,s}$ connect time-space nodes and describe the feasible movements among locations considering travel time in scenario s. Four types of arcs are defined in the time-space network as follows. *1) Moving arcs* $\tilde{\mathcal{E}}_S^{\omega,s}$: a moving arc connects two microgrid time-space nodes and represents a movement in spatial and time dimensions in scenario s. For example, as shown in Fig. 4.2, the specified moving arc represents that it is available for an MESS to move from microgrid #1 at t_1 to microgrid #3 at t_5. The movement takes 4 time intervals, which is obtained from the aforementioned travel time matrix $\mathfrak{T}$. All moving arcs that are beyond the time horizon are infeasible and removed from the $\tilde{\mathcal{E}}_{\mathrm{S}}^{\omega,s}$. In addition, the moving arcs will trigger transportation costs for MESSs. *2) Holding arcs* $\bar{\mathcal{E}}_S^{\omega,s}$: a holding arc connects two time-space nodes for the same microgrids in a time interval in scenario s. As shown in Fig. 4.2, holding arcs indicate that MESSs can stay at microgrids for an interval. Only when an MESS stays on the holding arc can it charge from or discharge to distribution systems. *3) Source arcs* $\hat{\mathcal{E}}_S^{\omega,s}$: a source arc connects a source node to a microgrid time-space node in scenario s, which implies that MESS ω is initially located at a depot and moves to a microgrid. *4) Sink arcs* $\check{\mathcal{E}}_S^{\omega,s}$: a sink arc connects a microgrid time-space node to a sink node in the scenario s, indicating that MESS ω return from a microgrid time-space node to a depot at the end of the time horizon.

4.2.2 Impact Analysis of Damage and Repair to Roads on Time-space Network

The damage and repair to the roads in transportation networks have impacts on the matrix $\mathfrak{P}^s$, $\mathfrak{D}^s$, $\mathfrak{T}^{\omega,s}$, leading to the reconstruction of time-space arcs in the time-space network. For example in Fig. 4.1(a), suppose in one of the scenarios the road 4-5 is at fault in the first interval and will be repaired in interval 3. The shortest path from depot #1 to microgrid #3 changes due to the road damage, so do the distance and travel time. The original routes and updated routes are denoted as the blue and green dash lines, respectively in Fig 4.1(a). It indicates that an MESS now takes four intervals to travel from depot #1 to microgrid #3, compared to two intervals before the road damage. Thus, in the time-space network, the corresponding arcs connecting depot #1 at time t_0 to microgrid #3 should be modified from t_2 to t_4. Furthermore, after the road 4-5 gets repaired, the travel time is reduced to two intervals and corresponding arcs are modified.

In addition, a rolling optimization framework is utilized to update the scheduling of MESS fleet at each interval. The detailed description of the rolling optimization framework is given in Section 4.3.2. In this formulation, MESSs' current locations are obtained at each interval as the initial condition for the optimization over the new prediction horizon,MESSs can be re-dispatched to any microgrids or depots. For instance, an MESS is dispatched from microgrid #4 to microgrid #3 via the route 10-9-8, indicated as the blue dash line in Fig .4.1(b). When it implements the decision for the first interval and gets to a new location, as indicated by the current location. The matrix $\mathfrak{P}^s$, $\mathfrak{D}^s$, $\mathfrak{T}^{\omega,s}$ are updated to reconstruct the time-space network. Based on the updated initial condition and system information, the MESS does not have to go the microgrid #3, it can go to other microgrids or even go back to microgrid #4. Moreover, this formulation can

also deal with subsequent road damage occurring during the MESS's movement. For example, as shown in Fig. 4.1(b), the damage to road edge 8-9 occurs when the MESS move to microgrid #3, the designated route is no longer available, the matrix $\mathfrak{P}^s$, $\mathfrak{D}^s$, $\mathfrak{T}^{\omega,s}$ need to be updated considering the road damage to provide the initial condition for the next decision. It is also assumed that if the current road is damaged, the MESS needs to move back to the nearest intersection node with the same road. For example, if the MESS is already on the road edge 8-9 when the damage occurs, it is assumed that the MESS cannot move forward and can only move back to the node 9. Similarly, the repair can also be taken into account by updating the matrix $\mathfrak{P}^s$, $\mathfrak{D}^s$, $\mathfrak{T}^{\omega,s}$. Therefore, the time-space network is modified based on the updated travel time matrix $\mathfrak{T}^{\omega,s}$.

4.2.3 Temporal-spatial Constraints of Mobile Energy Storage Systems

The temporal-spatial behavior of MESSs over the transportation network $\mathcal{G}_{\mathrm{T}}$ is transformed into the multi-layer time-space network $\mathcal{G}_{\mathrm{S}}^s = (\mathcal{N}_{\mathrm{S}}^s, \mathcal{E}_{\mathrm{S}}^s)$. The scheduling of vehicles is defined as a sequence of trips by time-space arcs starting from a source node to microgrid time-space nodes and finally returning to a sink node. The formulation is based on arc-wise binary variables $\zeta_{\hat{n}\check{n}}^{\omega,s}$, which are 1 if the MESS ω (corresponding to the ω^{th} layer) is on an arc $(\hat{n}, \check{n}) \in \tilde{\mathcal{E}}_{\mathrm{S}}^{\omega,s}$ in scenario s, otherwise set to 0.

Consider the time-space network in Fig. 4.2, a cut $(\mathcal{N}_1^s, \mathcal{N}_2^s)$ of $\mathcal{G}_{\mathrm{S}}^{\omega,s} = (\mathcal{N}_{\mathrm{S}}^{\omega,s}, \mathcal{E}_{\mathrm{S}}^{\omega,s})$ is defined as a partition of $\mathcal{N}_{\mathrm{S}}^{\omega,s}$ into two disjoint subsets (where $\mathcal{N}_1^s$ represents the nodes on the left side of the cut while $\mathcal{N}_2^s$ denotes ones on the right). The cut-set of the cut $(\mathcal{N}_1^s, \mathcal{N}_2^s)$ is a set $\{(n_1, n_2) \in \mathcal{E}_{\mathrm{S}}^{\omega,s} | n_1 \in \mathcal{N}_1^s, n_2 \in \mathcal{N}_2^s\}$. Any edge in the cut-set has one endpoint at each side of the cut $(\mathcal{N}_1^s, \mathcal{N}_2^s)$. There

is a cut for each time interval in time-space network and an associated cut-set, which is denoted by $\mathbf{C}_{\omega}^{t,s}$ representing the one for MESS ω in the interval t. For example, a cut for interval t_2 is depicted in Fig. 4.2. The cut-set $\mathbf{C}_{\omega}^{t_2}$ involves all the time-space arcs that crossing the cut, indicating all the feasible states of the MESS ω in the interval and an MESS can only be on exact one arc in any time interval. The MESS's states can be described by constraint (4.4):

$$\sum_{(\hat{n},\check{n})\in\mathbf{C}_{\omega}^{t,s}} \zeta_{\hat{n}\check{n}}^{\omega,s} = 1, \forall\omega, s, t \tag{4.4}$$

$$\sum_{(\hat{n},\check{n})\in\acute{\mathcal{E}}_{\mathrm{S},n}^{\omega,s}} \zeta_{\hat{n}\check{n}}^{\omega,s} = \sum_{(\hat{n},\check{n})\in\grave{\mathcal{E}}_{\mathrm{S},n}^{\omega,s}} \zeta_{\hat{n}\check{n}}^{\omega,s}, \forall n \in \tilde{\mathcal{N}}_{\mathrm{S}}^{\omega,s}, \omega, s \tag{4.5}$$

$$\sum_{(\hat{n},\check{n})\in\acute{\mathcal{E}}_{\mathrm{S},n}^{\omega,s}} \zeta_{\hat{n}\check{n}}^{\omega,s} = \zeta_{\mathrm{init}}^{\omega,s}, \forall n \in \hat{\mathcal{N}}_{\mathrm{S}}^{\omega,s}, \omega, s \tag{4.6}$$

In addition, for each time-space node $n \in \tilde{\mathcal{N}}_{\mathrm{S}}^{\omega,s}$ in scenario s, the time-space arcs connecting the n can be classified into two groups of in-flows $\grave{\mathcal{E}}_{\mathrm{S},n}^{\omega,s}$ and out-flows $\acute{\mathcal{E}}_{\mathrm{S},n}^{\omega,s}$, which represent the arcs entering or leaving the n, respectively. For source nodes $n \in \hat{\mathcal{N}}_{\mathrm{S}}^{\omega,s}$, there are out-flows with the initial location of MESSs. Each time-space node n needs to satisfy the network flow conservation, that is, an MESS ω ends trips at time-space node n, which serves as the starting point of the subsequent trip. The $\zeta_{\mathrm{init}}^{\omega,s}$ indicates the MESS's initial location. The time-space network flow conservation is suggested by constraint (4.5)-(4.6).

4.2.4 Operation Constraints of Mobile Energy Storage Systems

When staying on a holding arc, an MESS can exchange power through charging from or discharging to distribution systems. The holding arcs for microgrid m

at time interval t in scenario s is denoted by $\bar{\mathcal{E}}_{\mathrm{S},m}^{\omega,t,s}$, which can be obtained by determining the holding arc that involves time-space nodes for microgrid m in time interval t in scenario s. The charging/discharging behaviors are constrained as follows.

$$0 \leq P_{\mathrm{ch},m}^{\omega,t,s} \leq \zeta_{\hat{n}\check{n}}^{\omega,s} \overline{P}_{\mathrm{ch}}^{\omega}, \forall (\hat{n},\check{n}) \in \bar{\mathcal{E}}_{\mathrm{S},m}^{\omega,t,s}, \omega, m, t, s \tag{4.7}$$

$$0 \leq P_{\mathrm{dch},m}^{\omega,t,s} \leq \zeta_{\hat{n}\check{n}}^{\omega,s} \overline{P}_{\mathrm{dch}}^{\omega}, \forall (\hat{n},\check{n}) \in \bar{\mathcal{E}}_{\mathrm{S},m}^{\omega,t,s}, \omega, m, t, s \tag{4.8}$$

$$0 \leq \sum_{m \in \mathcal{M}} P_{\mathrm{ch},m}^{\omega,t,s} \leq I_{\mathrm{ch}}^{\omega,t,s} \overline{P}_{\mathrm{ch}}^{\omega}, \forall \omega, t, s \tag{4.9}$$

$$0 \leq \sum_{m \in \mathcal{M}} P_{\mathrm{dch},m}^{\omega,t,s} \leq I_{\mathrm{dch}}^{\omega,t,s} \overline{P}_{\mathrm{dch}}^{\omega}, \forall \omega, t, s \tag{4.10}$$

$$I_{\mathrm{dch}}^{\omega,t,s} + I_{\mathrm{dch}}^{\omega,t,s} \leq \sum_{(\hat{n},\check{n}) \in \bar{\mathcal{E}}_{\mathrm{S},m}^{\omega,t,s}} \zeta_{\hat{n}\check{n}}^{\omega,s}, \forall m, \omega, t, s \tag{4.11}$$

$$E_{\omega}^{t+1,s} = E_{\omega}^{t,s} - \Delta t \Big(\frac{\sum_{m \in \mathcal{M}} P_{\mathrm{dch},m}^{\omega,t,s}}{\eta_{\mathrm{dch}}^{\omega}} - \eta_{\mathrm{ch}}^{\omega} \sum_{m \in \mathcal{M}} P_{\mathrm{ch},m}^{\omega,t+1,s} \Big), \quad \forall \omega, t \in \mathcal{T} \setminus \{T\}, s \tag{4.12}$$

$$E_{\mathrm{c}}^{\omega} \underline{SOC}^{\omega} \leq E_{\omega}^{t,s} \leq E_{\mathrm{c}}^{\omega} \overline{SOC}^{\omega}, \forall \omega, t, s \tag{4.13}$$

where $P_{\mathrm{ch},m}^{\omega,t,s}, P_{\mathrm{dch},m}^{\omega,t,s}$ are charging/discharging power of MESS ω from/to microgrid m in interval t in scenario s. $I_{\mathrm{ch}}^{\omega,t,s}$, $I_{\mathrm{dch}}^{\omega,t,s}$ are binary variables, battery status of MESS ω in interval t in scenario s, 1 if the status is on, 0 otherwise. $\zeta_{\hat{n}\check{n}}^{\omega,s}$ are Binary variables, 1 if the MESS ω is on an arc $(\hat{n},\check{n}) \in \mathcal{E}_{\mathrm{S}}^{\omega,s}$ in scenario s, otherwise set to 0. $E_{\omega}^{t,s}$ represents energy of the MESS ω by the end point of interval t in scenario s. E_{c}^{ω} is battery's capacity of MESSs. $\overline{SOC}^{\omega}$, $\underline{SOC}^{\omega}$ are maximum and minimum level of SOC of the MESS. $\eta_{\mathrm{ch}}^{\omega}$, $\eta_{\mathrm{dch}}^{\omega}$ represent charging/discharging efficiency.

Constraints (4.7)-(4.8) state the relation between charging/discharging power

and temporal-spatial behaviors. Equations (4.9)-(4.10) express the charging/discharging power associated with battery status, which is also constrained by temporal-spatial behaviors in (4.11). Constraint (4.12) calculates the energy and constraint (4.13) sets the upper and lower range.

4.2.5 Complexity Analysis of Time-space Network

References [59], [67] add virtual nodes to form time-space arcs that span more than one interval. The time-space network can be extended to an extremely large model, leading to high computational complexity when applied to practical transportation networks. For instance, it takes four time spans from microgrid #3 to microgrid #4, three virtual nodes need to be added to represent the time-space arcs from microgrid #3 at t to microgrid #4 at $t + 4$. Then the arcs between virtual nodes and original nodes are added. This would significantly increase the numbers of binary variables and constraints.

This chapter proposes a time-space network without virtual nodes for the arcs that span more than one interval, resulting in fewer numbers of binary variables and constraints. The number of virtual nodes is indicated by $\Delta\eta_{\mathrm{V}}^{\omega}$, which is determined by the travel time matrix $\mathfrak{T}^{\omega,s}$, the comparison of numbers of variables and constraints are presented in Table 4.1, where the P is the permutation. Take the case in Fig. 4.2 and Fig. 4.1 for instance, suppose the time horizon is 6 hours and the length of interval is 1 hour. For this scenario, the proposed time-space network reduces the numbers of binary variables and constraints by 58.01% and 67.53%, respectively.

Table 4.1: Comparison of Numbers of Variables and Constraints

	Ref. [59], [67]	Proposed model
# of Binary Variables	$\sum_{s\in\mathcal{S},\omega\in\Omega}\lvert\mathcal{E}_{\mathrm{S}}^{\omega,s}\rvert+$ $\sum_{s\in\mathcal{S},\omega\in\Omega}[(\lvert\Delta\mathcal{N}_{\mathrm{V}}^{\omega,s}\rvert+1)$ $\times 2\lvert\mathcal{T}\rvert]$ $-P_2^{\lvert\mathcal{M}\cup\mathcal{D}\rvert}\times\lvert\mathcal{S}\rvert$	$\sum_{s\in\mathcal{S},\omega\in\Omega}\lvert\mathcal{E}_{\mathrm{S}}^{\omega,s}\rvert$
# of Constraints	$\sum_{s\in\mathcal{S},\omega\in\Omega}\lvert\mathcal{N}_{\mathrm{S}}^{\omega,s}\rvert+$ $\sum_{s\in\mathcal{S},\omega\in\Omega}(\lvert\Delta\mathcal{N}_{\mathrm{V}}^{\omega,s}\rvert\times\lvert\mathcal{T}\rvert)$	$\sum_{s\in\mathcal{S},\omega\in\Omega}\lvert\mathcal{N}_{\mathrm{S}}^{\omega,s}\rvert$

4.3 Rolling Integrated Service Restoration

This section proposes a rolling optimal service restoration that coordinates the scheduling of MESS fleets, resource dispatching of microgrids and distribution network reconfiguration. The objective is to minimize the total cost, considering the customer interruption cost, microgrid generation cost, and MESS transportation cost and battery maintenance cost. Partial load curtailment is used as in [43]. Customer interruption cost is adopted to differentiate between critical and non-critical loads [25]. In order to take into account the subsequent damage during the restoration process in both distribution systems and transportation networks, a rolling optimization is adopted for dynamic updating of system damage status. The detailed problem statement, rolling optimization framework, and mathematical formulation are described as follows.

4.3.1 Problem Statement

A conceptual resilience curve associated with an event in [31] is adopted for better illustration, as shown in Fig. 2.7. It is assumed in this manuscript

that extreme events cause the complete outages of transmission grids and the distribution systems can no longer be supplied by transmission grids. Under this circumstance, microgrids can be utilized to coordinate multiple stationary and mobile resources for service restoration at distribution level. It is noted that each load is powered by only one microgrid [38], [61], [62], there is no loop or overlap region. However, the model can be further extended to consider control strategies in network reconfiguration [9].

Previous studies generally assume that all the faults have been identified at t_{r} [38], [67] and the restoration starts with accurate damage information. However, the extreme events may involve multiple stages, i.e., after the major strikes, the extreme events can still last and cause subsequent damage. Therefore, the proposed integrated restoration strategy is implemented right after the major strikes of an extreme event until the main grid is restored, i.e., from t_{pe} to t_{ir}, to enhance the system resilience level. In this case, restoration gets started with incomplete damage information. A two-stage stochastic optimization is adopted to account for uncertainties and a rolling optimization framework is used to dynamically update system information over the prediction horizon at each interval.

4.3.2 Uncertainty Modeling and Scenario Generation

A scenario-based method is used to model uncertainties, by generating a large number of scenarios and doing scenario reduction to ensure the computational tractability.

There are several uncertainties considered in this chapter, including forecasting errors in load, the status of the roads in transportation networks and the branches in distribution systems. A normal distribution is used to represent the forecasting

error of load, in which, the mean value of the normal distribution is the predicted load and the standard deviation is set to be 2% of the predicted load [96]. A two-state continuous-time Markov model is applied to represent the availability of roads and branches [97], while available and unavailable hours are subject to exponential distributions with mean uptime and mean downtime values [59]. The repair efforts are also taken into account during the optimization time horizon. Then Monte-Carlo simulation is utilized to generate scenarios. In order to reduce the computation efforts, a scenario reduction is implemented to reduce the number of scenarios while maintaining a good approximation of the system uncertainty. This chapter adopts a simultaneous backward reduction method [97] for scenario reduction.

4.3.3 Rolling Optimization Framework

During the restoration process, it is challenging to obtain the accurate load forecast and damage status at the very beginning and to solve the optimization problem only once to acquire an acceptable solution. In addition, the load forecast and damage status are dynamically updated from multiple sources of information, with the short-term forecast being more accurate. Therefore, in order to deal with the inaccuracy of forecast over the long horizon and leverage dynamically updated forecasts, a rolling optimization framework is adopted to solve the problem recursively in a finite-moving-horizon of intervals [98]. Specifically, the entire time horizon $\mathcal{T}_{\mathrm{H}}$ is discretized into equal time intervals by Δt and the optimization problem is formulated and solved at each time interval over the prediction horizon $\mathcal{T}_{\mathrm{P}}$, but only the decisions in the first interval are implemented. Then the prediction horizon is shifted forward and the calculation is repeated for the new prediction horizon until the end of the entire time horizon $\mathcal{T}_{\mathrm{H}}$, based on the updated system

information and initial conditions [99]. The final decisions are the sequence of the decisions in the first interval of each prediction horizon.

The forecasts for uncertainties in each scenario s are denoted with superscript s, while the realization of uncertain parameters is indicated with superscript ξ. The proposed rolling optimization framework adopts a two-stage stochastic programming approach, in which the decision variables are divided into two different groups: *1)* First-stage variables involve the decision variables $\zeta^{\omega,s}_{\hat{n}\check{n}}$, α_{ij} in the first interval of prediction horizon $\mathcal{T}_{\mathrm{P}}$, and are determined before the realization of uncertain parameters and scenario independent by nonanticipativity constraint, as described in the next subsection. 2) The second-stage decisions are scenario-dependent and can be adjusted once uncertain parameters reveal, consisting of decision variables $\zeta^{\omega}_{\hat{n}\check{n}}$ in the rest intervals of $\mathcal{T}_{\mathrm{P}}$ and $P^{\omega,t,s}_{\mathrm{ch},m}$, $P^{\omega,t,s}_{\mathrm{dch},m}$, $P^{t,s}_{\mathrm{DG},m}$, $Q^{t,s}_{\mathrm{DG},m}$ in all intervals of $\mathcal{T}_{\mathrm{P}}$. The solution of the two-stage stochastic program is a single first-stage policy and a collection of second-stage recourse decisions defining recourse actions in response to each scenario s.

The first-stage decisions $\zeta^{\omega}_{\hat{n}\check{n}}$, α_{ij} are implemented at the beginning of the interval t. At the end of the interval t, the actual decisions $P^{\omega,t}_{\mathrm{ch},m}$, $P^{\omega,t}_{\mathrm{dch},m}$, $P^{t}_{\mathrm{DG},m}$, $Q^{t}_{\mathrm{DG},m}$ can be obtained by a deterministic re-optimization based on the implementation of $\zeta^{\omega}_{\hat{n}\check{n}}$, α_{ij} and realization of uncertainties of $P^{t,\xi}_{\mathrm{D},i}$, $Q^{t,\xi}_{\mathrm{D},i}$, $\ddot{\mathcal{E}}^{\xi}_{\mathrm{D}}$, $\ddot{\mathcal{E}}^{\xi}_{\mathrm{T}}$. Then the rolling optimization proceeds to the next time interval $t+1$, the initial condition will be updated by the realization of uncertainties of $P^{t,\xi}_{\mathrm{D},i}$, $Q^{t,\xi}_{\mathrm{D},i}$, $\ddot{\mathcal{E}}^{\xi}_{\mathrm{D}}$, $\ddot{\mathcal{E}}^{\xi}_{\mathrm{T}}$ and actual decisions of $\zeta^{\omega}_{\hat{n}\check{n}}$, α_{ij}, $P^{\omega,t}_{\mathrm{ch},m}$, $P^{\omega,t}_{\mathrm{dch},m}$, $P^{t}_{\mathrm{DG},m}$, $Q^{t}_{\mathrm{DG},m}$ in the interval t.

4.3.4 Mathematical Formulation

A distribution network is modeled as a graph $\mathcal{G}_{\mathrm{D}} = (\mathcal{N}_{\mathrm{D}}, \mathcal{E}_{\mathrm{D}})$ [38], where $\mathcal{N}_{\mathrm{D}}$ is the set of distribution system buses, indexed by i and $\mathcal{E}_{\mathrm{D}}$ is the set of distribution

system branches, indexed by (i, j). The mapping $\mathfrak{G}_{\mathrm{D}} : \mathcal{M} \rightarrow \mathcal{N}_{\mathrm{D}}$ indicates the microgrid locations in the distribution network.

The network reconfiguration is formulated by a fictitious network model [9], [43], [100] to describe the spanning forest constraints. A linearized DistFlow model [43], [61] is employed for power flow analysis. It is noted that the linearized three-phase power flow [51] can be included for further extension of this model to unbalanced three-phase conditions. The mathematical formulations are described as follows.

$$\sum_{i \in \delta^s(j)} \mathfrak{f}_{ji}^s - \sum_{i \in \pi^s(j)} \mathfrak{f}_{ij}^s = -1, \forall j \in \mathcal{N}_{\mathrm{D}} \setminus \mathcal{G}_{\mathrm{D}}(\mathcal{M}), s \tag{4.14}$$

$$\sum_{i \in \delta^s(j)} \mathfrak{f}_{ji}^s - \sum_{i \in \pi^s(j)} \mathfrak{f}_{ij}^s = \mathfrak{b}_j^s, \forall j \in \mathcal{G}_{\mathrm{D}}(\mathcal{M}), s \tag{4.15}$$

$$-M\alpha_{ij}^s \leq \mathfrak{f}_{ij}^s \leq M\alpha_{ij}^s, \forall (i, j), s \tag{4.16}$$

$$-M(2 - \alpha_{ij}^s) \leq \mathfrak{f}_{ij}^s \leq M(2 - \alpha_{ij}^s), \forall (i, j), s \tag{4.17}$$

$$\mathfrak{b}_j^s \geq 1, \forall j \in \mathcal{G}_{\mathrm{D}}(\mathcal{M}), s \tag{4.18}$$

$$\sum_{(i,j) \in \mathcal{E}_{\mathrm{D}}} \alpha_{ij}^s = |\mathcal{N}_{\mathrm{D}}| - |\mathcal{M}|, \forall s \tag{4.19}$$

$$\alpha_{ij}^s = 0, \forall (i, j) \in \ddot{\mathcal{E}}_{\mathrm{D}}^s, s \tag{4.20}$$

$$P_{\mathrm{G},i}^{t,s} - P_{\mathrm{r},i}^{t,s} = \sum_{(i,j) \in \mathcal{E}_{\mathrm{D}}} P_{ij}^{t,s} - \sum_{(k,i) \in \mathcal{E}_{\mathrm{D}}} P_{ki}^{t,s}, \forall i, t, s \tag{4.21}$$

$$Q_{\mathrm{G},i}^{t,s} - Q_{\mathrm{r},i}^{t,s} = \sum_{(i,j) \in \mathcal{E}_{\mathrm{D}}} Q_{ij}^{t,s} - \sum_{(k,i) \in \mathcal{E}_{\mathrm{D}}} Q_{ki}^{t,s}, \forall i, t, s \tag{4.22}$$

$$v_j^{t,s} - v_i^{t,s} \leq M(1 - \alpha_{ij}^s) + \frac{r_{ij} P_{ij}^{t,s} + x_{ij} Q_{ij}^{t,s}}{v_0}, \forall (i, j), t, s \tag{4.23}$$

$$v_j^{t,s} - v_i^{t,s} \geq -M(1 - \alpha_{ij}^s) + \frac{r_{ij} P_{ij}^{t,s} + x_{ij} Q_{ij}^{t,s}}{v_0}, \forall (i, j), t, s \tag{4.24}$$

$$-\alpha_{ij}^s \overline{S}_{ij} \leq P_{ij}^{t,s} \leq \alpha_{ij}^s \overline{S}_{ij}, \forall (i, j), t, s \tag{4.25}$$

$$-\alpha_{ij}^{s}\overline{S}_{ij} \leq Q_{ij}^{t,s} \leq \alpha_{ij}^{s}\overline{S}_{ij}, \forall (i,j), t, s \tag{4.26}$$

$$-\sqrt{2}\alpha_{ij}^{s}\overline{S}_{ij} \leq P_{ij}^{t,s} + Q_{ij}^{t,s} \leq \sqrt{2}\alpha_{ij}^{s}\overline{S}_{ij}, \forall (i,j), t, s \tag{4.27}$$

$$-\sqrt{2}\alpha_{ij}^{s}\overline{S}_{ij} \leq P_{ij}^{t,s} - Q_{ij}^{t,s} \leq \sqrt{2}\alpha_{ij}^{s}\overline{S}_{ij}, \forall (i,j), t, s \tag{4.28}$$

$$\underline{v}_{i} \leq v_{i}^{t,s} \leq \overline{v}_{i}, \forall i \in \mathcal{N}_{\mathrm{D}} \setminus \mathcal{G}_{\mathrm{D}}(\mathcal{M}), t, s \tag{4.29}$$

$$v_{i}^{t,s} = v_{0}, \forall i \in \mathcal{G}_{\mathrm{D}}(\mathcal{M}), t, s \tag{4.30}$$

$$0 \leq P_{\mathrm{r},i}^{t,s} \leq P_{\mathrm{D},i}^{t,s}, \forall i, t, s \tag{4.31}$$

$$Q_{\mathrm{r},i}^{t,s} = P_{\mathrm{r},i}^{t,s} \tan\left(\cos^{-1}\varphi_{i}\right), \forall i, t, s \tag{4.32}$$

$$P_{\mathrm{G},m}^{t,s} = P_{\mathrm{DG},m}^{t,s} - \sum_{\omega \in \Omega}(P_{\mathrm{ch},m}^{\omega,t,s} + P_{\mathrm{dch},m}^{\omega,t,s}) - P_{\mathrm{d},m}^{t,s}, \forall m, t, s \tag{4.33}$$

$$Q_{\mathrm{G},m}^{t,s} = Q_{\mathrm{DG},m}^{t,s} - Q_{\mathrm{d},m}^{t,s}, \forall m, t, s \tag{4.34}$$

$$0 \leq P_{\mathrm{DG},m}^{t,s} \leq \overline{P}_{\mathrm{DG},m}, \forall m, t, s \tag{4.35}$$

$$-\overline{Q}_{\mathrm{DG},m} \leq Q_{\mathrm{DG},m}^{t,s} \leq \overline{Q}_{\mathrm{DG},m}, \forall m, t, s \tag{4.36}$$

$$E_{\mathrm{DG},m}^{t+1,s} = E_{\mathrm{DG},m}^{t,s} - P_{\mathrm{DG},m}^{t+1,s}\Delta t, \forall m, t \in \mathcal{T}_{\mathrm{P}} \setminus \{T\}, s \tag{4.37}$$

$$\underline{E}_{\mathrm{DG},m} \leq E_{\mathrm{DG},m}^{t,s} \leq \overline{E}_{\mathrm{DG},m}, \forall m, t, s \tag{4.38}$$

where $|\mathcal{N}_{\mathrm{D}}|, |\mathcal{M}|$ represent the cardinality of the sets, $\delta^{s}(j)$ and $\pi^{s}(j)$ are the set of children nodes and parent nodes of bus j in scenario s, respectively. $\mathfrak{f}_{ij}$ is the power transferred on the line (i,j) in the fictitious network; $\mathfrak{b}_{j}$ is the power supplied by the "source" buses in the fictitious network. M is a large number. Since the fictitious network has the same topology structure as the original power network, they have the same connectivity. Equations (4.14)-(4.18) indicates that the satisfaction of energy balance at each bus in the fictitious network implies at least one path exists between the "source" bus and all other buses, so that the sub-graph must be connected. Equation (4.19) guarantees the necessary condition for radiality. Equation (4.20) represents the damaged branch status. Constraints (4.21) and (4.22) describe the active and reactive

power balance at bus i. Constraints (4.23) and (4.24) indicate the branch voltage drop by the big-M method [80]. Equations (4.25)-(4.28) provide a linearized approximation regarding branch capacity. Equation (4.29) suggests the range of voltage magnitude. Equation (4.30) sets the voltage of microgrid buses to v_0. Equations (4.31) and (4.32) constrain the load restoration and power factor. Constraints (4.33) and (4.34) express the aggregated real and reactive power considering the charging or discharging of MESS fleets. Equations (4.35) and (4.36) depict the power capacity constraints of equivalent dispatchable DG. Equation (4.37) calculates the energy in each microgrid. Equation (4.38) presents the range of energy.

Considering that the first stage variables are scenario independent, the nonanticipativity constraints are enforced to ensure that all the realizations of the first-stage decision variables are equal to each other [101]. The nonanticipativity constraints are described as follows.

$$\zeta_{\hat{n}\check{n}}^{\omega,s} = \sum_{\mathfrak{s}\in\mathcal{S}} \gamma_{\mathfrak{s}} \zeta_{\hat{n}\check{n}}^{\omega,\mathfrak{s}}, \forall(\hat{n},\check{n}) \in \mathbf{C}_{\omega}^{0,s}, \omega, s \tag{4.39}$$

$$\alpha_{ij}^{s} = \sum_{\mathfrak{s}\in\mathcal{S}} \gamma_{\mathfrak{s}} \alpha_{ij}^{\mathfrak{s}}, \forall(i,j), s \tag{4.40}$$

where $\mathbf{C}_{\omega}^{0,s}$ denotes the cut set of time-space arcs in the first interval of the prediction horizon $\mathcal{T}_{\mathrm{P}}$ in the scenario s.

The objective function is formulated as follows to minimize the total cost.

$$\min \sum_{t\in\mathcal{T}_{\mathrm{P}}} \gamma_s \sum_{s\in\mathcal{S}} \Bigg[\Bigg[\sum_{i\in\mathcal{N}} W_i (P_{\mathrm{D},i}^{t,s} - P_{\mathrm{r},i}^{t,s}) + \sum_{m\in\mathcal{M}} C_{\mathrm{gen},m} P_{\mathrm{DG},m}^{t,s} + \sum_{\omega\in\Omega} C_{\mathrm{bat},\omega} \sum_{m\in\mathcal{M}} (P_{\mathrm{ch},m}^{\omega,t,s} + P_{\mathrm{dch},m}^{\omega,t,s}) \Bigg] \Delta t$$

$$+\sum_{\omega\in\Omega} C_{\text{tran},\omega} \sum_{(\hat{n},\check{n})\in\mathcal{E}_{\text{S}}^{\omega,s}} \zeta_{\hat{n}\check{n}}^{\omega,s}\Bigg] \tag{4.41}$$

where the term $\sum_{t\in\mathcal{T}}\sum_{s\in\mathcal{S}}\sum_{i\in\mathcal{N}} W_i(P_{\text{D},i}^{t,s}-P_{\text{r},i}^{t,s})\Delta T$ is the customer interruption cost. The term $\sum_{t\in\mathcal{T}}\sum_{s\in\mathcal{S}}\sum_{m\in\mathcal{M}} C_{\text{gen},m}P_{\text{DG},m}^{t,s}\Delta T$ shows the microgrids generation cost. The third term $\sum_{t\in\mathcal{T}}\sum_{s\in\mathcal{S}}\sum_{\omega\in\Omega} C_{\text{bat},\omega}\sum_{m\in\mathcal{M}}(P_{\text{ch},m}^{\omega,t,s}+P_{\text{dch},m}^{\omega,t,s})\Delta T$ calculates the MESS battery maintenance cost. The last term $\sum_{s\in\mathcal{S}}\sum_{\omega\in\Omega} C_{\text{tran},\omega}\sum_{(\hat{n},\check{n})\in\mathcal{E}_{\text{S}}^{\omega,s}}\zeta_{\hat{n}\check{n}}^{\omega}$ denotes the transportation cost.

The framework of the integrated restoration strategy is illustrated in Algorithm 1.

4.4 Case Studies

The simulations are studied on two integrated distribution and transportation systems to verify the effectiveness of the proposed service restoration strategy, one is with a Sioux Falls transportation network [102] and four 33-bus distribution systems [85], the other is based on the Singapore transportation network and six 33-bus distribution systems. The proposed model is implemented using Python 3.6 and the two-stage stochastic MILP at each interval over the prediction horizon is solved by CPLEX 12.8.0 [103].

4.4.1 Case I : Sioux Falls Transportation Networks with four 33-bus Distribution Systems

A. Test Systems

As the scheduling of MESS fleets involves multiple distribution systems, an integrated test system with four 33-bus distribution systems connected by the

Algorithm 1: Framework for integrated service restoration

▷ ***Initialization***:

Input the distribution system $\mathcal{G}_{\mathrm{D}} = (\mathcal{N}_{\mathrm{D}}, \mathcal{E}_{\mathrm{D}})$, transportation network $\mathcal{G}_{\mathrm{T}} = (\mathcal{N}_{\mathrm{T}}, \mathcal{E}_{\mathrm{T}})$, microgrids $m \in \mathcal{M}$ and depots $d \in \mathcal{D}$, MESSs $\omega \in \Omega$;

Generate scenarios and do scenario reduction to obtain $\mathcal{S}$;

▷ ***Rolling optimization***:

for each interval $t \in$ time horizon $\mathcal{T}_{\mathrm{H}}$ **do**

  Move forward the prediction horizon $\mathcal{T}_{\mathrm{P}}$;

  Update initial condition by the realization of uncertainties of $P_{\mathrm{D},i}^{t-1,\xi}$, $Q_{\mathrm{D},i}^{t-1,\xi}$, $\ddot{\mathcal{E}}_{\mathrm{D}}^{\xi}$, $\ddot{\mathcal{E}}_{\mathrm{T}}^{\xi}$ and actual decisions of $\zeta_{\hat{n}\check{n}}^{\omega}$, α_{ij}, $P_{\mathrm{ch},m}^{\omega,t-1}$, $P_{\mathrm{dch},m}^{\omega,t-1}$, $P_{\mathrm{DG},m}^{t-1}$, $Q_{\mathrm{DG},m}^{t-1}$ in the previous interval;

  for each scenario $s \in \mathcal{S}$ **do**

    Update the set of damaged branches $\ddot{\mathcal{E}}_{\mathrm{D}}^{s}$ and and the set of damaged roads $\ddot{\mathcal{E}}_{\mathrm{T}}^{s}$;

    for each MESS $\omega \in \Omega$ **do**

      Update MESS ω's current location;

      Compute path matrix $\mathfrak{P}^{\omega,s}$, distance matrix $\mathfrak{D}^{\omega,s}$ and time matrix $\mathfrak{T}^{\omega,s}$ via (4.1) - (4.3),

      Construct time-space network $\mathcal{G}_{\mathrm{S}}^{\omega,s} = (\mathcal{N}_{\mathrm{S}}^{\omega,s}, \mathcal{E}_{\mathrm{S}}^{\omega,s})$;

    end

  end

  The optimization problem over the prediction horizon $\mathcal{T}_{\mathrm{P}}$ is formulated as a two-stage stochastic MILP and solved by CPLEX:

$$\begin{aligned} &\min \ (4.41) \\ &\text{s.t. } (4.4) - (4.40) \end{aligned}$$

  Implement optimal solution $\zeta_{\hat{n}\check{n}}^{\omega\star}$, $\alpha_{ij}^{\star}$ in the first interval of $\mathcal{T}_{\mathrm{P}}$;

  Actual decisions for $P_{\mathrm{ch},m}^{\omega,t}$, $P_{\mathrm{dch},m}^{\omega,t}$, $P_{\mathrm{DG},m}^{t}$, $Q_{\mathrm{DG},m}^{t}$ are obtained by a deterministic re-optimization based on the implementation of $\zeta_{\hat{n}\check{n}}^{\omega}$, α_{ij} and realization of uncertainties of $P_{\mathrm{D},i}^{t,\xi}$, $Q_{\mathrm{D},i}^{t,\xi}$, $\ddot{\mathcal{E}}_{\mathrm{D}}^{\xi}$, $\ddot{\mathcal{E}}_{\mathrm{T}}^{\xi}$ in interval t;

end

return the solution $\zeta_{\hat{n}\check{n}}^{\omega\star}$, $P_{\mathrm{ch},m}^{\omega,t\star}$, $P_{\mathrm{dch},m}^{\omega,t\star}$, $\alpha_{ij}^{\star}$, $P_{\mathrm{DG},m}^{t\star}$, $Q_{\mathrm{DG},m}^{t\star}$ for the entire time horizon $\mathcal{T}_{\mathrm{H}}$.

Sioux Falls transportation network is proposed, as shown in Fig. 4.3. The distance of each edge in the transportation network is double. As the interfaces between the transportation network and distribution systems are microgrids, other buses and branches of the distribution systems can not directly be linked to the transportation network. Thus, only microgrids' locations are explicitly indicated in Fig. 4.3 and the boundary of distribution systems are drawn for illustration. Each distribution system has identical topologies (shown in Fig. 4.4) but different categories of loads such as residential (R), commercial (C) and industrial (I). Monte Carlo simulation is used to generate 2000 random scenarios, which are reduced to 10 scenarios as described in Section 4.3-B. The realization of damage and repair to the roads in the transportation network and the branches in distribution systems are depicted in Fig. 4.3 and 4.4, respectively. Fig. 4.5 shows predicted value of industrial, commercial and residential loads, as well as prediction intervals and actual realization.

The length of entire time horizon $\mathcal{T}_{\mathrm{H}}$ is set to 24-h while the length of prediction horizon $\mathcal{T}_{\mathrm{P}}$ is 12-h. Unit interruption costs are adopted to distinguish critical and non-critical loads, with \$10/kWh and \$2/kWh, respectively. Critical loads are randomly selected. The microgrid unit generation cost is \$0.5/kWh. The unit battery maintenance cost is \$0.2/kWh. The unit transportation cost is \$80/h. A depot is located at intersection node #10 in the transportation network. Microgrid set comprises four microgrids located at bus #14 in each distribution system and intersection nodes #2, #3, #17, #24 in the transportation network, respectively, as depicted in Fig. 4.3 and Fig. 4.4. The parameters for microgrids and the MESS fleet are described in Table 4.2 and Table 4.3, respectively.

In the remaining section, three sub-cases are considered to show the effectiveness of MESS mobility for service restoration as follows.

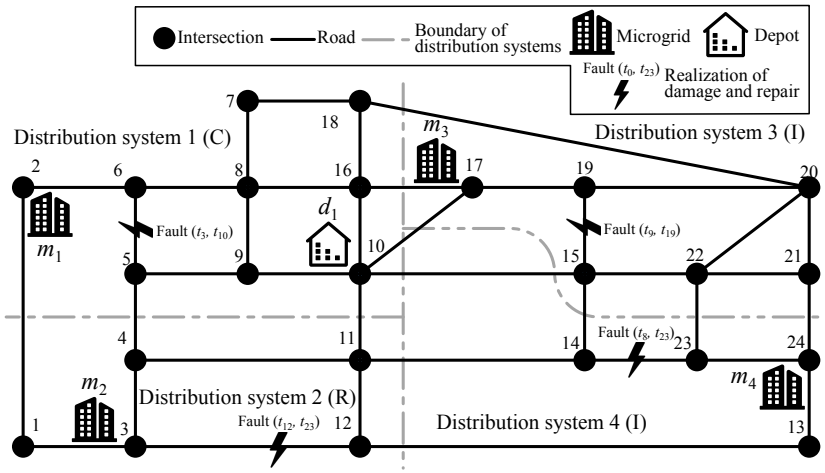

Figure 4.3: An integrated test system with a Sioux Falls transportation network connecting four distribution systems.

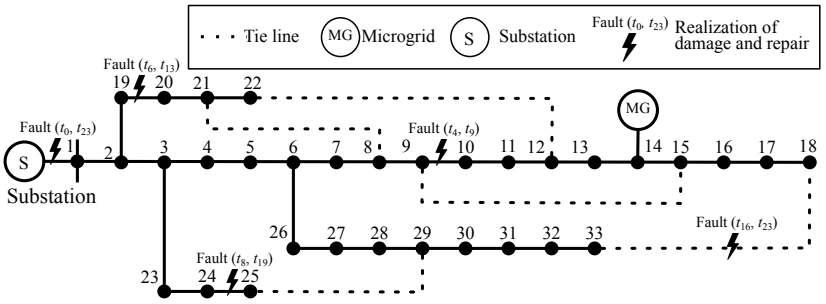

Figure 4.4: Distribution system: a modified 33-bus test system.

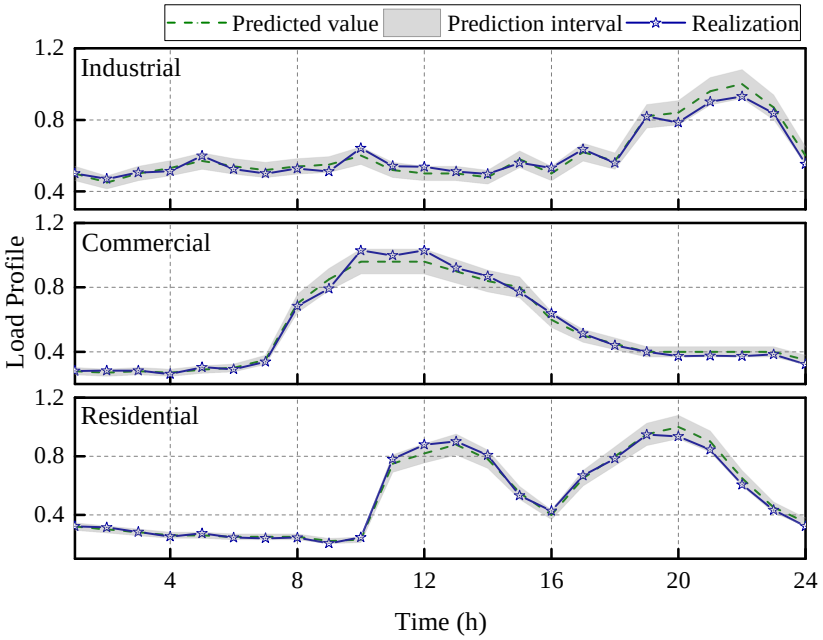

Figure 4.5: Load profile.

Table 4.2: Generation Resources and Local Loads for microgrids

Microgrid #		1	2	3	4
Generation	$\overline{P}_{\mathrm{DG},m}$ (MW)	1.80	1.60	1.80	1.60
	$\overline{Q}_{\mathrm{DG},m}$ (MVar)	1.35	1.20	1.35	1.20
	$\overline{E}_{\mathrm{DG},m}$ (MWh)	34.5	30.7	34.5	30.7
	$\underline{E}_{\mathrm{DG},m}$ (MWh)	3.5	3.0	3.5	3.0
Local load	Peak load (MW)	0.5			
	Power factor	0.9			
	Load type	C	R	I	I

Note: C - commercial, R - residential, I - industrial

Table 4.3: Parameters of the MESS fleet

MESS #	$\overline{P}^{\omega}_{\mathrm{ch}}$ / $\overline{P}^{\omega}_{\mathrm{dch}}$ (MW)	$\overline{E}^{\omega}_{\mathrm{c}}$ (MWh)	Initial SOC (%)	$\overline{SOC}^{\omega}$ / $\underline{SOC}^{\omega}$ (%)	$\eta^{\omega}_{\mathrm{ch}}/\eta^{\omega}_{\mathrm{dch}}$ (%)	V_{avg} (km/h)
1						20
2	0.5	2.0	50	90/10	95/95	30
3						40

Table 4.4: Comparison in Case I

Results		Case I-a)	Case I-b)	Case I-c)
Objective values ($)	Interruption cost	288535	272202	231662
	MG generation cost	58752	58752	58752
	Transportation cost	0	640	1920
	Battery maintenance cost	0	1022	2709
	Total cost	347287	332616	295043
Load restoration (%)	Critical	80.98	82.26	88.61
	Non-critical	41.73	43.57	36.24
	Total	58.33	59.62	59.48

Case I-a) There are no MESSs;

Case I-b) Allocation of MESSs;

Case I-c) Dynamic scheduling of MESSs.

B. Simulation Results

Table 4.4 compares the three cases in terms of objective value and load restoration.

Case I-a) There are no MESSs: The base case assumes that there are no MESSs, microgrids only use local generating resources for service restoration in

distribution systems. The total cost is $347287, restoration of critical, non-critical and total loads are 80.98%, 41.73%, 58.33%, respectively.

Case I-b) Allocation of MESSs: In the second case, resource allocation is introduced to dispatch MESSs from the depot to microgrids in the initial stage of restoration, then MESSs stay at the microgrid to coordinate with local stationary resources. The MESSs are dispatched to microgrids #2, #4 and #2, respectively, to provide support for local resources. In comparison with Case I-a), the total cost decreases by 4.22% to $332616 while incorporating MESSs only introduces about 1.4% additional energy. The restoration of critical, non-critical and total loads are 82.26%, 43.57%, and 59.62%, respectively. The results show the benefits of properly positioning MESSs to coordinate with microgrids for service restoration. However, after the allocation of MESSs from depots to microgrids, the MESSs is then served as stationary resources, the mobility and flexibility are underutilized.

Case I-c) Dynamic scheduling of MESSs: This case co-optimize the dynamic scheduling of MESSs, resource dispatching of microgrids and network reconfiguration. The total cost reduces by 11.29% than Case I-b) to $295043. All the microgrid generation costs in the three cases are the same, this is due to the fact that three cases have the same condition of energy capacity $\overline{E}_{\mathrm{DG},m}$ and minimum reserve $\underline{E}_{\mathrm{DG},m}$ in corresponding microgrids, and the results indicate that all the microgrids get to the minimum reserve and are fully utilized for service restoration. The restoration of critical, non-critical and total loads are 88.61%, 36.24% and 59.48%, respectively. It is noted that the total load restoration is a little bit less than Case I-c), this is because MESSs transport energy among microgrids and have more charging/discharging behaviors, thus having more charging/discharging losses.

Fig. 4.6 provides the charging/discharging schedule with respect to the

position of MESS. The bar shows the charging/discharging active power while the dash lines with asterisks and right Y-axis indicates the MESSs' movements. The d1 represents the depot and m1-m4 represent microgrid #1 - #4, respectively. In contrast to the allocation of MESSs in Case I-b), the dynamic scheduling of MESSs optimizes the sequence of movements and associated charging/discharging behaviors. Since the limited power and energy capacity, the MESSs need to move among microgrids back and forth considering the transportation cost.

For instance, MESS #1 initially starts from depot #1 to microgrid #3 in (00:00-01:00) and discharges in (01:00-02:00). Then it takes three intervals to get to microgrid #1 and stay there to charge in (04:00-06:00), followed by going to microgrid #2 to discharge. Next, it moves back to microgrid #2 to achieve energy transfer. Finally, it returns to depot #1 in (22:00-24:00). It is also observed that the MESS #1 is mainly dispatched back and forth between microgrid #1 and #2, MESS #2 is mainly back and forth between microgrid #3 and #4, while MESS #3 generally moves among more locations (microgrid #1-#3). This is due to the difference in the average speed of MESSs, as compared to MESS #1 and #2, MESS #3 is faster and more effective to transfer energy among microgrids.

Fig. 4.7 denotes the coordinated generation dispatch and load restoration in each distribution system. By coordinating multiple sources, the generation capacities are fully utilized to restore critical loads with higher customer interruption cost. Fig. 4.8 describes the energy transfer among microgrids through charging or discharging of MESSs. A microgrid with positive energy transfer means it receives energy from MESSs whereas negative one means outputting energy from this microgrid. It is observed that energy transfer is mainly from microgrids #1, #3 to microgrids #2, #4.

(a) Effect of Temporal-spatial Dynamics of MESSs

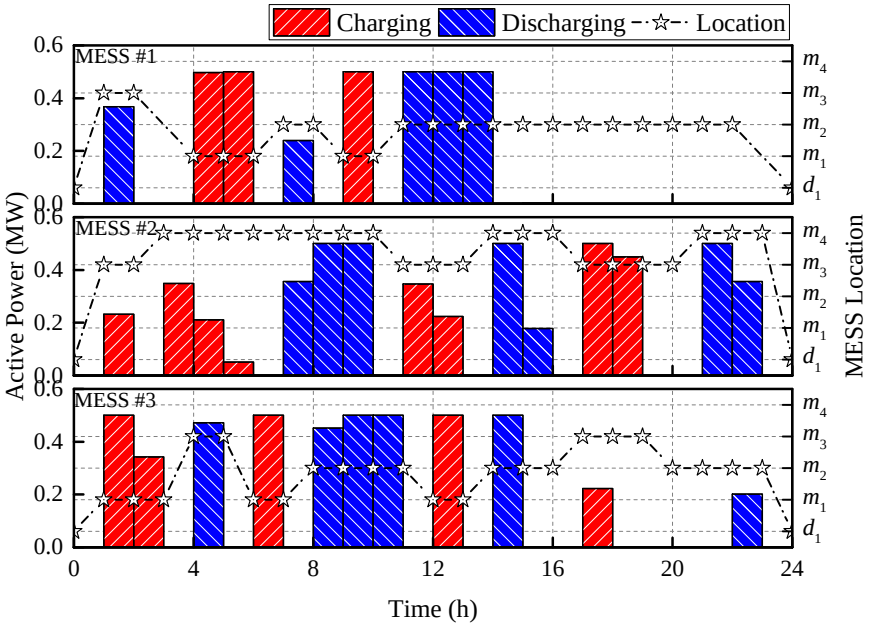

Figure 4.6: Scheduling results of the MESS fleet in Case I-c).

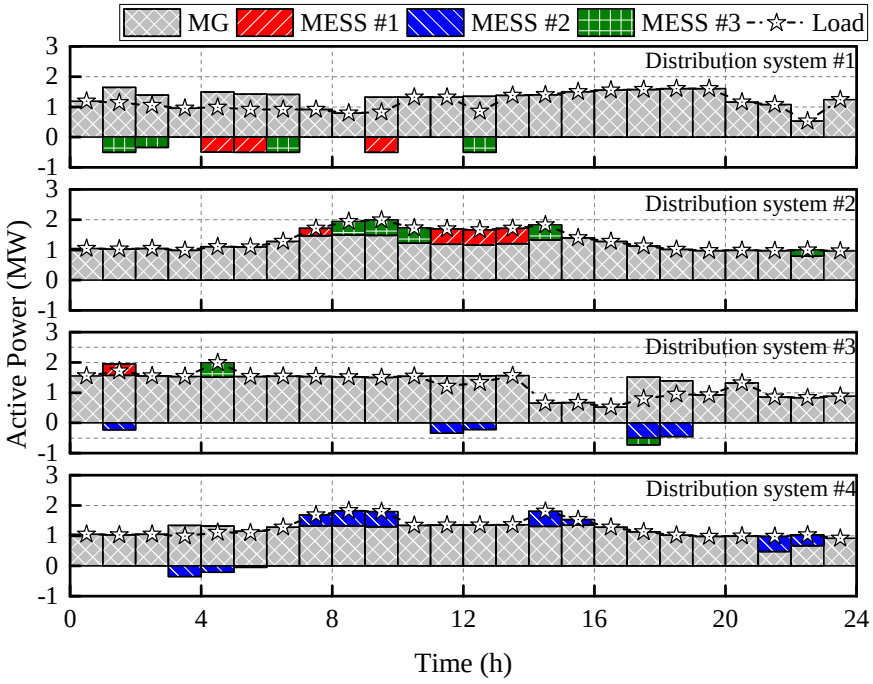

Figure 4.7: Coordinated generation dispatch and load restoration in Case I-c).

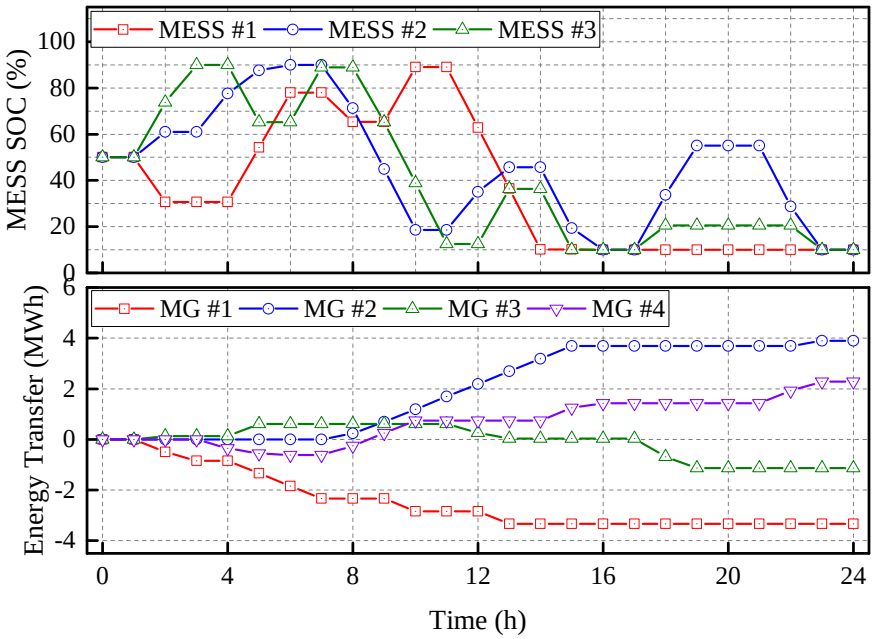

Figure 4.8: Energy transfer through MESSs in Case I-c).

The simulation demonstrates that MESSs supplement energy by charging from some microgrids with relatively surplus resources and transfer to other microgrids to minimize the total cost. During the restoration process, the energy imbalance between distribution systems is caused by topology and operation constraints, which impedes the effective utilization of local stationary resources. Therefore, the integration of MESSs and coordination with microgrids can make the most of MESSs mobility to deal with the energy imbalance. MESSs can transfer power and energy among microgrids to restore critical loads and reduces system total costs. It can be seen in Table 4.4 that total load restoration for Case I-b) and Case I-c) are almost the same whereas the load restoration for critical loads increases by 6.93% and 5.37% in Case I-c) than Cases I-a) and I-b) because MESSs mobility is better utilized to serve more critical loads. For instance, the MESS #3 initially moves to microgrid #1 from depot #1 and charges in (01:00-03:00) to get to maximum SOC of 90% (see Fig. 4.6 and Fig. 4.8). Next it moves to microgrid

#3 to discharge, with SOC reduced to 65.19%. Then it moves back and forth between microgrid #1 and #2 in (06:00-16:00) to transfer energy from microgrid #1 to #2. The SOC ranges from 10% to 88.94% and MESS #3 is fully discharged to the minimum SOC of 10% at 15:00. Next it moves to microgrid #3 to charge and back to microgrid #2 to discharge. So the energy is mainly transferred from microgrids #1 and #3 to microgrid #2. Similar temporal-spatial dynamics and associated charging/discharging behaviors can be observed for other MESSs.

Also, it is noticed that MESSs can perform load shifting within the same microgrid. For example, MESS #2 charges at microgrid #4 in (03:00-06:00) and discharges at the same location in (07:00-10:00). This is because the load is relatively low during some intervals, so MESS #2 charges in energy sufficient hours and prepares for peak hours to obtain effective use of energy resources in microgrid #4.

The comparison of three cases highlights the importance of effective utilization of MESSs mobility. The integrated restoration strategy reduces the total cost by coordinating the dynamic scheduling of MESSs, resource dispatching of microgrids and distribution network reconfiguration. In comparison with the allocation of MESSs only in the very initial stage of the restoration process, the MESSs mobility is fully utilized by dynamic scheduling to deal with energy imbalance in distribution systems posed by topology and operation constraints.

(b) Impact of Damage and Repair to Branches

To consider the subsequent damage and repair to branches in distribution systems, the system damage status is updated at each interval and the network topology is reconfigured, as shown in Fig. 4.9. For example, there are two faults in distribution system #3 at $t = 5$: substation fault and damage to branch (9, 10). The opening line switches are (6, 7), (8, 9), (27, 28), (30, 31), as shown in Fig.

4.9(a). At $t = 6$, new damage to branch (19, 20) occurs, and the distribution system #3 is reconfigured to new topology with opening switches (4, 5), (6, 7), (13, 14), as shown in Fig. 4.9(b). Similarly, subsequent damage to branches (24, 25), (18, 33) change the network topology and reconfiguration is needed.

In addition, the repair to branches is considered. Once the repair is finished, the branch can be controlled again. For example, as shown in Fig. 4.9(c), branch (9, 10) is repaired at $t = 10$, and the topology is reconfigured by opening switches (9, 15), (12, 22), (27, 28). At $t = 20$, branch (24, 25) is repaired, the distribution network takes the new topology and switches (6, 26), (8, 21), (9, 10), (12, 22) are open.

(c) Impact of Damage and Repair to Roads

Extreme events also cause damage to transportation networks, which in turn will impact the scheduling of the MESS fleet. In order to leverage the updated information on subsequent damage and repair to roads, the scheduling of the MESS fleet is optimized at each interval over the prediction horizon based on the updated information and current locations. The scheduling results are shown in Fig. 4.10(a). In general, MESSs have two choices when damage occurs, one is to discard the original scheduling and be rescheduled to another microgrid, the other option is to be rerouted to the original destination via a different route. For example, the MESS #1 is dispatched from microgrid #3 to microgrid #2 at $t = 2$, as depicted by the blue dot line. At $t = 3$, the current location of MESS #1 is obtained, shown as the blue node in Fig. 4.10(a). The subsequent damage causes road 5-6 to fail, thus the originally designated route is no longer available. The optimization takes into account the updated information and the current location, consequently MESS #1 is rescheduled to microgrid #1 via a new route, as depicted by the green dot line. Meanwhile, MESSs can be rerouted to the

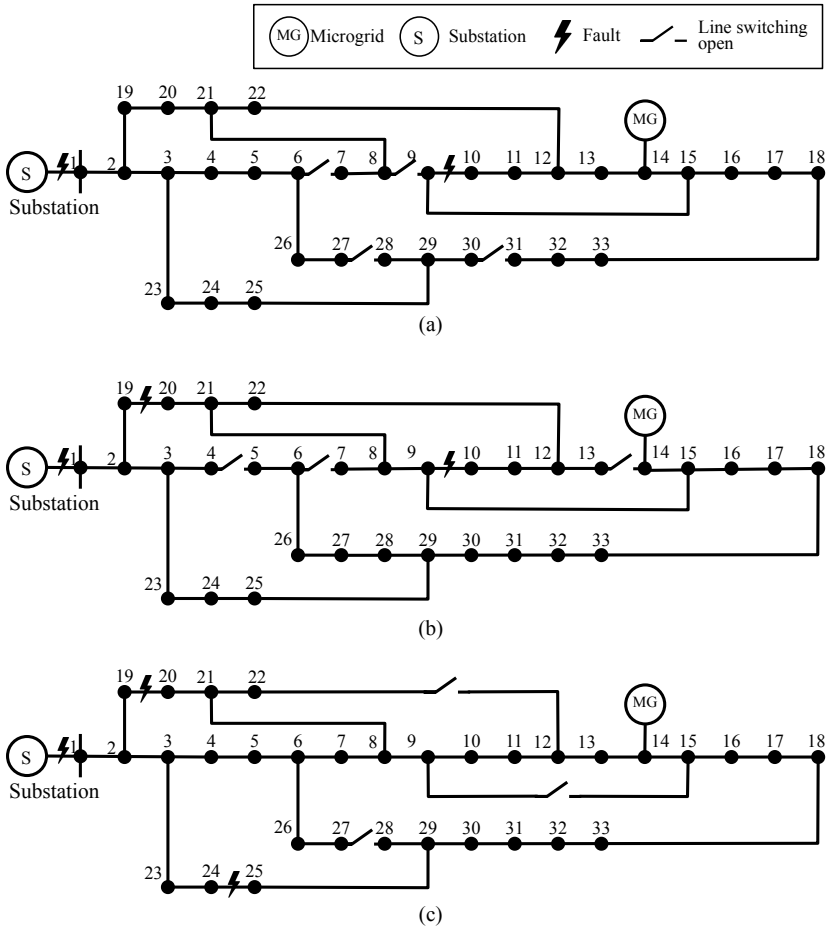

Figure 4.9: Network reconfiguration for distribution system #3: (a) t=5, faults: substation, branch (9, 10); (b) t=6, faults: substation, branches (9, 10), (19, 20); (c) t=10, faults: substation, branches (19, 20), (24, 25), repair: branch (9, 10).

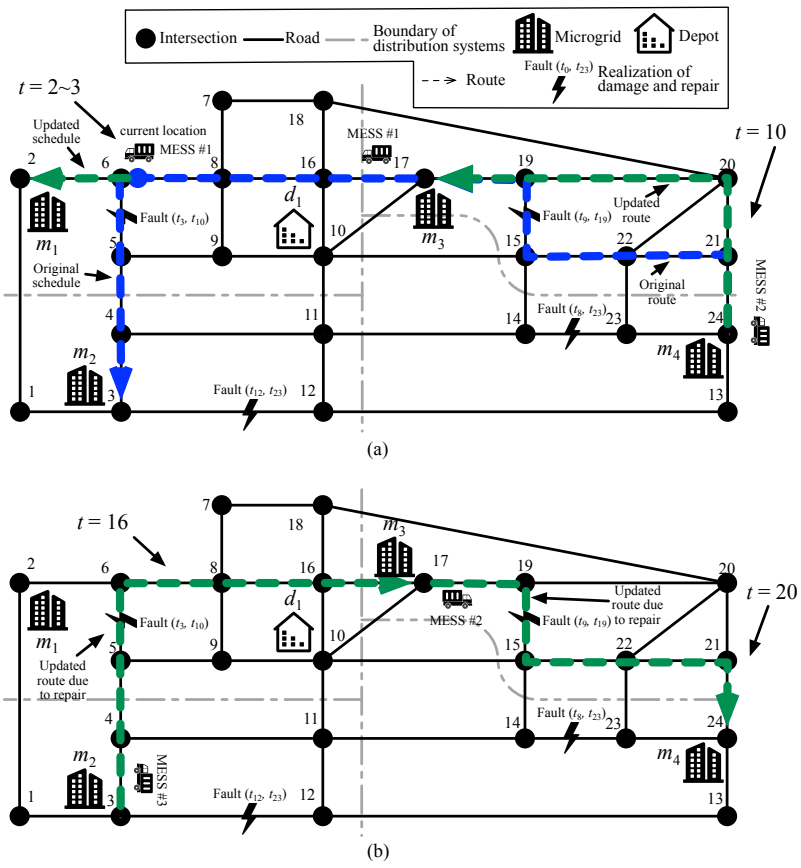

Figure 4.10: Impact analysis of damage and repair to roads: (a) impacts of damage to roads on vehicle scheduling and routing, (b) impacts of repair to roads on vehicle scheduling and routing.

same destination when damage occurs. The originally designated route for MESS #2 from microgrid #4 to microgrid #3 is shown by the blue dash line. The road (15, 19) is damaged at $t = 10$, so the MESS #2 takes another route to microgrid #3, which is depicted by the green dash line in Fig. 4.10(a).

In addition, Fig. 4.10(b) illustrates the impact of repair to roads. Once a road is repaired, scheduling and routing of the MESS fleet can be updated. At $t = 16$, the road 5-6 is repaired and available again, thus the MESS #3 is dispatched from microgrid #2 to #3 via the designated route, which is represented by the green dash line. Similarly, after the repair of road 15-19, MESS #2 is dispatched from microgrid #3 to microgrid #4 via the route with the shortest travel time.

The results reveal the flexibility of the proposed model that MESS fleets can be rescheduled or rerouted at each interval considering the damage and repair to roads.

(d) Sensitivity Analysis of Scenario Generations

The stability test is adopted to verify the effectiveness of scenario trees to represent the uncertainties [104]. A sensitivity analysis with varying number of scenarios is carried out on the integrated test system. The stability requirements is to have small optimality gaps and approximately same optimal objective value [104]. Fig. 4.11 shows that the solution is stable as the variation range is small. Therefore, the scenario tree with 10 scenarios can be suitable for the stochastic programming problem.

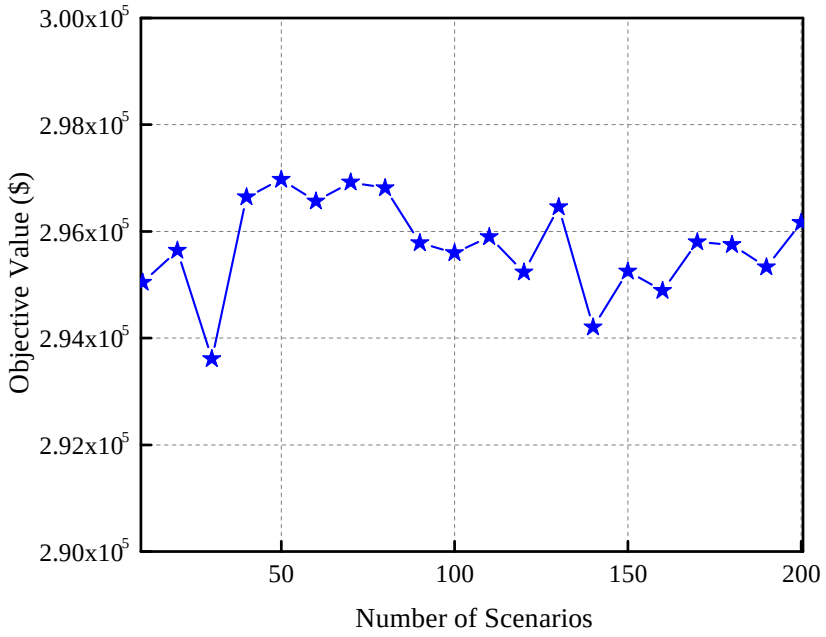

Figure 4.11: Evaluation of scenario generation.

4.4.2 Case II: Singapore Transportation Network with Six 33-bus Distribution Systems

A. Test systems

To verify the scalability of the proposed integrated restoration strategy, the case study on an integrated test system with Singapore transportation network connecting six 33-bus distribution systems is carried out for illustration. Each distribution system has one microgrid located at bus 14. Fig. 4.12 shows the transportation network with microgrids and depots' locations. The Python client for Google Maps API [105] is used to retrieve geospatial data for Singapore transportation network. Six microgrids and two depots are located across the map. Microgrids #5 and #6 have the same properties as Microgrids #1 and #3, respectively. A fleet of five MESSs is considered, with three MESSs initially

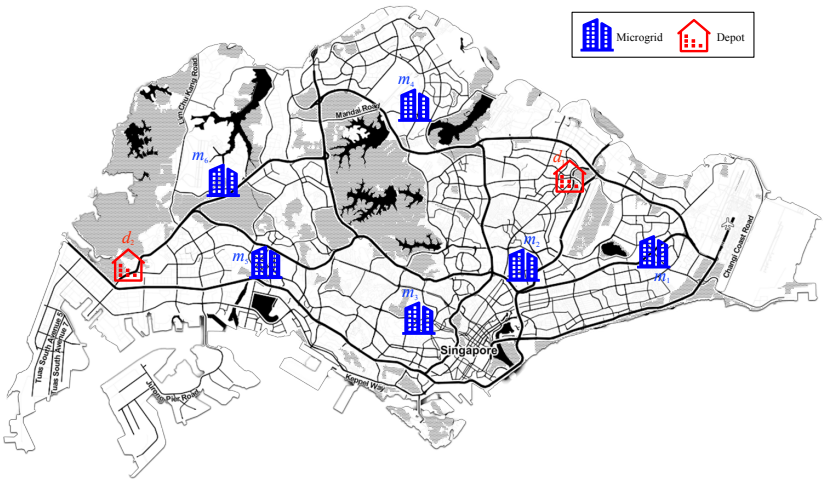

Figure 4.12: Singapore transportation network with microgrids and depots.

located at depot #1, and the other two at depot #2. Other parameter settings follow the Case I-c). Similarly, three cases are implemented as follows.

Case II-a) There are no MESSs;

Case II-b) Allocation of MESSs;

Case II-c) Dynamic scheduling of MESSs.

B. Simulation Results

Table 4.5 depicts the objective value and load restoration in Case II. The total costs in Case II-c) reduce by 16.89% than Case II-a) and 13.91% than Case II-b). In Case II-c), the restoration of critical, non-critical and total loads are 91.64%, 48.92% and 61.66%, respectively. More critical loads with higher importance are restored. Fig. 4.13 depicts the scheduling results for the MESS fleet. The dynamic scheduling optimizes the sequence of movements and charging/discharging behaviors. MESSs get charged from some microgrids with surplus resources and transport energy to other microgrids to minimize the total system cost. Fig. 4.14

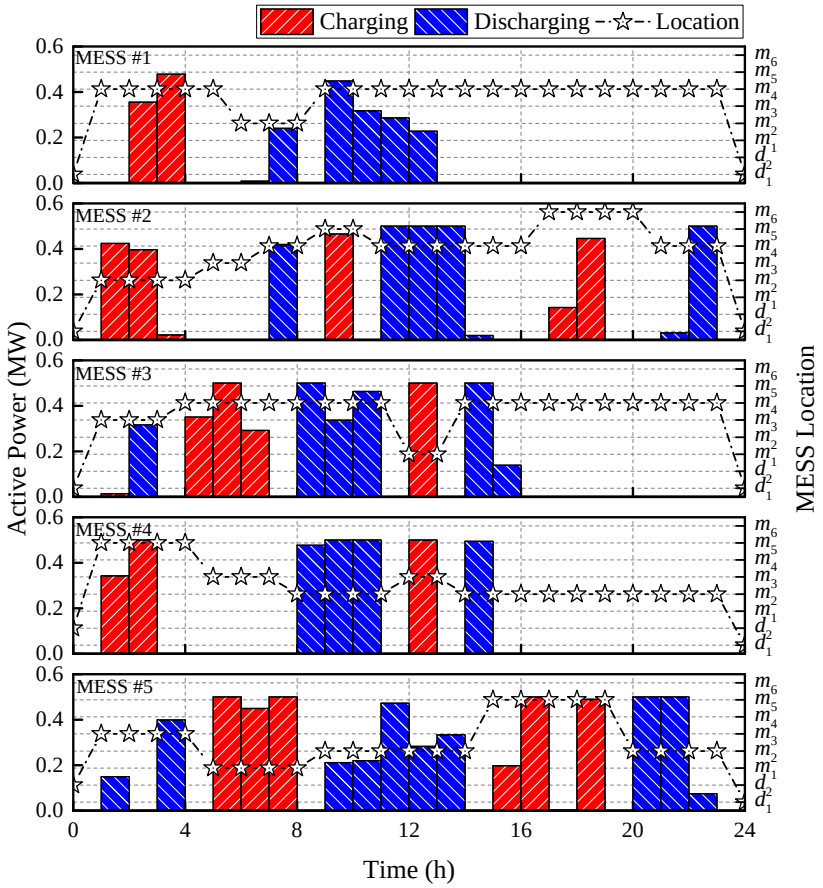

Figure 4.13: Scheduling results of the MESS fleet in Case II-c).

Table 4.5: Comparison in Case II

	Results	Case II-a)	Case II-b)	Case II-c)
Objective values ($)	Interruption cost	362892	344747	280455
	MG generation cost	87990	87990	87990
	Transportation cost	0	800	2320
	Battery maintenance cost	0	1694	3947
	Total cost	450882	435231	374712
Load restoration (%)	Critical	81.12	85.62	91.64
	Non-critical	51.03	56.48	48.92
	Total	60.01	61.85	61.66

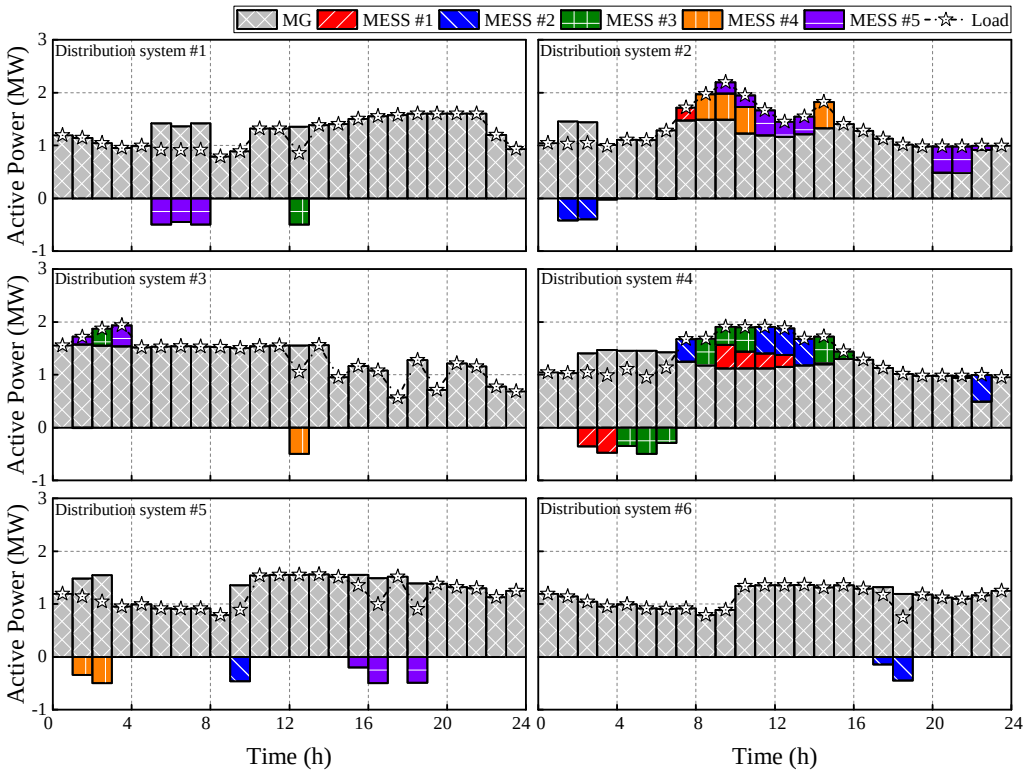

Figure 4.14: Coordinated generation dispatch and load restoration in Case II-c).

shows the coordinated generation dispatch and load restoration. By coordinating stationary and mobile resources, the generation capacities of microgrids and MESSs are better utilized for service restoration.

The simulation results demonstrate the potential applications of the proposed integrated restoration strategy to enhance distribution system resilience.

4.5 Conclusions

This chapter proposes a rolling integrated service restoration strategy to minimize the total system cost by coordinating MESS fleets, microgrids and distribution systems. The proposed service restoration strategy takes into account damage and repair to both the roads in transportation systems and the branches in distribution systems. The uncertainties in load consumption and the status of roads and branches are considered to generate scenarios using Monte Carlo simulation method. A rolling optimization framework is adopted to consider subsequent damage and repair during the restoration process. The operation of MESS fleets is modeled by a stochastic multi-layer time-space network technique and MESS fleets can be rescheduled and rerouted at each interval. The coordinated scheduling at each interval over the prediction horizon is formulated as a two-stage stochastic MILP. The simulation results demonstrate the effectiveness of MESSs mobility that transfers energy across multiple distribution systems and coordinates with microgrids during the disasters, and highlight that the mobile and stationary resources can be well coordinated to enhance distribution system resilience.

Chapter 5

Resilient Service Restoration in Microgrids Considering Mobile Energy Storage Fleets: A Deep Reinforcement Learning Approach

MESSs provide mobility and flexibility to enhance distribution system resilience. The chapter proposes an MDP formulation for an integrated service restoration strategy that coordinates the scheduling of MESSs and resource dispatching of microgrids. The uncertainties in load consumption are taken into account. The DRL algorithm is utilized to solve the MDP for optimal scheduling. Specifically, the DDPG and TD3 are applied to train the deep Q-network and policy network, then the well-trained policy can be deployed in on-line manner to perform multiple actions simultaneously. The proposed model is demonstrated on an integrated test system with three microgrids connected by Sioux Falls transportation network. The simulation results indicate that mobile and stationary energy resources can be well coordinated to improve system resilience.

5.1 Introduction

Recent major blackouts caused by extreme events lead to catastrophic consequences for the economy and society [9]. Load restoration is of paramount importance in resilient smart grids [11]. When severe blackouts occur, a variety of local resources, e.g., microgrids and DERs (ESSs, etc.), can be utilized to restore critical loads in distribution systems. Moreover, the emerging MESSs [20] can provide temporal-spatial mobility and coordinate with stationary local resources for an integrated distribution system restoration. Great progress has been made in coordinating multiple energy resources to effectively restore electricity supply to critical loads after major blackouts [38]. Microgrids are well utilized to consolidate stationary energy resources [14]. Moreover, with the increasing installation of charging/discharging facilities [67], microgrids can provide plug-and-play integration of MESSs for effective service restoration. MESSs are generally vehicle-mounted container battery ESSs with standard interfaces that allow for plug-and-play [20]. The importance of integrating mobile energy resources into critical load restoration in smart grid has been increasingly recognized in recent studies [60], [66], [106]. Reference [62] formulates a proactive resource allocation scheme of electric buses and transportable batteries to restore critical loads. Reference [64] proposes a microgrid-based critical load restoration by adaptively forming microgrids and positioning mobile emergency resources after power disruptions. Reference [65] implements resilient routing and scheduling of mobile power sources via a two-stage framework. A resilient scheme for disaster recovery logistics is proposed in [66], involving scheduling of repair crews and mobile power source and network reconfiguration. Reference [67] presents a joint post-disaster restoration scheme for distribution systems with critical loads by integrating the dynamic scheduling of MESSs. Reference [107]

proposed a rolling horizon-based integrated restoration strategy to effectively restore electricity supply to critical loads by MESSs considering uncertainties. However, the optimal scheduling is generally formulated as a mixed-integer convex program, which is NP-hard and computationally expensive, in terms of a large number of integer or binary variables in large-scale systems [108]. In addition, accurate forecast information is necessary in the optimization model [109].

Recent advances in DRL give rise to tremendous success in solving challenging decision-making problems [110]–[112]. In general, the decision-making problem under uncertainties is formulated using MDPs [113] and solved iteratively by data-driven DRL algorithms [111]. The application of DRL in energy management systems has been increasingly recognized. Reference [114] presents a reinforcement learning approach for optimal distributed energy management in a microgrid. A DRL-based economic dispatch in microgrid is proposed in [115]. Reference [116] developed an MDP formulation for the joint bidding and pricing problem and applied DRL algorithm to solve it. Reference [108] proposes a demand response for home energy management based on DRL. Optimal energy management strategies for energy internet via DRL are demonstrated in [117]. An MDP formulation for electrical vehicle charging is proposed to jointly coordinate a set of charging stations [118]. However, research in this area is still in the early stage, the benefit of applying DRL in coordinated scheduling of stationary and mobile energy resources has not yet been fully investigated and further studies are needed.

To address the aforementioned issue, a novel MDP formulation for critical load restoration in microgrids is proposed considering the stationary and mobile energy resources. Uncertainties in load consumption are taken into account. The agent aims to maximize the service restoration in microgrids by jointly coordinating the resource dispatching of microgrids and scheduling of MESS. The MESS fleets

are dynamically dispatched among microgrids for load restoration in coordination with microgrid operation. The proposed model is solved by TD3 [119], which is an actor-critic algorithm that can deal with discrete or continuous variables in state and action space.

The remainder of this chapter is organized as follows. Section 5.2 mathematically describes the scheduling of MESSs and integrated service restoration strategy. Section 5.3 develops the MDP formulation and DRL algorithm. Section 5.4 provides case studies and this chapter is concluded in Section 5.5.

5.2 Mathematical modeling

5.2.1 Uncertainty Modeling

Uncertainties have been considered including forecasting errors in load consumption. A normal distribution is used to represent the forecasting error of load consumption [39]. At each time step t, the load will be simulated as exogenous information input. It is worth noting that the learning-based approach, which is illustrated later in Section 5.3, does not rely on prior knowledge of the random variables and can be adaptive to different uncertainty modeling methods.

5.2.2 Scheduling of Mobile Energy Storage Fleets

A transportation network is modeled as a weighted graph $\mathcal{G}_{\mathrm{T}} = (\mathcal{N}_{\mathrm{T}}, \mathcal{E}_{\mathrm{T}}, \mathcal{W}_{\mathrm{T}})$, where $\mathcal{N}_{\mathrm{T}}$ is the nodes set, while $\mathcal{E}_{\mathrm{T}}$ denotes the edges set of roads with the edge distance $w \in \mathcal{W}_{\mathrm{T}}$. A set of microgrids $\mathcal{M}$ indexed by m and a set of depots $\mathcal{D}$ are located in the transportation network $\mathcal{G}_{\mathrm{T}}$. Location mappings $f_{\mathrm{M}} : \mathcal{M} \rightarrow \mathcal{N}_{\mathrm{T}}$ and $f_{\mathrm{D}} : \mathcal{D} \rightarrow \mathcal{N}_{\mathrm{T}}$ denotes microgrids and depots' locations in the transportation

network, respectively. Ω represents an MESS fleet. An MESS $\omega \in \Omega$ is initially located at a depot $d \in \mathcal{D}$, where it starts and travels among microgrids to provide power supply to power grids, finally it goes back to a depot.

The scheduling of MESS fleets is defined as a sequence of trips. An MESS ω's current location at t is represented by n_ω^t, which is generally defined as the node in the transportation network [120]. In addition, MESS may change destination during its' movement without having to arrive at the next destination, that is, MESS may be on the edge at t, so the location of MESS is defined as $n_\omega^t \in \mathcal{N}_\mathrm{T} \cup \{(\hat{n}, \delta_{\hat{n}}, \check{n}, \delta_{\check{n}}) | (\hat{n}, \check{n}) \in E_\mathrm{T}, \delta_{\hat{n}} + \delta_{\check{n}} = w_{\hat{n}\check{n}}, \delta_{\hat{n}} \geq 0, \delta_{\check{n}} \geq 0\}$, where the $\{(\hat{n}, \delta_{\hat{n}}, \check{n}, \delta_{\check{n}}) | (\hat{n}, \check{n}) \in E_\mathrm{T}, \delta_{\hat{n}} + \delta_{\check{n}} = w_{\hat{n}\check{n}}, \delta_{\hat{n}} \geq 0, \delta_{\check{n}} \geq 0\}$ denotes a location on the edge $(\hat{n}, \check{n}) \in E_T$, $\delta_{\hat{n}}$ and $\delta_{\check{n}}$ depict the location's distance to corresponding nodes, and $w_{\hat{n}\check{n}}$ represents the edge length.

The movement decision for MESS ω at t is to designate the destination κ_ω^t, which specifies the destination to one of microgrids or stations. The MESS ω moves from the current location n_ω^t and follows the movement decision κ_ω^t to the designated destination. And It is assumed that the MESS ω always takes the shortest path, which is determined by the Dijkstra's algorithm [93]. Therefore, a location function f_L is defined to obtain the next location n_ω^{t+1} in graph G_T, by using Dijkstra algorithm based on current location n_ω^t and designated destination κ_ω^t. Thus, we have

$$n_\omega^{t+1} = f_\mathrm{L}(n_\omega^t, \kappa_\omega^t), \forall \omega, t \tag{5.1}$$

where $\kappa_\omega^t \in \mathcal{M} \cup \mathcal{D}$ is a categorical variable indicating the destination to microgrids or depots.

Binary variables $\zeta_{\omega m}^t$ denote if MESS ω stays at microgrid m during the

interval t, which is described as follows.

$$\zeta_{\omega m}^{t} = \begin{cases} 1, & \text{If } n_{\omega}^{t} = n_{\omega}^{t+1} \text{ and } n_{\omega}^{t} \in f_{\mathrm{M}}(m) \\ 0, & \text{Otherwise} \end{cases}, \forall \omega, m, t \tag{5.2}$$

MESS fleets can exchange power with microgrids by charging from or discharging to microgrids. The operation constraints are described as follows.

$$\sum_{m \in M} \zeta_{\omega m}^{t} \leq 1, \forall \omega, t \tag{5.3}$$

$$-\overline{P}_{\mathrm{ch}}^{\omega} \sum_{m \in M} \xi_{\omega m}^{t} \leq P_{\omega}^{t} \leq \overline{P}_{\mathrm{dch}}^{\omega} \sum_{m \in M} \xi_{\omega m}^{t}, \forall \omega, t \tag{5.4}$$

$$\mathrm{SOC}_{\omega}^{t+1} = \begin{cases} \mathrm{SOC}_{\omega}^{t} - \frac{\eta_{\mathrm{ch}}^{\omega} P_{\omega}^{t}}{E_{\mathrm{c}}^{\omega}} \Delta_t, & \text{if } P_{\omega}^{t} < 0 \\ \mathrm{SOC}_{\omega}^{t} - \frac{P_{\omega}^{t}}{\eta_{\mathrm{dch}}^{\omega} E_{\mathrm{c}}^{\omega}} \Delta_t, & \text{if } P_{\omega}^{t} \geq 0 \end{cases}, \forall \omega, t \tag{5.5}$$

$$\underline{\mathrm{SOC}}_{\omega} \leq \mathrm{SOC}_{\omega}^{t} \leq \overline{\mathrm{SOC}}_{\omega}, \forall \omega, t \tag{5.6}$$

where P_{ω}^{t} represents the charging/discharging power of MESS ω from/to microgrid m at interval t, negative power depicts that MESS charges from microgrids while positive power means that MESS discharge to microgrid. $\overline{P}_{\mathrm{ch}}^{\omega}$ and $\overline{P}_{\mathrm{dch}}^{\omega}$ are maximum charging/discharging power of MESS ω. $\mathrm{SOC}_{\omega}^{t}$ indicates the state-of-charge (SOC) of MESS ω at time point t. $\underline{\mathrm{SOC}}_{\omega}$ and $\overline{\mathrm{SOC}}_{\omega}$ provide the prescribed minimum and maximum level of SOC. $\eta_{\mathrm{ch}}^{\omega}$ and $\eta_{\mathrm{dch}}^{\omega}$ are charging/discharging efficiency. Constraints (5.3) indicates that an MESS can only stay at no more than one microgrid, which is also implicated in the Equation (5.2). Constraint (5.4) shows the relation between charging/discharging and temporal-spatial behaviors. That is, only when staying at a microgrid m can MESS ω charge or discharge to exchange power. Equation (5.5) calculates the SOC of MESS ω and Constraint (5.6) sets the upper and lower bound for SOC.

5.2.3 Joint Service Restoration

The operation constraints of microgrids are as follows.

$$P^t_{\mathrm{dg},m} + \sum_{\omega\in\Omega} \xi^t_{\omega m} P^t_{\omega} = P^t_{\mathrm{r},m}, \forall m, t \tag{5.7}$$

$$Q^t_{\mathrm{dg},m} = Q^t_{\mathrm{r},m}, \forall m, t \tag{5.8}$$

$$0 \le P^t_{\mathrm{r},m} \le P^t_{\mathrm{load},m}, \forall m, t \tag{5.9}$$

$$Q^t_{\mathrm{r},m} = P^t_{\mathrm{r},m} \tan\Big(\cos^{-1}\varphi_m\Big), \forall m, t \tag{5.10}$$

$$0 \le P^t_{\mathrm{dg},m} \le \overline{P}_{\mathrm{dg},m}, \forall m, t \tag{5.11}$$

$$-\overline{Q}_{\mathrm{dg},m} \le Q^t_{\mathrm{dg},m} \le \overline{Q}_{\mathrm{dg},m}, \forall m, t \tag{5.12}$$

$$E^{t+1}_{\mathrm{dg},m} = E^t_{\mathrm{dg},m} - P^{t+1}_{\mathrm{dg},m}\Delta t, \forall m, t \tag{5.13}$$

$$\underline{E}^{\min}_{\mathrm{dg},m} \le E^t_{\mathrm{dg},m} \le \overline{E}_{\mathrm{dg},m} \forall m, t \tag{5.14}$$

where $P^t_{\mathrm{dg},m}, Q^t_{\mathrm{dg},m}$ are the active/reactive power generation of equivalent dispatchable DG in microgrid m in interval t, respectively. $\overline{P}_{\mathrm{dg},m}, \overline{Q}_{\mathrm{dg},m}$ are the maximum active/reactive power generation, respectively. $P^t_{\mathrm{r},m}, Q^t_{\mathrm{r},m}$ are active/reactive load restoration in microgrid m, respectively. φ_m is the power factor. $E^t_{\mathrm{dg},m}$ is the energy of equivalent DG. $\overline{E}^t_{\mathrm{dg},m}$ and $\underline{E}^t_{\mathrm{dg},m}$ are the energy capacity and minimum energy reserve in microgrid m. Constraints (5.7)-(5.8) describe the active/reactive power balance at microgrid m in interval t. It takes into account the power generation of dispatachable DG and mobile energy storage by considering if the location of MESSs. Equations (5.9)-(5.10) constrain the load restoration and power factor. Constraints (5.11)-(5.12) depict the power generation capacity. Equation (5.13) calculates the energy in each microgrid. Constraint (5.14) presents the upper and lower bounds of energy.

The objective is formulated as follows to minimize the system overall cost.

$$\min \sum_{t\in T}\Bigg[\sum_{m\in\mathcal{M}} W_m(P^t_{\text{load},m}-P^t_{\text{r},m})+\sum_{m\in\mathcal{M}} C_{\text{gen},m}P^t_{\text{dg},m} + \sum_{\omega\in\Omega} C_{\text{bat},\omega}|P^t_{\omega}|+\sum_{\omega\in\Omega} C_{\text{tran},\omega}(1-\sum_{m\in\mathcal{M}}\zeta^t_{\omega m})\Bigg]\Delta T \tag{5.15}$$

where the overall cost is composed of four parts. The first term $\sum_{t\in T}\sum_{m\in\mathcal{M}} W_m(P^t_{\text{load},m}-P^t_{\text{r},m})$ represents the customer interruption cost. $\sum_{t\in T}\sum_{m\in\mathcal{M}} C_{\text{gen},m}P^t_{\text{dg},m}$ is the microgrids generation cost. The third term $\sum_{t\in T}\sum_{\omega\in\Omega} C_{\text{bat},\omega}|P^t_{\omega}|$ shows the MESS battery maintenance cost. The last term $\sum_{t\in T}\sum_{\omega\in\Omega} C_{\text{tran},\omega}V_{\text{avg},\omega}(1-\sum_{m\in\mathcal{M}}\zeta^t_{\omega m})$ calculates the transportation cost of MESSs.

5.3 Deep Reinforcement Learning Algorithm

5.3.1 Markov Decision Process

The sequential decision-making problem in a stochastic environment is formulated by MDPs. In an MDP, an agent observes the state s_t at each time step $t \in \mathcal{T}$ and continually interacts with an environment by following a policy π to select actions a [111]. In response to the actions, the environment presents new states s_{t+1} and give rise to rewards r_t to the agent. An MDP is defined by a 4-tuple $(\mathcal{S},\mathcal{A},\mathcal{P},\mathcal{R})$, where $\mathcal{S},\mathcal{A},\mathcal{P},\mathcal{R}$ are the state space, action space, transition probability functions that satisfy Markov property [113] (i.e., the next state is only dependent on present state and action), and reward functions. The detailed formulation is described as follows.

A. State

The state is a vector reflecting current state of the system, involving time step t, load information $P^t_{\text{load},m}$, the MESSs' location n^t_ω, SOC of MESSs SOC^t_ω and energy in microgrids $E^t_{\text{dg},m}$. The state vector is defined as:

$$s_t = \{t, P^t_{\text{load},m}, n^t_\omega, \text{SOC}^t_\omega, E^t_{\text{dg},m}\} \in \mathcal{S} \tag{5.16}$$

B. Action

The action is a vector consisting of decision variables on the designated destination of MESSs κ^t_ω, charging/discharging behavior of MESSs P^t_ω and generation output in microgrids $P^t_{\text{dg},m}$. The action vector is defined as

$$a_t = \{\kappa^t_\omega, P^t_\omega, P^t_{\text{dg},m}\} \in \mathcal{A} \tag{5.17}$$

I t is noted that κ^t_ω represents categorical action and needs to be one-hot encoded.

C. State Transition

The state transition $\mathcal{P} : \mathcal{S} \times \mathcal{A} \times \mathcal{S} \rightarrow [0, 1]$ represents the dynamics of the environment, the transition function indicating the probability of transitioning to next state given current state and action. To model the uncertainties in load consumption. the exogenous information $P^t_{\text{load},m}$ in state vector s_t are random variables. Based on the realization of random variables, the next state s_{t+1} can be obtained. In reinforcement learning, the $\mathcal{P}$ is unknown and needs to be learned through interactions between the agent and the environment [121].

D. Reward

The reward function is defined as $\mathcal{R} : \mathcal{S} \times \mathcal{A} \times \mathcal{S} \rightarrow \mathbb{R}$, where $r_t = \mathcal{R}(s_t, a_t, s_{t+1})$ is the immediate reward the agent receives by taking action a_t given state s_t. The immediate reward r_t has two components to take into account objectives and penalty by violating constraints [115]. The detailed definition is as follows.

$$r_t = \lambda_1 R_{\text{obj},t} + \lambda_2 C_{\text{pen},t} \tag{5.18}$$

where λ_1, λ_2 are coefficients. $R_{\text{obj},t} = [\sum_{m\in\mathcal{M}} W_i P^t_{\text{r},m} - \sum_{m\in\mathcal{M}} C_{\text{gen},m} P^t_{\text{dg},m} - \sum_{\omega\in\Omega} C_{\text{bat},\omega} |P^t_\omega| - \sum_{\omega\in\Omega} C_{\text{tran},\omega} V_{\text{avg},\omega} (1 - \sum_{m\in\mathcal{M}} \zeta^t_{\omega m})]\Delta T$ relates to objective function (5.15) and is obtained by ignoring the constant term and taking minus sign, thus the cost minimization is transformed into a reward maximization problem. The second term $C_{\text{pen},t}$ is Lagrangian penalty term incurred by violation of constraints. The penalty term is proportional to the violations of acceptable ranges.

5.3.2 Deep Deterministic Policy Gradient

In reinforcement learning, the return is defined as the sum of discounted reward $G_t = \sum_{i=t}^{T} \gamma^{(i-t)} r(s_i, a_i)$, where $\gamma \in [0, 1]$ is the discount factor. A policy $\pi : \mathcal{S} \rightarrow \mathcal{A}$ is a mapping from states to selecting actions, i.e., stochastic policy $a_t \sim \pi(\cdot|s_t)$ or deterministic policy $a_t = \pi(s_t)$ []. Solving an MDP is to find a policy π that maximizes the expected return $\mathbb{E}_{a_t, s_t}[G_0]$.

In order to deal with continuous and discrete variables in state and action space, an actor-critic algorithm is adopted [122], e.g. DDPG, which concurrently learns a Q-function and a policy. It uses off-policy data and the Bellman equation

to learn the Q-function, and uses the Q-function to learn the policy [121].

A. Q-learning of DDPG

For Q-learning in DDPG, the action-value function $Q_\pi(s, a)$ denotes the expected return starting from s, taking the action a and thereafter following policy π, the Q-function is defined as follows.

$$Q_\pi(s_t, a_t) = \mathbb{E}_\pi[G_t|s_t, a_t] = \mathbb{E}_\pi[\sum_{i=t}^{T} \gamma^{(i-t)} r(s_i, a_i)] \tag{5.19}$$

where $\mathbb{E}_\pi[\cdot]$ depicts the expected values of random variables given the policy π, and the Q_π is the action-value function for policy π.

The optimal Q-function $Q^*(s_t, a_t)$ is to maximize the expected return by observing state and following any policy to take action, i.e., $Q^*(s_t, a_t) = \max \mathbb{E}_\pi[G_t|s_t, a_t]$. The optimal Q function obeys the Bellman equation, which describes the optimal $Q^*(s_t, a_t)$ in recursive form [123]:

$$Q^*(s_t, a_t) = \mathbb{E}_{s_{t+1}, a_{t+1}}[r_t + \gamma \max_{a_{t+1}} Q^*(s_{t+1}, a_{t+1})] \tag{5.20}$$

The basic solution to the Bellman equation is to iteratively update the Q-function and converge to optimal Q-function [121]. However, the approach is impractical as different sequences separately estimate the Q-function [111]. Generally, the Q-function and policy are estimated by a neural networks $Q_\theta(s_t, a_t)$ and π_ϕ as a Q-network and a policy network, parameterized with weights θ and ϕ, respectively. Fig. 5.1 and Fig. 5.2 shows the architecture of Q-network and policy network.

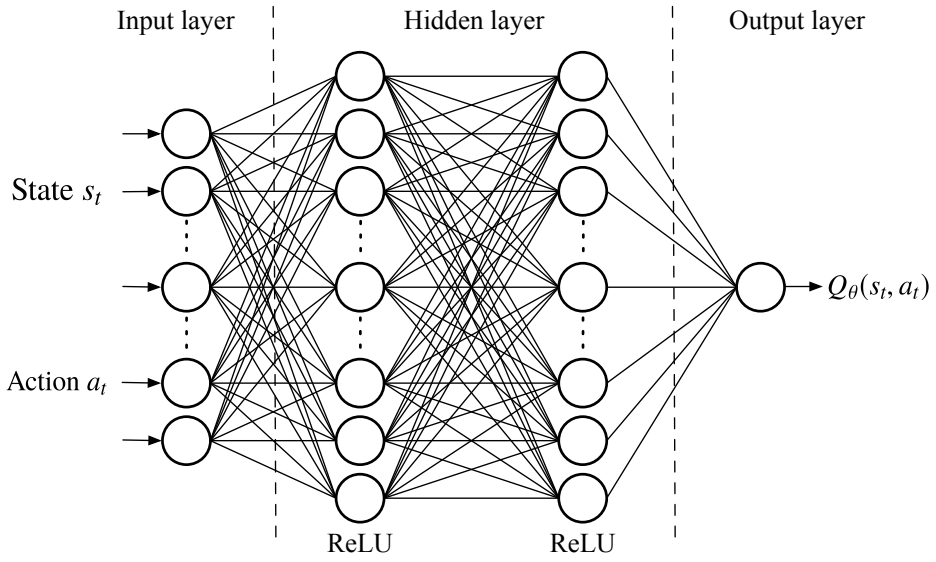

Figure 5.1: Q-network.

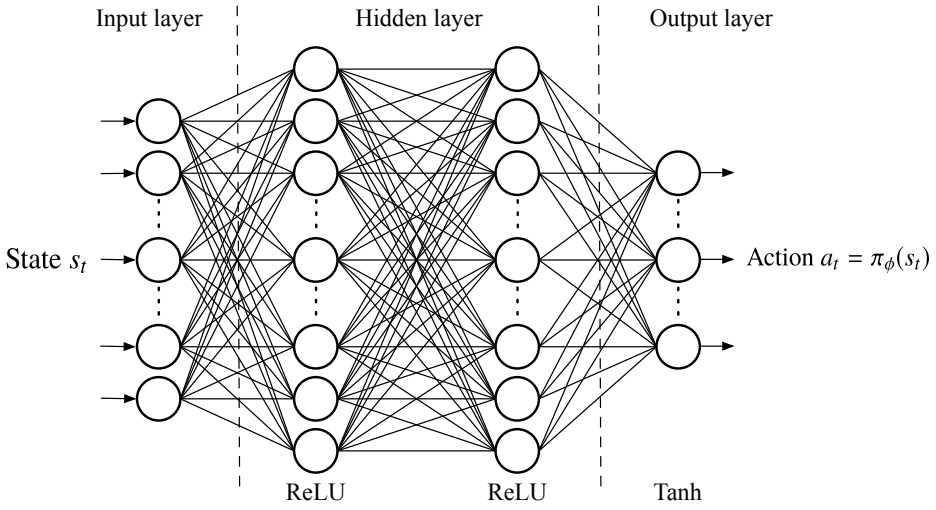

Figure 5.2: Policy network.

The Q-network can be learned to reduce the mean-squared error in the Bellman equation by adjusting the parameters θ. A sequence of loss functions $L(\theta)$ is set up by the mean-squared Bellman error as follows:

$$L(\theta) = \mathbb{E}_{s_t, a_t, r_t}[(Q_\theta(s_t, a_t) - y_t)^2] \tag{5.21}$$

where the optimal target value $r_t + \gamma \max_{a_{t+1}} Q^*(s_{t+1}, a_{t+1})$ is substituted with approximate target values:

$$y_t = \begin{cases} r_t, & \text{If episode terminates at step } t+1 \\ r_t + \gamma \max_{a_{t+1}} Q_\theta(s_{t+1}, a_{t+1}), & \text{Otherwise} \end{cases} \tag{5.22}$$

when s_{t+1} is a terminal state, the target value indicates that the agent gets no additional rewards after current state [111]. The Q-functions are updated by one step gradient descent using $L(\theta_t)$.

Introducing deep neural network architectures in reinforcement learning may cause training diverge [121]. One challenge is that the samples are assumed to be independently and identically distributed. As in deep Q-learning [111], an experience replay buffer is adopted to randomize over the data, thereby removing correlations in the observation sequence and smoothing over changes in the data distribution. The successful integration of reinforcement learning with deep neural networks is demonstrated in [124]. The replay buffer is a data set $\mathcal{D}$ that stores the agent's experience at each time-step (s_t, a_t, r_t, s_{t+1}). A mini-batch of samples $\mathcal{B} = \{(s_t, a_t, r_t, s_{t+1})\}$ is randomly drawn from the replay buffer $\mathcal{D}$ at each time-step for Q-network updates.

Another method to improve the stability of deep Q-learning is to utilize a separate network for generating the target value y_t in Q-learning updates. As in

Equations (5.21), (5.22), the Q-network $Q_\theta(s_t, a_t)$ being updated is also used to calculate the target value, resulting in that the network update is unstable and diverge. So, a soft target update [122] is adopted for actor-critic algorithm. More specifically, separate target networks are defined for both Q-network and policy network as $Q_{\theta'}(s_t, a_t)$ and $\pi_{\phi'}(s_t)$ with parameters θ' and ϕ', respectively. The target networks are updated by Polyak averaging [125]:

$$\theta' = \tau\theta + (1 - \tau)\theta' \tag{5.23}$$

$$\phi' = \tau\phi + (1 - \tau)\phi' \tag{5.24}$$

where $\tau \in [0, 1]$ is the Polyak hyperparameter (usually $\tau \ll 1$). Therefore the target values are updated by slowly tracking the learned networks and this would greatly improve the stability of learning [122].

Furthermore, computing the maximum over actions in the target values is challenging in continuous action spaces. Instead, a simple and computationally attractive alternative is to move the policy in the direction of the gradient of the target Q-network $Q_{\theta'}$ [122], rather than globally maximizing it. Specifically, the target values are updated by approximating the $\max_{a_t} Q_{\theta'}(s_t, a_t)$ with $Q_{\theta'}(s_t, \pi_{\theta'}(s_t))$. Thus the target value in Equation (5.22) is rewritten as:

$$y_t = r_t + \gamma Q_{\theta'}(s_{t+1}, \pi_{\phi'}(s_{t+1})) \tag{5.25}$$

B. Policy Learning of DDPG

Policy learning is to find a policy $\pi_\phi(s_t)$ that maximizes the expected discounted return $J(\phi) = \mathbb{E}_{s_t,a_t}[G_0] \approx \mathbb{E}_{s_t}[Q_\theta(s_t, \pi_\phi(s_t))]$ [121]. The policy network is

updated by applying the chain rule to the $J(\phi)$ with respect to the actor parameters ϕ and gradient ascent is implemented [123]. Thus, we have policy learning algorithm as follows.

$$\nabla_{\phi} J(\phi) = \mathbb{E}_{s_t}[\nabla_a Q_{\theta}(s_t, a_t)|_{a_t=\pi_{\phi}(s_t)} \nabla_{\phi} \pi_{\phi}(s_t)] \tag{5.26}$$

It is noted that the Q-function parameters θ are treated as constants here.

C. Exploration and Exploitation

Exploration is challenging in continuous action spaces [122]. The agent has to exploit to obtain a reward, but it also explores in order to make better actions in the future. An advantage of off-policy algorithms is that the exploration can be implemented independently from the learning algorithm [121]. A temporally-correlated noise Ornstein-Hulenbeck process [126] ϵ' with standard deviation σ' is added to the actions in the training process. Thus, the action with noise is denoted by a' as:

$$a'_t = \pi_{\phi}(s_t) + \epsilon', \ \epsilon' \sim \text{OU} \tag{5.27}$$

At evaluation process, the policy focuses on exploitation and there is no noise adding to the actions.

D. Pseudocode

Overall, the DDPG is illustrated in Algorithm 2.

Algorithm 2: DDPG Algorithm

Initialize critic networks Q_{θ_1}, and policy network π_ϕ with random parameters θ, ϕ, initialize replay buffer $\mathcal{D}$
Initialize target networks $\theta' \leftarrow \theta, \phi' \leftarrow \phi$
for Episode = $0, M$ **do**
    Initialize Ornstein-Hulenbeck process for action exploration
    Initialize environment state s_0
    for $t = 0, T$ **do**
        Observe state s_t and select action a_t with exploration noise by (5.27). Observe reward r_t and next state s_{t+1}
        Store transition (s_t, a_t, r_t, s_{t+1}) in $\mathcal{D}$
        Randomly sample mini-batch of N transitions (s_t, a_t, r_t, s_{t+1}) from $\mathcal{D}$
        Compute target values by (5.25)
        Update Q-networks by performing one step gradient descent on the loss (5.21) with respect to θ:

$$\nabla_\theta L(\theta) = \nabla_\theta \frac{1}{N} \sum [(Q_\theta(s_t, a_t) - y_t)^2]$$

        Update policy network by applying (5.26) to the mini-batch and implementing one step gradient ascent:

$$\nabla_\phi J(\phi) = \frac{1}{N} \sum [\nabla_a Q_\theta(s_t, a_t)|_{a_t = \pi_\phi(s_t)} \nabla_\phi \pi_\phi(s_t)] \tag{5.28}$$

        Update target networks by (5.23), (5.24)
    end
end

5.3.3 Twin Delayed Deep Deterministic Policy Gradient

Value overestimation with actor-critic algorithms in continuous space is of great concern [119]. TD3 algorithm is proposed to address overestimation bias and variance reduction. First, a pair of Q-networks are adopted based on double Q-learning [127]. Second, delayed policy updates are utilized to address the coupling of value and policy. Finally, a target smoothing regularization is introduced to reduce variance.

A. Clipped Double Q-learning

A clipped variant of Double Q-learning is adopted to reduce overestimation bias [127]. A pair of Q-networks $(Q_{\theta_1}, Q_{\theta_2})$ are defined along with corresponding target Q-networks $(Q_{\theta'_1}, Q_{\theta'_2})$. There is still only single actor π_ϕ optimized with respect to ϕ, while the target policy network $\pi_{\phi'}$ with parameters ϕ'. By upper-bounding the less biased value approximator Q_{θ_2} with the biased estimate Q_{θ_1}, a single target update for clipped Double Q-learning is obtained by taking the minimum between the two Q-networks [119]:

$$y_t = r_t + \gamma \min_{i=1,2} Q'_{\theta'_i}(s_{t+1}, \pi'_{\phi'}(s_{t+1})) \tag{5.29}$$

Then Q_{θ_1} and Q_{θ_2} are updated by minimizing the corresponding mean-squared Bellman error as follows, while the target networks $Q_{\theta'_1}$ and $Q_{\theta'_2}$ are updated by Polyak averaging as in Equation (5.23):

$$L(\theta_i) = \mathbb{E}_{s_t, a_t, r_t}[(Q_{\theta_i}(s_t, a_t) - y_t)^2], \forall i = 1, 2 \tag{5.30}$$

If $Q_{\theta_1} > Q_{\theta_2}$, the update is actually identical to the standard update without inducing additional bias. Otherwise, this indicates that overestimation occurs and the value is reduced similar to Double Q-learning.

B. Target Policy Smoothing Regularization

When updating the critics Q_{θ_1} and Q_{θ_2}, a learning target using a deterministic policy is highly susceptible to inaccuracies induced by function approximation error, increasing the variance of the target value. This induced variance can be reduced through regularization by target policy smoothing, which is similar to learning update from SARSA [121]. Since deterministic policies can overfit to narrow peas in the value estimate, the Q-function over similar actions is smoothed out to have similar value, by adding a small amount of random noise $\tilde{\epsilon}$ to the target policy network in target update and averaging over mini-batches. The modified target actions $\tilde{a}$ and target values y_t are thus:

$$\tilde{a}_{t+1} = \pi'_{\phi'}(s_{t+1}) + \tilde{\epsilon},\ \tilde{\epsilon} \sim \text{clip}(\mathcal{N}(0, \tilde{\sigma}^2), -c, c) \tag{5.31}$$

$$y_t = r_t + \gamma \min_{i=1,2} Q'_{\theta'_i}(s_{t+1}, \tilde{a}) \tag{5.32}$$

where the added noise is a normal distribution with zero-mean and standard deviation $\tilde{\sigma}$, and clipped by a hyperparameter c.

C. Delayed Policy Updates

The policy π_ϕ is optimized with respect to Q_{θ_1} to maximize the expected return $J(\phi)$, so the Equation (5.26) is rewritten as:

$$\nabla_{\phi} J(\phi) = \mathbb{E}_{s_t}[\nabla_a Q_{\theta_1}(s_t, a_t)|_{a_t=\pi_{\phi}(s_t)} \nabla_{\phi} \pi_{\phi}(s_t)] \tag{5.33}$$

In addition, the policy network π_{ϕ} is updated at a lower frequency than the value network Q_{θ_1}, in order to reduce error before introducing a policy update [119]. More specifically, the delaying policy updates only optimize the policy and target policy networks after a fixed number of updates d to critic networks. This modification uses a value estimate with lower variance and result in higher quality policy updates [128].

D. Pseudocode

The TD3 algorithm is illustrated in Algorithm 3.

5.4 Case Studies

The case studies are implemented on an integrated test system, based on Sioux Falls transportation network [102] and three microgrids, to verify the effectiveness of the proposed service restoration strategy.

5.4.1 Test Systems

Fig. 5.3 shows an integrated test system with microgrids connected by the Sioux Falls transportation network. A depot is located at node #10 in the transportation network. There are three microgrids located at nodes #2, #12, #21 in the transportation network, respectively. The operational parameters for microgrids and MESSs are shown in Table 5.1 and Table 5.2, respectively. The predicted value

Algorithm 3: TD3 Algorithm

Initialize critic networks Q_{θ_1}, Q_{θ_2}, and policy network π_ϕ with random parameters θ_1, θ_2, ϕ, initialize replay buffer $\mathcal{D}$
Initialize target networks $\theta_1' \leftarrow \theta_1, \theta_2' \leftarrow \theta_2, \phi' \leftarrow \phi$
for Episode = $0, M$ **do**
    Initialize Ornstein-Hulenbeck process for action exploration and Gaussian process for target policy smoothing
    Initialize environment state s_0
    for $t = 0, T$ **do**
        Observe state s_t and select action a_t with exploration noise by (5.27). Observe reward r_t and next state s_{t+1}
        Store transition (s_t, a_t, r_t, s_{t+1}) in $\mathcal{D}$
        Randomly sample mini-batch of N transitions (s_t, a_t, r_t, s_{t+1}) from $\mathcal{D}$
        Compute target actions by (5.31) and target values by (5.32)
        Update double Q-networks by minimizing the loss (5.30) of the mini-batch:

$$\nabla_{\theta_i} L(\theta_i) = \nabla_{\theta_i} \frac{1}{N} \sum [(Q_{\theta_i}(s_t, a_t) - y_t)^2], \forall i = 1, 2 \tag{5.34}$$

        if $t \bmod d = 0$ **then**
            Update policy network by applying (5.33) to the mini-batch and performing one step gradient ascent:

$$\nabla_\phi J(\phi) = \frac{1}{N} \sum [\nabla_a Q_{\theta_1}(s_t, a_t)|_{a_t = \pi_\phi(s_t)} \nabla_\phi \pi_\phi(s_t)] \tag{5.35}$$

            Update target Q-networks and policy network by (5.23), (5.24)
        end
    end
end

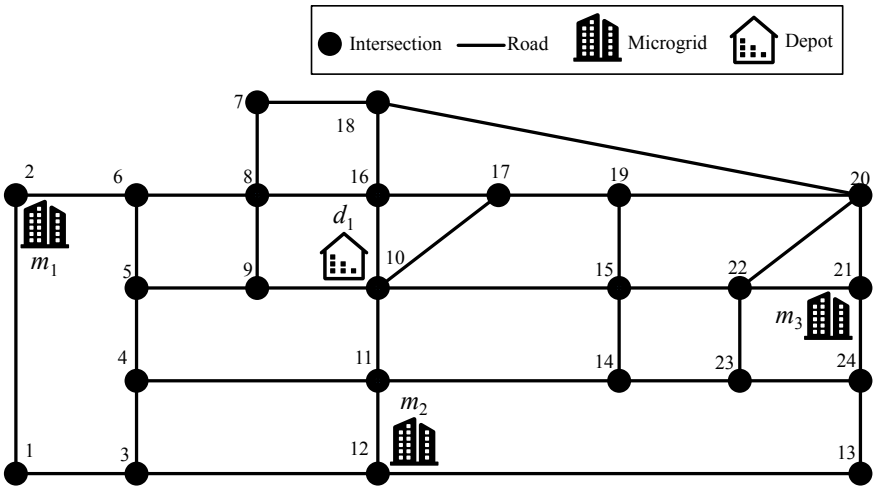

Figure 5.3: An integrated test system with a Sioux Falls transportation network connecting three microgrids.

of industrial, commercial and residential loads, as well as prediction intervals are shown in Fig. 5.4.

The length of the entire time horizon T_{H} is set to 24-h and the length of interval is 1-h. The customer interruption cost for industrial, commercial and residential loads are \$8/kWh, \$10/kWh and \$2/kWh, respectively. The unit generation cost in microgrid is \$0.5/kWh. The unit battery maintenance cost is \$0.2/kWh. The unit transportation cost is \$80/h.

To demonstrate the effectiveness of the proposed DRL-based service restoration strategy, DDPG and TD3 algorithms are adopted for training the agent in stochastic environment, the evaluation results are benchmarked with rolling optimization approach, which is illustrated in chapter 4. It is noted that the DDPG and TD3 algorithms do not need prior uncertainty model while rolling optimization needs forecast information over the optimization horizon to generate scenarios.

Table 5.1: Generation Resources and Local Loads for Microgrids

Microgrid #		1	2	3
Generation	$\overline{P}_{\mathrm{dg},m}$ (MW)	1.0	1.80	1.20
	$\overline{Q}_{\mathrm{dg},m}$ (MVar)	0.8	1.5	1.0
	$\overline{E}_{\mathrm{dg},m}$ (MWh)	20	35	23
	$\underline{E}_{\mathrm{dg},m}$ (MWh)	2.0	3.5	2.3
Load	Peak load (MW)	3.0	3.0	3.0
	Power factor	0.9	0.9	0.9
	Load type	C	R	I

Note: C - commercial, R - residential, I - industrial

Table 5.2: MESS Parameters

MESS #	1	2	3	4
Charging/discharging power (MW)	0.5			
Energy capacity (MWh)	2.0			
Initial SOC (%)	50			
$SOC_{\max}/SOC_{\min}$ (%)	90/10			
Charging/discharging efficiency (%)	95/95			
Average speed (km/h)	20	30	40	40

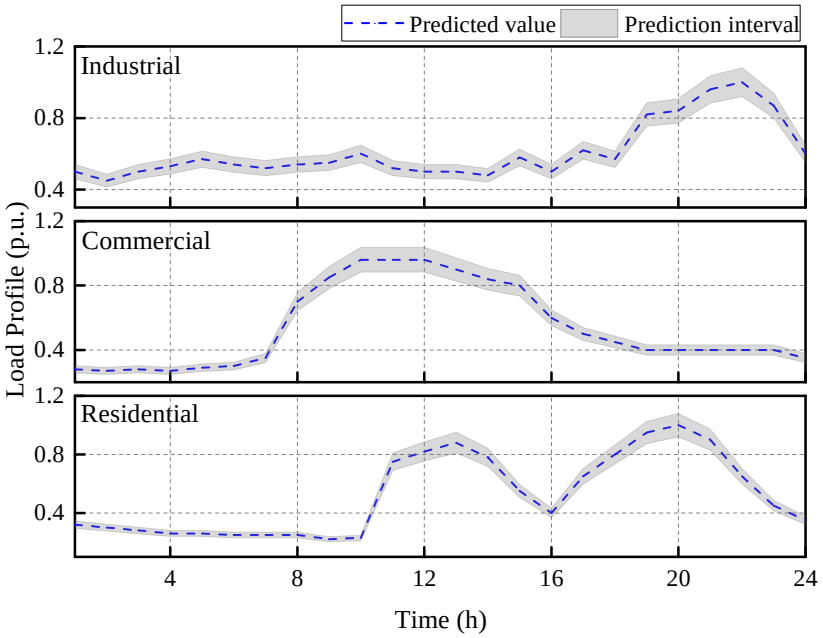

Figure 5.4: Load profile.

5.4.2 Training Settings

The Q-networks are with four dense layers, as shown in Fig. 5.1. The input layer receives both the state vector and action vector. Two hidden layers have 100 and 50 neurons, respectively. The output layer outputs one value for evaluating the state-action pair.ReLU is utilized as an activation function for the two hidden layers and Tanh is for the output layer. For policy network (Fig. 5.2), there are four dense layers, the input layer take the system state vector, the two hidden layers have 100 and 50 neurons, respectively. The output layer outputs action vector. ReLU is utilized as activation function for the two hidden layers and output layer is with linear activation function.

The neural networks are implemented in PyTorch 1.1 [129]. Adam optimizer with a learning rate of 0.001 is used to train the networks. The networks are updated using a mini-batch of 256 samples. Discount factor is 0.99. For TD3, the

target policy smoothing is performed by adding Gaussian noise $\tilde{\epsilon} \sim \mathcal{N}(0, 0.2)$ and clipped by $(-0.5, 0.5)$. The delayed policy update is to update the policy network and target policy network every $d = 2$ iterations. Both target Q-networks and target policy network are updated with $\tau = 0.005$.

A purely exploratory policy is carried out for the first 3000 episodes. Then, an off-policy exploration strategy is adopted with Ornstein-Hulenbeck noise. In the learning process, the average and standard deviation are obtained every 10 episodes. In the validation process, the policy is evaluated every 500 episodes over 20 episodes with no exploration noise.

5.4.3 Simulation Results

A. Performance Comparison

To evaluate the DRL-based algorithms, the rolling optimization is solved as the baseline to benchmark the proposed algorithms. In rolling optimization, which is illustrated in great detail in chapter 4, a rolling time horizon framework is adopted, the service restoration strategy is formulated as two-stage stochastic program over the prediction horizon and solved by MILP solver Cplex. This benchmark make use of exact model on system operations and knowledge on uncertainty information to generate scenarios. Since the original optimization problem is cost minimization, similarly, it is transformed into reward maximization problem by taking the minus sign of the objective function (5.15), ignoring constant terms and multiplying by coefficient.

Fig. 5.5 illustrates the evolution of learning and validation rewards compared with baseline rewards over 60000 episodes. It can be seen that the gaps between DRL-based algorithms and baseline value are decreasing with training episodes

and keep stable then. The DRL-algorithms do not work well at the beginning since it is still undergoing trial and error. The learning process gradually converges to a suboptimal policy in 40000 episodes. The results indicate that the proposed approach can learn a policy to maximize the cumulative rewards.

In addition, the performance of rolling optimization is greatly dependent on the accuracy of uncertainty modeling while the DRL-based approaches do not need a forecasting model. In comparison with the baseline of rolling optimization, after the agent is well-trained, it can make decisions in online manner (several milliseconds to seconds), while optimization method needs to re-run the time-consuming optimization process for every new decision.

Furthermore, the DDPG and TD3 present different learning capabilities. TD3 outperforms DDPG in both performance and learning speed. The Double Q-learning is more effective in reducing overestimation bias with continuous actions, leading to great performance improvement. The target smoothing regularization modifies the temporal difference target to limit errors from function approximation.

B. Effect of Temporal-spatial Dynamics of MESSs

Fig. 5.6 presents the charging/discharging schedule with respect to the position of MESS. The bar shows the charging/discharging active power while the dash lines with asterisks and right Y-axis indicates the MESS's movements. The dynamic scheduling of MESS optimizes the trip chain of MESSs and corresponding charging/discharging behaviors. It can be observed that MESSs move among microgrids back and forth due to limited power and energy capacity.

Fig. 5.7 denotes the SOC of MESSs and the energy transfer among microgrids through charging or discharging of MESSs. A microgrid with positive energy

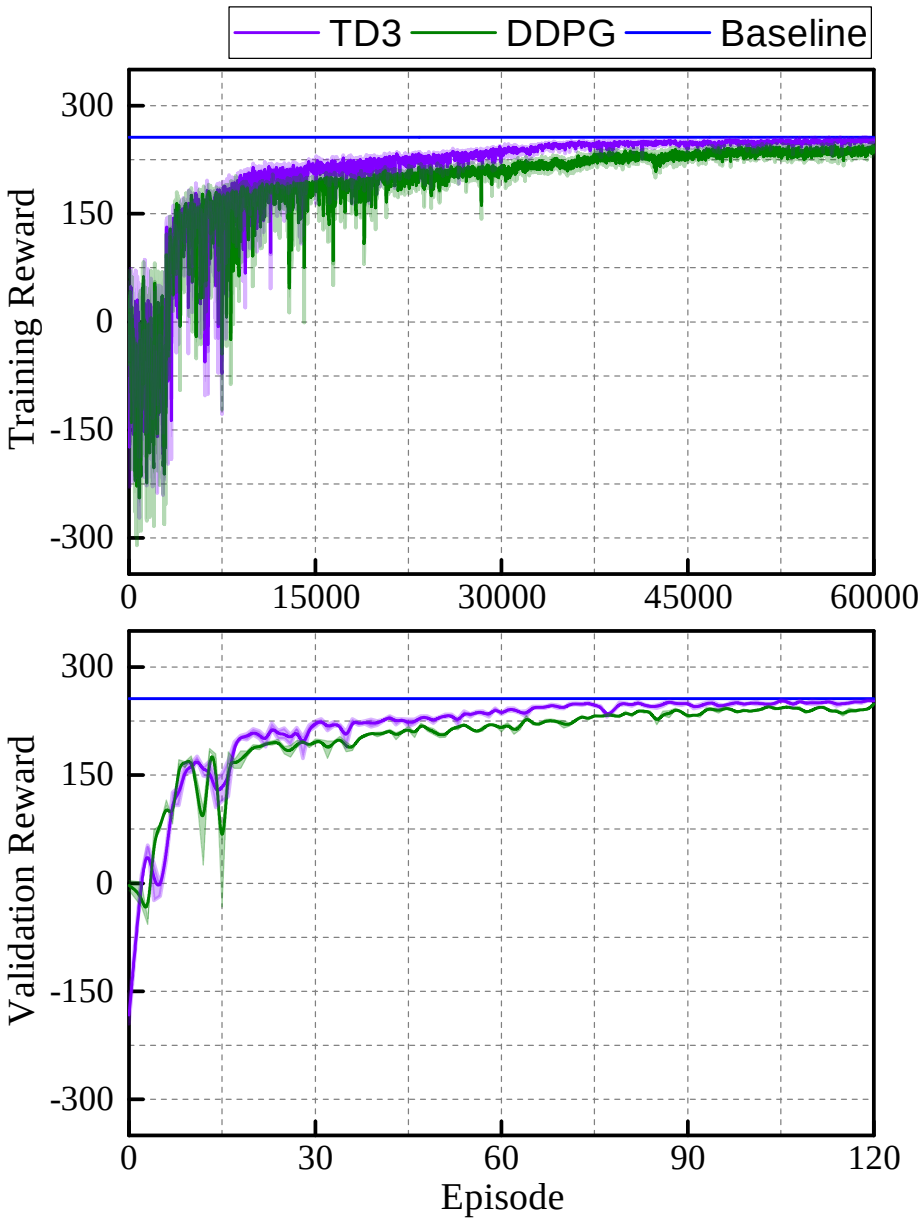

Figure 5.5: Learning and validation curves.

transfer means it receives energy from MESSs whereas negative one means outputting energy from this microgrid. It is observed that energy transfer is mainly from microgrid #1 to microgrid #2.

The simulation result shows that MESSs transport energy among microgrids to restore critical loads by charging from some microgrids and discharging to others. For example, it is observed that MESS #1 is dispatched between microgrid #1 and microgrid #2. The MESS #1 initially moves to microgrid #2 from depot and charges at microgrid #2. Next, it moves back and forth between microgrid #2 and microgrid #1 in (07:00-22:00) to transfer energy. The integration of MESSs and coordination with microgrids can leverage the MESSs mobility. Also, the MESSs can carry out load shifting within the same microgrid. For instance, MESS #3 charges at microgrid #2 in (01:00-02:00) and discharges in (02:00-07:00). The results highlight the importance of effective utilization of MESSs mobility and flexibility.

5.5 Conclusions

This chapter presents a novel MDP formulation for service restoration strategy in microgrids by coordinating the scheduling of MESSs and resource dispatching of microgrids. The DRL algorithms are leveraged to solve the formulated sequential decision-making problem with consideration of uncertainties in load consumption. The well-trained policy can be deployed in on-line manner and is computationally efficient. The simulation results verify the effectiveness of MESSs mobility that transport energy among microgrids to facilitate load restoration. Mobile and stationary resources can be jointly coordinated to enhance system resilience.

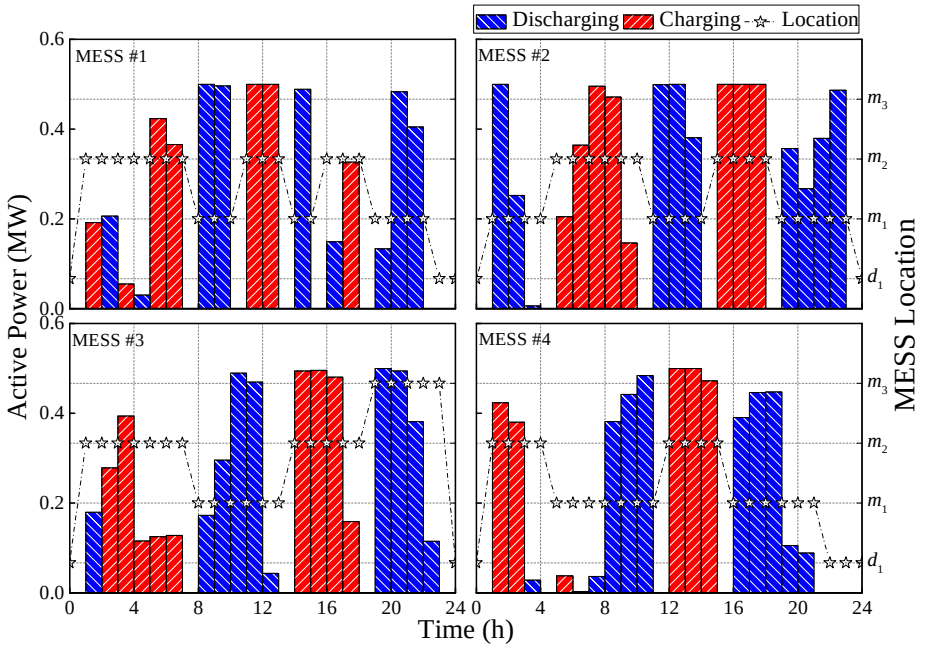

Figure 5.6: Scheduling results of the MESS fleet.

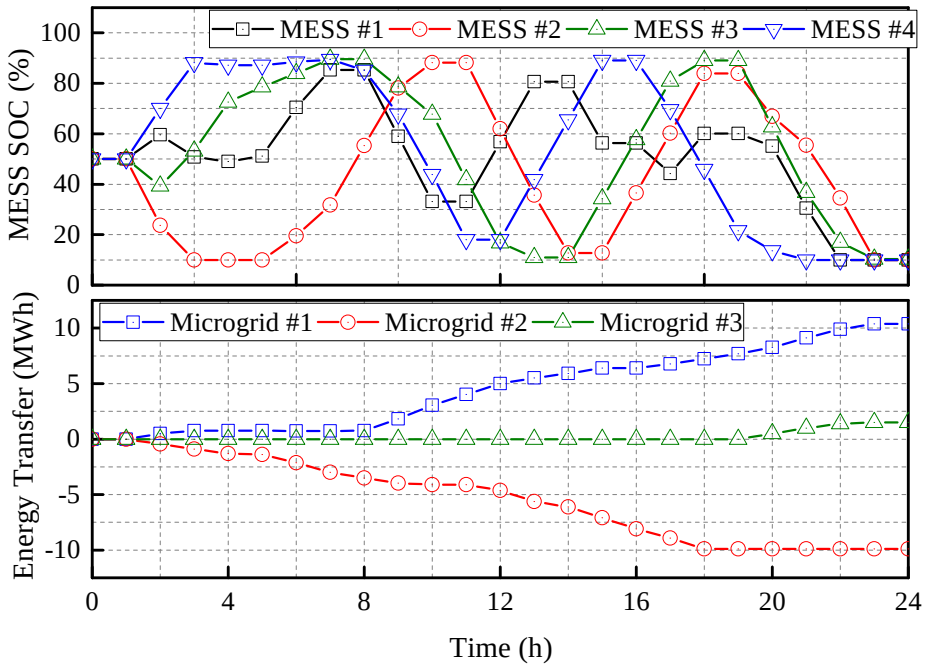

Figure 5.7: SOC of MESSs and energy transfer among microgrids.

Chapter 6

Conclusions and Future Works

The summary and overall conclusion of this thesis are presented in this chapter. The thesis begins with reviews on current research work on smart grid resilience. Service restoration strategy considering stationary and mobile energy resources are demonstrated and verified. The main outcomes are carefully summarized. The research results have highlighted the importance of coordination of multiple energy resources in facilitating service restoration after major blackouts. Furthermore, future works are presented as well.

6.1 Conclusions

MESSs provide promising solutions to enhance distribution system resilience. The importance of coordinating mobile and stationary energy resources has been increasingly recognized. This thesis developed a novel holistic management framework for MESS fleets to enhance smart grid resilience. The conclusions are summarized as follows.

Chapter 3 and Chapter 4 target at integrated restoration strategies from a mathematical optimization perspective. The optimization models are formulated as MILP. In particular, Chapter 3 presents a novel deterministic model that applies MESSs into distribution system restoration. A modified time-space network-based MESS scheduling model is presented and integrated into distribution network reconfiguration to allocate MESSs among microgrids. The MESSs can efficiently transfer energy among multiple microgrids within the distribution system in appropriate times and locations to facilitate critical loads service restoration without violating network topology and operation constraints. Meanwhile, MESSs can also serve as stationary ESSs to implement load shifting within microgrids. Mobile and stationary resources can be jointly coordinated to enhance system resilience.

Subsequently, to address uncertain information and thoroughly investigate the potential subsequent damage and repair during the restoration process, Chapter 4 further develops the deterministic model in Chapter 3 to a stochastic one. The scheduling of MESS fleet is modeled by a stochastic multi-layer time-space network, which reduces the computational complexity with a fewer number of binary variables and constraints and can be utilized for practical transportation networks. In addition, a rolling optimization framework is adopted to dynamically

update system information and the coordinated scheduling over the prediction horizon. The integrated restoration strategy is demonstrated to perform effectively under uncertainties in coupled transportation and distribution systems. The results reveal the flexibility of the proposed model that MESS fleets can be rescheduled or rerouted at each interval considering the damage and repair to roads.

To deal with scalability issues and the need for accurate uncertainty modeling. Chapter 5 investigates an on-line optimization framework inspired by DRL. Chapter 5 presents a novel MDP formulation for service restoration strategy in microgrids by coordinating the scheduling of MESSs and resource dispatching of microgrids. The DRL algorithms are leveraged to solve the formulated sequential decision-making problem with consideration of uncertainties in load consumption. The well-trained policy can be deployed in on-line manner and is computationally efficient.

To summarize, MESSs have been demonstrated to coordinate well with stationary resources for more resilient service restoration. Three novel restoration strategies are proposed to bridge the gap of applying MESSs into distribution system restorations. The effectiveness and improvements of these strategies have been highlighted with favorable results.

6.2 Recommendations for Further Research

This thesis developed a novel holistic management framework for MESS fleets that coordinates the stationary and mobile energy resources to improve smart grid resilience. Due to its applicability and versatility, the development for the coordination of multiple energy resources still requires more extensive research. Considering the assumptions and limitations of the modeling methods in this

thesis, further investigation can be conducted in several potential areas, as listed bellow.

6.2.1 Impacts of Transportation Systems

The road damages in a transportation network have been considered in this thesis. However, this might not be the only factor to impact the restoration process. The key point in the vehicle scheduling problem is the estimated time of arrival, which is mainly determined by 1) the vehicle properties, 2) damage and repair to roads, 3) system traffic flow and 4) road capacities.

In this manuscript, we consider the 1) vehicle properties and 2) damage and repair to roads. We adopt the shortest path and vehicle average speed to obtain the travel time among microgrids and depots over the transportation network, which is a static method to approximate the estimated time of arrival. This method only takes into account the vehicle properties and the distance between microgrids or depots, which can be reasonable under certain circumstances since emergency response actions do have higher priorities in the aftermath of catastrophes. In addition, the 2) damage and repair to roads also affect the restoration process. In this revised manuscript, we have extended the proposed model with considerations of uncertainties in the status of roads in transportation networks, i.e., the roads can be repaired in the optimization time horizon, and simulation results have been analyzed to indicate the impact of damage and repair to roads in transportation networks.

However, to consider the impacts of 3) traffic flow and 4) road capacities on the scheduling of MESS over the transportation networks, this model can be further extended in the formulation of travel time matrix for MESS in the future work, i.e, the travel time of MESSs is obtained not only considering the shortest path in

the transportation network and the average speed of MESSs, but also the traffic flow and the road capacities.

6.2.2 Three-phase Unbalanced Conditions

The three-phase unbalanced model provides more details about unbalanced configurations in distribution systems than single-phase models. But as the main concern of this thesis is to illustrate the coordinated scheduling of mobile and stationary resources, a linearized DistFlow model is adopted in this manuscript and it is assumed a balanced power flow model.

However, the proposed model can be extended to consider the unbalanced three-phase power flow in distribution systems. Some relevant researches have been implemented. Reference [51] proposes a service restoration method that coordinates multiple sources to restore critical load considering unbalanced three-phase power flow. constraint. Microgrid formation schemes considering an unbalanced three-phase network model are proposed in [130] to restore critical loads and the coordinated operation of DGs and ESSs is explored. Reference [131] presents a soft open points-based operation strategy for unbalanced active distribution networks. A multi-period optimization is performed to minimize the cost of EV charging considering three-phase unbalanced load flow in [96].

Thus, the linearized three-phase power flow can be included in the future work for further extension of this model to unbalanced conditions.

6.2.3 Critical Load Restoration

Regarding the customer interruption cost, there is still debate on the definition of critical load. When major blackouts happen, some life-matter infrastructures

should be prioritized in the restoration to provide emergency services [29], [132]. These critical loads generally involve data center, hospitals, police stations, fire stations, emergency response centers, and other infrastructures that are associated with the basic needs of human life [45], [62], [64].

Priority weight-based method has been widely adopted to distinguish between critical loads and non-critical loads. In general, the priority weight is based on the reliability worth [77] (also the value of customer reliability [78] or value of lost load [133]), which represents the willingness of customers to pay for the reliable supply of electricity and is measured in dollars per unit of power (e.g., kilowatt-hour or megawatt-hour). The customer interruption costs are most often used to provide a comprehensive measure of reliability worth [59], [77] and to evaluate the impacts of interruptions to customer service due to failure in electric energy supply [134]. Nevertheless, it is noted that accurately estimating interruption costs for a given region and a specific type of outage is quite challenging as the customer interruption costs depend on multiple factors such as the type of customer affected, regional economic conditions and demographics, time of the outage, and other specific traits of an outage [133].

Therefore, the parameter setting for the priority weight of loads is still an open question. In this manuscript, we adopt the customer interruption costs as priority weights to distinguish between the critical load and non-critical load. The interruption costs are set following the general value range from the above references, that is, \$10/kWh and \$2/kWh for critical and non-critical loads, respectively. This parameter setting is only for illustration purpose and more accurate customer interruption costs can be adopted.

In addition, research works for critical load restoration are mainly for generic critical loads without considering particular operation properties, e.g., hospitals,

water stations, gas stations, internet data centers and other critical infrastructures. To leverage the coordination of multiple energy resources to facilitate service restoration fro critical infrastructures, more detailed and integrated service restoration strategies are needed.

List of Publications

Journal Publications

[1]. **S. Yao**, P. Wang, X. Liu, H. Zhang, T. Zhao, "Rolling Optimization of Mobile Energy Storage Fleets for Resilient Service Restoration," *IEEE Trans. Smart Grid*, vol. 11, no. 2, pp. 1030-1043, 2020.

[2]. **S. Yao**, P. Wang, T. Zhao, "Transportable Energy Storage for More Resilient Distribution Systems with Multiple Microgrids," *IEEE Trans. Smart Grid*, vol. 10, no. 3, pp. 3331-3341, 2019.

[3]. T. Zhao, X. Pan, **S. Yao**, C. Ju, L. Li, "Strategic Bidding of Hybrid AC/DC Microgrid Embedded Energy Hubs: A Two-stage Chance Constrained Stochastic Programming Approach," *IEEE Trans. Sustain. Energy*, vol. 11, no. 1, pp. 116-125, 2020.

[4]. H. Zhang, P. Wang, **S. Yao**, T. Zhao, "Spatial-temporal Reliability and Damage Assessment of Transmission Networks under Hurricanes", *IEEE Trans. Smart Grid*, vol. 11, no.2, pp. 1044-1054, 2020.

[5]. H. Zhang, P. Wang, **S. Yao**, X. Liu, T. Zhao, “Resilience Assessment of Interdependent Energy Systems under Hurricanes”, *IEEE Trans. Power Syst.*, Early Access, 2020.

[6]. X. Liu, T. Zhao, **S. Yao**, C. Soh, P. Wang, "Distributed Operation Management of Battery Swapping-Charging Systems," *IEEE Trans. Smart Grid*, vol. 10, no. 5, pp. 5320-5333 , 2019.

Conference Proceedings

[1]. **S. Yao**, J. Gu, P. Wang, T. Zhao, H. Zhang, X. Liu, "Resilient Load Restoration in Microgrids Considering Mobile Energy Storage Fleets: A Deep Reinforcement Learning Approach", *2020 IEEE Power & Energy Society General Meeting*, 2020.

[2]. **S. Yao**, T. Zhao, H. Zhang, P. Wang, L. Goel, "Two-stage Stochastic Scheduling of Transportable Energy Storage Systems for Resilient Distribution Systems," *2018 IEEE International Conference on Probabilistic Methods Applied to Power Systems (PMAPS)*, 2018.

[3]. P. Tu, **S. Yao**, P. Wang, L. Goel, "Hierarchical Reliability Modeling of an Island Hybrid AC/DC Microgrid," *2018 IEEE International Conference on Probabilistic Methods Applied to Power Systems (PMAPS)*, 2018.

[4]. **S. Yao**, T. Zhao, P. Wang, H. Zhang, "Resilience-oriented Distribution System Reconfiguration for Service Restoration Considering Distributed Generations," *2017 IEEE Power & Energy Society General Meeting*, 2017.

[5]. *(Best Conference Paper Award)* C. Ju, **S. Yao**, P. Wang, "Resilient Post-disaster System Reconfigure for Multiple Energy Service Restoration," *2017 IEEE Conference on Energy Internet and Energy System Integration (EI2)*, 2017.

[6]. T. Zhao, X. Pan, **S. Yao**, P. Wang, "Stackelberg Game Based Energy and Reserve Management for a Fast Electric Vehicle Charging Station, " *2017 IEEE Energy Conversion Congress and Exposition (ECCE)*, 2017.

Bibliography

[1] IEC, "Coping with the Energy Challenge The IEC ' s role from 2010 to 2030: Smart Electrification - The Key to Energy Efficiency," Tech. Rep., 2019. [Online]. Available: https://basecamp.iec.ch/download/iec-white-paper-coping-with-the-energy-challenge-the-iecs-role-from-2010-to-2030/

[2] U.S. Energy Information Administration, "International Energy Outlook 2019," Tech. Rep., 2019. [Online]. Available: https://www.eia.gov/outlooks/ieo/pdf/ieo2019.pdf

[3] M. Mendiluce, "Risky Business: Building a Resilient Power Sector," *IEEE Power Energy Mag.*, vol. 12, no. 5, pp. 34–41, 2014.

[4] Executive Office of the President, "Economic Benefits of Increasing Electric Grid Resilience to Weather Outages," Tech. Rep., 2013. [Online]. Available: https://www.energy.gov/sites/prod/files/2013/08/f2/Grid%20Resiliency%20Report_FINAL.pdf

[5] A. McAslan, "The concept of resilience: Understanding its origins, meaning and utility," *Adelaide Torrens Resil. Inst.*, 2010.

[6] Presidential Policy Directive PPD-21, "Critical Infrastructure Security and Resilience," Tech. Rep., 2013. [Online]. Available: https://www.whitehouse.gov/the-press-office/2013/02/12/presidential-policy-directive-critical-infrastructure-security-and-resil

[7] D. T. Ton and W. T. P. Wang, "A More Resilient Grid: The U.S. Department of Energy Joins with Stakeholders in an R&D Plan," *IEEE Power Energy Mag.*, vol. 13, no. 3, pp. 26–34, 2015.

[8] U.S. Department of Energy, "Quadrennial Energy Review First Installment: Transforming U.S. Energy Infrastructures in a Time of Rapid Change," Department of Energy, Tech. Rep., 2015. [Online]. Available: https://www.energy.gov/policy/initiatives/quadrennial-energy-review-qer/quadrennial-energy-review-first-installment

[9] Z. Bie, Y. Lin, G. Li, and F. Li, "Battling the Extreme: A Study on the

Power System Resilience," *Proc. IEEE*, vol. 105, no. 7, pp. 1253–1266, 2017.

[10] M. Panteli, D. N. Trakas, P. Mancarella, and N. D. Hatziargyriou, "Power Systems Resilience Assessment: Hardening and Smart Operational Enhancement Strategies," *Proc. IEEE*, vol. 105, no. 7, pp. 1202–1213, 2017.

[11] Y. Wang, C. Chen, J. Wang, and R. Baldick, "Research on Resilience of Power Systems Under Natural Disasters—A Review," *IEEE Trans. Power Syst.*, vol. 31, no. 2, pp. 1604–1613, 2016.

[12] Y. Li, K. Xie, L. Wang, and Y. Xiang, "Exploiting network topology optimization and demand side management to improve bulk power system resilience under windstorms," *Electr. Power Syst. Res.*, vol. 171, pp. 127–140, 2019.

[13] N. M. Tabatabaei, S. N. Ravadanegh, and N. Bizon, *Power Systems Resilience: Modeling, Analysis and Practice*. Springer, 2019.

[14] C. Chen, J. Wang, and D. Ton, "Modernizing Distribution System Restoration to Achieve Grid Resiliency Against Extreme Weather Events: An Integrated Solution," *Proc. IEEE*, vol. 105, no. 7, pp. 1267–1288, 2017.

[15] C. Liang, M. Khodayar, and M. Shahidehpour, "Only Connect: Microgrids for Distribution System Restoration," *IEEE Power Energy Mag.*, vol. 12, no. 1, pp. 70–81, 2014.

[16] G. Jiménez-Estévez, A. Navarro-Espinosa, R. Palma-Behnke, L. Lanuzza, and N. Velázquez, "Achieving resilience at distribution level: Learning from isolated community microgrids," *IEEE Power Energy Mag.*, vol. 15, no. 3, pp. 64–73, 2017.

[17] A. M. Cuomo, R. L. Kauffman, J. B. Rhodes, A. Zibelman, and J. M. Hauer, "Microgrids for critical facility resiliency in New York state," New York State Energy Research and Development Authority, Tech. Rep., 2014. [Online]. Available: https://www.nyserda.ny.gov/-/media/Microgrids-Report-Summary.pdf

[18] Maryland Energy Administration, "Maryland Resiliency

Through Microgrids Task Force Report," Tech. Rep., 2014. [Online]. Available: https://energy.maryland.gov/Documents/MarylandResiliencyThroughMicrogridsTaskForceReport_000.pdf

[19] H. Kumar Nunna, S. Battula, S. Doolla, and D. Srinivasan, "Energy Management in Smart Distribution Systems with Vehicle-to-Grid Integrated Microgrids," *IEEE Trans. Smart Grid*, vol. 9, no. 5, pp. 4004–4016, 2018.

[20] *IEEE Draft Guide for Design, Operation, and Maintenance of Battery Energy Storage Systems, both Stationary and Mobile, and Applications Integrated with Electric Power Systems*. IEEE Standard P2030.2.1/D9.0, 2019.

[21] U.S. Department of Energy, "Quadrennial Energy Review Second Installment: Transforming the Nation's Electricity System," Tech. Rep., 2017. [Online]. Available: https://www.energy.gov/policy/initiatives/quadrennial-energy-review-qer/quadrennial-energy-review-second-installment

[22] International Energy Agency, "World Energy Outlook 2019," Tech. Rep., 2019. [Online]. Available: https://www.iea.org/weo2019/

[23] BP plc, "BP Energy Outlook 2019 edition The Energy Outlook explores the forces shaping the global energy transition out to 2040 and the key uncertainties surrounding that," Tech. Rep., 2019. [Online]. Available: https://www.bp.com/content/dam/bp/business-sites/en/global/corporate/pdfs/energy-economics/energy-outlook/bp-energy-outlook-2019.pdf

[24] Lawrence Livermore National Laboratory, "Energy Flow Charts." [Online]. Available: https://flowcharts.llnl.gov/commodities/energy

[25] W. Li, *Risk assessment of power systems: models, methods, and applications*. John Wiley & Sons, 2014.

[26] WBCSD electric utilities, "Building a Resilient Power Sector," Tech. Rep., 2014. [Online]. Available: http://docs.wbcsd.org/2014/03/Building_A_Resilient_Power_Sector.pdf

[27] Munich Re, "NatCatSERVICE." [Online]. Available: https://www.munichre.com/en/solutions/for-industry-clients/natcatservice.html

[28] U.S. Department of Energy, "Electric Disturbance Events (OE-417)." [Online]. Available: https://www.oe.netl.doe.gov/OE417_annual_summary.aspx

[29] K. Schneider, F. Tuffner, M. Elizondo, C. C. Liu, Y. Xu, and D. Ton, "Evaluating the Feasibility to Use Microgrids as a Resiliency Resource," *IEEE Trans. Smart Grid*, vol. 8, no. 2, pp. 687 – 696, 2016.

[30] M. Panteli, D. N. Trakas, P. Mancarella, and N. D. Hatziargyriou, "Boosting the Power Grid Resilience to Extreme Weather Events Using Defensive Islanding," *IEEE Trans. Smart Grid*, vol. 7, no. 6, pp. 2913–2922, 2016.

[31] M. Panteli and P. Mancarella, "The Grid: Stronger, Bigger, Smarter?" *IEEE Power Energy Mag.*, vol. 13, no. 3, pp. 58–66, 2015.

[32] University of Tokyo, "Resilience Engineering Research Center (RERC)."

[33] Tohoku University, "International Research Institute of Disaster Science (IRIDeS)." [Online]. Available: http://irides.tohoku.ac.jp/eng

[34] Public Law 111-5, "American Recovery and Reinvestment Act 2009," Tech. Rep., 2009. [Online]. Available: http://www.gpo.gov/fdsys/pkg/PLAW-111publ5/pdf/PLAW-111publ5.pdf

[35] U.S. Department of Energy, "Smart Grid Research & Development," Tech. Rep., 2012. [Online]. Available: https://energy.gov/sites/prod/files/SG_MYPP_2012Update.pdf

[36] Executive Order, "Preparing the United States for the Impacts of Climate Change," 2013. [Online]. Available: https://obamawhitehouse.archives.gov/the-press-office/2013/11/01/executive-order-prEPAring-united-states-impacts-climate-change

[37] R. Das, V. Madani, F. Aminifar, J. McDonald, S. S. Venkata, D. Novosel, A. Bose, and M. Shahidehpour, "Distribution Automation Strategies: Evolution of Technologies and the Business Case," *IEEE Trans. Smart Grid*, vol. 6, no. 4, pp. 2166–2175, 2015.

[38] Y. Xu, C. C. Liu, K. P. Schneider, F. K. Tuffner, and D. T. Ton, "Microgrids for service restoration to critical load in a resilient distribution system," *IEEE Trans. Smart Grid*, vol. 9, no. 1, pp. 426–437, 2018.

[39] Z. Wang and J. Wang, "Self-Healing Resilient Distribution Systems Based on Sectionalization Into Microgrids," *IEEE Trans. Power Syst.*, vol. 30, no. 6, pp. 3139–3149, 2015.

[40] C. Chen, J. Wang, F. Qiu, and D. Zhao, "Resilient Distribution System by Microgrids Formation After Natural Disasters," *IEEE Trans. Smart Grid*, vol. 7, no. 2, pp. 958 – 966, 2016.

[41] CIGRE, "WG C6.22 Microgrids." [Online]. Available: http://c6.cigre.org/WG-Area/WG-C6.22-Microgrids

[42] P. L. Cavalcante, J. C. Lopez, J. F. Franco, M. J. Rider, A. V. Garcia, M. R. R. Malveira, L. L. Martins, and L. C. M. Direito, "Centralized Self-Healing Scheme for Electrical Distribution Systems," *IEEE Trans. Smart Grid*, vol. 7, no. 1, pp. 145–155, 2016.

[43] T. Ding, Y. Lin, G. Li, and Z. Bie, "A New Model for Resilient Distribution Systems by Microgrids Formation," *IEEE Trans. Power Syst.*, vol. 32, no. 5, pp. 4145–4147, 2017.

[44] J. Li, X. Y. Ma, C. C. Liu, and K. P. Schneider, "Distribution System Restoration With Microgrids Using Spanning Tree Search," *IEEE Trans. Power Syst.*, vol. 29, no. 6, pp. 3021–3029, 2014.

[45] H. Gao, Y. Chen, Y. Xu, and C. C. Liu, "Resilience-Oriented Critical Load Restoration Using Microgrids in Distribution Systems," *IEEE Trans. Smart Grid*, vol. 7, no. 6, pp. 2837–2848, 2016.

[46] G. Huang, J. Wang, C. Chen, J. Qi, and C. Guo, "Integration of Preventive and Emergency Responses for Power Grid Resilience Enhancement," *IEEE Trans. Power Syst.*, vol. 32, no. 3, pp. 4451 – 4463, 2017.

[47] C. Wang, Y. Hou, F. Qiu, S. Lei, and K. Liu, "Resilience Enhancement with Sequentially Proactive Operation Strategies," *IEEE Trans. Power Syst.*, vol. 32, no. 4, pp. 2847–2857, 2017.

[48] M. H. Amirioun, F. Aminifar, and H. Lesani, "Resilience-Oriented Proactive Management of Microgrids Against Windstorms," *IEEE Trans. Power Syst.*, vol. 33, no. 4, pp. 4275–4284, 2018.

[49] M. H. Amirioun, F. Aminifar, and M. Shahidehpour, "Resilience-

Promoting Proactive Scheduling Against Hurricanes in Multiple Energy Carrier Microgrids," *IEEE Trans. Power Syst.*, vol. 34, no. 3, pp. 2160–2168, 2019.

[50] M. H. Amirioun, F. Aminifar, and H. Lesani, "Towards Proactive Scheduling of Microgrids Against Extreme Floods," *IEEE Trans. Smart Grid*, vol. 9, no. 4, pp. 3900–3902, 2018.

[51] Y. Wang, Y. Xu, J. He, C.-C. Liu, K. P. Schneider, M. Hong, and D. T. Ton, "Coordinating Multiple Sources for Service Restoration to Enhance Resilience of Distribution Systems," *IEEE Trans. Smart Grid*, vol. 10, no. 5, pp. 5781–5793, 2019.

[52] B. Zhou, D. Xu, C. Li, Y. Cao, K. W. Chan, Y. Xu, and M. Cao, "Multiobjective Generation Portfolio of Hybrid Energy Generating Station for Mobile Emergency Power Supplies," *IEEE Trans. Smart Grid*, vol. 9, no. 6, pp. 5786–5797, 2018.

[53] Electric Power Research Institute, "Electricity Energy Storage Technology Options," Tech. Rep., 2010. [Online]. Available: http://large.stanford.edu/courses/2012/ph240/doshay1/docs/EPRI.pdf

[54] Department of Defense, "Transportable Microgrid with Energy Storage," Tech. Rep., 2016. [Online]. Available: https://serdp-estcp.org/Program-Areas/Energy-and-Water/Energy/Microgrids-and-Storage/EW-201605

[55] Y. Sun, Z. Li, M. Shahidehpour, and B. Ai, "Battery-Based Energy Storage Transportation for Enhancing Power System Economics and Security," *IEEE Trans. Smart Grid*, vol. 6, no. 5, pp. 2395–2402, 2015.

[56] H. H. Abdeltawab and Y. A.-R. I. Mohamed, "Mobile Energy Storage Scheduling and Operation in Active Distribution Systems," *IEEE Trans. Ind. Electron.*, vol. 64, no. 9, pp. 6828–6840, 2017.

[57] M. E. Khodayar, L. Wu, and Z. Li, "Electric vehicle mobility in transmission-constrained hourly power generation scheduling," *IEEE Trans. Smart Grid*, vol. 4, no. 2, pp. 779–788, 2013.

[58] K. Knezovic, S. Martinenas, P. B. Andersen, A. Zecchino, and M. Marinelli,

"Enhancing the Role of Electric Vehicles in the Power Grid: Field Validation of Multiple Ancillary Services," *IEEE Trans. Transp. Electrif.*, vol. 3, no. 1, pp. 201–209, 2017.

[59] Y. Sun, J. Zhong, Z. Li, W. Tian, and M. Shahidehpour, "Stochastic Scheduling of Battery-Based Energy Storage Transportation System With the Penetration of Wind Power," *IEEE Trans. Sustain. Energy*, vol. 8, no. 1, pp. 135–144, 2017.

[60] J. Kim and Y. Dvorkin, "Enhancing Distribution System Resilience With Mobile Energy Storage and Microgrids," *IEEE Trans. Smart Grid*, vol. 10, no. 5, pp. 4996–5006, 2019.

[61] S. Lei, J. Wang, C. Chen, and Y. Hou, "Mobile emergency generator pre-positioning and real-time allocation for resilient response to natural disasters," *IEEE Trans. Smart Grid*, vol. 9, no. 3, pp. 2030 – 2041, 2018.

[62] H. Gao, Y. Chen, S. Mei, S. Huang, and Y. Xu, "Resilience-Oriented Pre-Hurricane Resource Allocation in Distribution Systems Considering Electric Buses," *Proc. IEEE*, vol. 105, no. 7, pp. 1214 – 1233, 2017.

[63] K. S. A. Sedzro, A. J. Lamadrid, and L. F. Zuluaga, "Allocation of Resources Using a Microgrid Formation Approach for Resilient Electric Grids," *IEEE Trans. Smart Grid*, vol. 33, no. 3, pp. 2633–2643, 2018.

[64] L. Che and M. Shahidehpour, "Adaptive Formation of Microgrids With Mobile Emergency Resources for Critical Service Restoration in Extreme Conditions," *IEEE Trans. Power Syst.*, vol. 34, no. 1, pp. 742–753, 2019.

[65] S. Lei, C. Chen, H. Zhou, and Y. Hou, "Routing and Scheduling of Mobile Power Sources for Distribution System Resilience Enhancement," *IEEE Trans. Smart Grid*, vol. 10, no. 5, pp. 5650–5662, 2019.

[66] S. Lei, C. Chen, Y. Li, and Y. Hou, "Resilient Disaster Recovery Logistics of Distribution Systems: Co-Optimize Service Restoration With Repair Crew and Mobile Power Source Dispatch," *IEEE Trans. Smart Grid*, vol. 10, no. 6, pp. 6187–6202, 2019.

[67] S. Yao, P. Wang, and T. Zhao, "Transportable Energy Storage for More Resilient Distribution Systems with Multiple Microgrids," *IEEE Trans.*

Smart Grid, vol. 10, no. 3, pp. 3331–3341, 2019.

[68] A. Arif, Z. Wang, J. Wang, and C. Chen, "Power Distribution System Outage Management With Co-Optimization of Repairs, Reconfiguration, and DG Dispatch," *IEEE Trans. Smart Grid*, vol. 9, no. 5, pp. 4109–4118, 2018.

[69] S. Chanda and A. K. Srivastava, "Defining and Enabling Resiliency of Electric Distribution Systems with Multiple Microgrids," *IEEE Trans. Smart Grid*, vol. 7, no. 6, pp. 2859–2868, 2016.

[70] T. Shekari, S. Golshannavaz, and F. Aminifar, "Techno-Economic Collaboration of PEV Fleets in Energy Management of Microgrids," *IEEE Trans. Power Syst.*, vol. 32, no. 5, pp. 3833–3841, 2017.

[71] IEEE, *IEEE Std 446-1995 : IEEE Recommended Practice for Emergency and Standby Power Systems for Industrial and Commercial Applications.* IEEE, 1996.

[72] N. Kliewer, T. Mellouli, and L. Suhl, "A time-space network based exact optimization model for multi-depot bus scheduling," *Eur. J. Oper. Res.*, vol. 175, no. 3, pp. 1616–1627, 2006.

[73] S. Bunte and N. Kliewer, "An overview on vehicle scheduling models," *Public Transp.*, vol. 1, no. 4, pp. 299–317, 2009.

[74] D. C. Paraskevopoulos, G. Laporte, P. P. Repoussis, and C. D. Tarantilis, "Resource constrained routing and scheduling: Review and research prospects," *Eur. J. Oper. Res.*, vol. 263, no. 3, pp. 737–754, 2017.

[75] N. Kliewer, B. Amberg, and B. Amberg, "Multiple depot vehicle and crew scheduling with time windows for scheduled trips," *Public Transp.*, vol. 3, no. 3, pp. 213–244, 2012.

[76] T. Ding, Y. Lin, Z. Bie, and C. Chen, "A resilient microgrid formation strategy for load restoration considering master-slave distributed generators and topology reconfiguration," *Appl. Energy*, vol. 199, pp. 205–216, 2017.

[77] R. Billinton and W. Li, *Reliability assessment of electric power systems using Monte Carlo methods*. New York : Plenum Press, 1994.

[78] Australian Energy Market Operator, "Value of Customer Reliability Review," Tech. Rep., 2014.

[79] R. A. Jabr, R. Singh, and B. C. Pal, "Minimum Loss Network Reconfiguration Using Mixed-Integer Convex Programming," *IEEE Trans. Power Syst.*, vol. 27, no. 2, pp. 1106–1115, 2012.

[80] M. R. Dorostkar-Ghamsari, M. Fotuhi-Firuzabad, M. Lehtonen, and A. Safdarian, "Value of Distribution Network Reconfiguration in Presence of Renewable Energy Resources," *IEEE Trans. Power Syst.*, vol. 31, no. 3, pp. 1879–1888, 2016.

[81] X. Chen, W. Wu, and B. Zhang, "Robust restoration method for active distribution networks," *IEEE Trans. Power Syst.*, vol. 31, no. 5, pp. 4005–4015, 2016.

[82] N. Hatziargyriou, H. Asano, R. Iravani, and C. Marnay, "Microgrids," *IEEE Power Energy Mag.*, vol. 5, no. 4, pp. 78–94, 2007.

[83] R. Rahmaniani, T. G. Crainic, M. Gendreau, and W. Rei, "The Benders decomposition algorithm: A literature review," *Eur. J. Oper. Res.*, vol. 259, no. 3, pp. 801–817, 2017.

[84] J. P. Watson and D. L. Woodruff, "Progressive hedging innovations for a class of stochastic mixed-integer resource allocation problems," *Comput. Manag. Sci.*, vol. 8, no. 4, pp. 355–370, 2011.

[85] M. E. Baran and F. F. Wu, "Network reconfiguration in distribution systems for loss reduction and load balancing," *IEEE Trans. Power Deliv.*, vol. 4, no. 2, pp. 1401–1407, 1989.

[86] Gurobi Optimization, "Gurobi optimizer quick start guide," 2017. [Online]. Available: http://www.gurobi.com/documentation/5.6/quick-start-guide/quickstart.pdf

[87] G. O'Brien, A. El Gamal, and R. Rajagopal, "Shapley Value Estimation for Compensation of Participants in Demand Response Programs," *IEEE Trans. Smart Grid*, vol. 6, no. 6, pp. 2837–2844, 2015.

[88] Y. Sun, Z. Li, W. Tian, and M. Shahidehpour, "A Lagrangian Decomposition Approach to Energy Storage Transportation Scheduling

in Power Systems," *IEEE Trans. Power Syst.*, vol. 31, no. 6, pp. 4348–4356, 2016.

[89] V. Madani, R. Das, F. Aminifar, J. McDonald, S. S. Venkata, D. Novosel, A. Bose, and M. Shahidehpour, "Distribution Automation Strategies Challenges and Opportunities in a Changing Landscape," *IEEE Trans. Smart Grid*, vol. 6, no. 4, pp. 2157–2165, 2015.

[90] S. Yan, J. C. Chu, and Y. L. Shih, "Optimal scheduling for highway emergency repairs under large-scale supply-demand perturbations," *IEEE Trans. Intell. Transp. Syst.*, vol. 15, no. 6, pp. 2378–2393, 2014.

[91] C.-C. Lu, S. Yan, and Y.-W. Huang, "Optimal scheduling of a taxi fleet with mixed electric and gasoline vehicles to service advance reservations," *Transp. Res. Part C Emerg. Technol.*, vol. 93, pp. 479–500, 2018.

[92] X. Liu, T. Zhao, S. Yao, C. B. Soh, and P. Wang, "Distributed Operation Management of Battery Swapping-Charging Systems," *IEEE Trans. Smart Grid*, vol. 10, no. 5, pp. 5320–5333, 2019.

[93] T. H. Cormen, *Introduction to algorithms*. MIT press, 2009.

[94] Z. Cao, H. Guo, J. Zhang, and U. Fastenrath, "Multiagent-based route guidance for increasing the chance of arrival on time," in *30th AAAI Conf. Artif. Intell. AAAI 2016*, 2016, pp. 3814–3820.

[95] Z. Cao, H. Guo, J. Zhang, D. Niyato, and U. Fastenrath, "Finding the Shortest Path in Stochastic Vehicle Routing: A Cardinality Minimization Approach," *IEEE Trans. Intell. Transp. Syst.*, vol. 17, no. 6, pp. 1688–1702, 2016.

[96] Z. Wang, J. Wang, B. Chen, M. M. Begovic, and Y. He, "MPC-based Voltage/Var optimization for distribution circuits with distributed generators and exponential load models," *IEEE Trans. Smart Grid*, vol. 5, no. 5, pp. 2412–2420, 2014.

[97] L. Wu, M. Shahidehpour, and T. Li, "Stochastic security-constrained unit commitment," *IEEE Trans. Power Syst.*, vol. 22, no. 2, pp. 800–811, 2007.

[98] A. O'Connell, D. Flynn, and A. Keane, "Rolling multi-period optimization to control electric vehicle charging in distribution networks," *IEEE Trans.*

Power Syst., vol. 29, no. 1, pp. 340–348, 2014.

[99] F. Li and Y. Du, "From AlphaGo to power system AI : What engineers can learn from solving the most complex board game," *IEEE Power Energy Mag.*, vol. 16, no. 2, pp. 76–84, 2018.

[100] Y. Liu, S. Lei, and Y. Hou, "Restoration of Power Distribution Systems With Multiple Data Centers as Critical Loads," *IEEE Trans. Smart Grid*, vol. 10, no. 5, pp. 5294–5307, sep 2019.

[101] A. Shapiro, D. Dentcheva, and A. Ruszczyński, *Lectures on Stochastic Programming: Modeling and Theory*, 2nd ed. Society for Industrial and Applied Mathematics, 2014.

[102] L. J. LeBlanc, E. K. Morlok, and W. P. Pierskalla, "An efficient approach to solving the road network equilibrium traffic assignment problem," *Transp. Res.*, vol. 9, no. 5, pp. 309–318, 1975.

[103] IBM, "CPLEX User's Manual 12.8.0," Tech. Rep., 2018. [Online]. Available: https://www.ibm.com/support/knowledgecenter/SSSA5P_12.8.0/ilog.odms.studio.help/pdf/usrcplex.pdf

[104] M. Kaut and S. W. Wallace, "Evaluation of Scenario-Generation Methods for Stochastic Programming," *Pacific J. Optim.*, vol. 3, no. 2, pp. 257–271, 2007.

[105] Google, "Python Client Library for Google Maps API Web Services." [Online]. Available: https://github.com/googlemaps/google-maps-services-python

[106] S. Yao, T. Zhao, H. Zhang, P. Wang, and L. Goel, "Two-stage stochastic scheduling of transportable energy storage systems for resilient distribution systems," in *2018 IEEE Int. Conf. Probabilistic Methods Appl. to Power Syst.*, 2018, pp. 1–6.

[107] S. Yao, P. Wang, X. Liu, H. Zhang, and T. Zhao, "Rolling Optimization of Mobile Energy Storage Fleets for Resilient Service Restoration," *IEEE Trans. Smart Grid*, vol. PP, no. 99, pp. 1–1, 2019.

[108] R. Lu, S. H. Hong, and M. Yu, "Demand Response for Home Energy Management Using Reinforcement Learning and Artificial Neural

Network," *IEEE Trans. Smart Grid*, vol. 10, no. 6, pp. 6629–6639, 2019.

[109] E. Mocanu, D. C. Mocanu, P. H. Nguyen, A. Liotta, M. E. Webber, M. Gibescu, and J. G. Slootweg, "On-Line Building Energy Optimization Using Deep Reinforcement Learning," *IEEE Trans. Smart Grid*, vol. 10, no. 4, pp. 3698–3708, 2019.

[110] D. Silver, J. Schrittwieser, K. Simonyan, I. Antonoglou, A. Huang, A. Guez, T. Hubert, L. Baker, M. Lai, A. Bolton, Y. Chen, T. Lillicrap, F. Hui, L. Sifre, G. Van Den Driessche, T. Graepel, and D. Hassabis, "Mastering the game of Go without human knowledge," *Nature*, vol. 550, no. 7676, pp. 354–359, 2017.

[111] V. Mnih, K. Kavukcuoglu, D. Silver, A. A. Rusu, J. Veness, M. G. Bellemare, A. Graves, M. Riedmiller, A. K. Fidjeland, G. Ostrovski, S. Petersen, C. Beattie, A. Sadik, I. Antonoglou, H. King, D. Kumaran, D. Wierstra, S. Legg, and D. Hassabis, "Human-level control through deep reinforcement learning," *Nature*, vol. 518, no. 7540, p. 529, 2015.

[112] M. Jaderberg, W. M. Czarnecki, I. Dunning, L. Marris, G. Lever, A. G. Castañeda, C. Beattie, N. C. Rabinowitz, A. S. Morcos, A. Ruderman, N. Sonnerat, T. Green, L. Deason, J. Z. Leibo, D. Silver, D. Hassabis, K. Kavukcuoglu, and T. Graepel, "Human-level performance in 3D multiplayer games with population-based reinforcement learning," *Science*, vol. 364, no. 6443, pp. 859–865, 2019.

[113] T. J. Sheskin, *Markov Chains and Decision Processes for Engineers and Managers*. CRC Press, 2011.

[114] E. Foruzan, L. K. Soh, and S. Asgarpoor, "Reinforcement Learning Approach for Optimal Distributed Energy Management in a Microgrid," *IEEE Trans. Power Syst.*, vol. 33, no. 5, pp. 5749–5758, 2018.

[115] W. Liu, P. Zhuang, H. Liang, J. Peng, and Z. Huang, "Distributed Economic Dispatch in Microgrids Based on Cooperative Reinforcement Learning," *IEEE Trans. Neural Networks Learn. Syst.*, vol. 29, no. 6, pp. 2192–2203, 2018.

[116] H. Xu, H. Sun, D. Nikovski, S. Kitamura, K. Mori, and H. Hashimoto, "Deep Reinforcement Learning for Joint Bidding and Pricing of Load

Serving Entity," *IEEE Trans. Smart Grid*, vol. 10, no. 6, pp. 6366–6375, 2019.

[117] H. Hua, Y. Qin, C. Hao, and J. Cao, "Optimal energy management strategies for energy Internet via deep reinforcement learning approach," *Appl. Energy*, vol. 239, pp. 598–609, 2019.

[118] N. Sadeghianpourhamami, J. Deleu, and C. Develder, "Definition and evaluation of model-free coordination of electrical vehicle charging with reinforcement learning," *IEEE Trans. Smart Grid*, vol. PP, no. 99, pp. 1–1, 2018.

[119] S. Fujimoto, H. van Hoof, and D. Meger, "Addressing Function Approximation Error in Actor-Critic Methods," in *35th Int. Conf. Mach. Learn.*, 2018.

[120] X. Yu, S. Gao, X. Hu, and H. Park, "A Markov decision process approach to vacant taxi routing with e-hailing," *Transp. Res. Part B Methodol.*, vol. 121, pp. 114–134, 2019.

[121] R. S. Sutton and A. G. Barto, *Reinforcement Learning: An Introduction*. The MIT Press, 2018.

[122] T. P. Lillicrap, J. J. Hunt, A. Pritzel, N. Heess, T. Erez, Y. Tassa, D. Silver, and D. Wierstra, "Continuous control with deep reinforcement learning," in *Int. Conf. Learn. Represent. (2016 ICLR)*, 2016.

[123] D. Silver, G. Lever, D. Technologies, G. U. Y. Lever, and U. C. L. Ac, "Deterministic Policy Gradient Algorithms," in *Proc. 31st Int. Conf. Mach. Learn. (ICML 2014)*, 2014.

[124] V. Mnih, K. Kavukcuoglu, D. Silver, A. Graves, I. Antonoglou, D. Wierstra, and M. Riedmiller, "Playing Atari with Deep Reinforcement Learning," in *2013 NIPS*, 2013.

[125] B. T. Polyak and A. B. Juditsky, "Acceleration of Stochastic Approximation by Averaging," *SIAM J. Control Optim.*, vol. 30, no. 4, pp. 838–855, 1992.

[126] G. E. Uhlenbeck and L. S. Ornstein, "On the Theory of the Brownian Motion," *Phys. Rev.*, vol. 36, no. 5, pp. 823–841, 1930.

[127] H. V. Hasselt, "Double Q-Learning," in *Adv. Neural Inf. Process. Syst.*, 2010, pp. 2613–2621.

[128] V. R. Konda and J. N. Tsitsiklis, "On Actor-Critic Algorithms," *SIAM J. Control Optim.*, vol. 42, no. 4, pp. 1143–1166, 2003.

[129] A. Paszke, S. Gross, S. Chintala, G. Chanan, E. Yang, Z. DeVito, Z. Lin, A. Desmaison, L. Antiga, and A. Lerer, "Automatic Differentiation in PyTorch," in *NeurIPS Autodiff Work.*, 2017.

[130] Z. Wang, J. Wang, and C. Chen, "A Three-Phase Microgrid Restoration Model Considering Unbalanced Operation of Distributed Generation," *IEEE Trans. Smart Grid*, vol. 9, no. 4, pp. 3594–3604, 2018.

[131] P. Li, H. Ji, C. Wang, J. Zhao, G. Song, F. Ding, and J. Wu, "Optimal Operation of Soft Open Points in Active Distribution Networks Under Three-Phase Unbalanced Conditions," *IEEE Trans. Smart Grid*, vol. 10, no. 1, pp. 380 – 391, 2019.

[132] Y. Xu, C. C. Liu, Z. Wang, K. Mo, K. P. Schneider, F. K. Tuffner, and D. T. Ton, "DGs for Service Restoration to Critical Loads in a Secondary Network," *IEEE Trans. Smart Grid*, vol. 10, no. 1, pp. 435–447, 2019.

[133] London Economics International, "Estimating the Value of Lost Load," Tech. Rep., 2013. [Online]. Available: https://hepg.hks.harvard.edu/files/hepg/files/06_18_13_ercot_voll_literature_review_and_macroeconomic_analysis_0613.pdf

[134] Y. Xu, C. C. Liu, K. P. Schneider, and D. T. Ton, "Placement of Remote-Controlled Switches to Enhance Distribution System Restoration Capability," *IEEE Trans. Power Syst.*, vol. 31, no. 2, pp. 1139–1150, 2016.